MH.

UNCLASSIFIED
Distribution: UNLIMITED

DIVISION OF MECHANICAL ENGINEERING

DIVISION DE GÉNIE MÉCANIQUE

CANADA

PAGES
PAGES

FIG.
DIAG.

REPORT
RAPPORT

REPORT
RAPPORT LTR-WE-38

DATE
DATE April 1983

SECTION
Western Lab.

LAB. ORDER
COMM. LAB. 22200

FILE
DOSSIER 3793-2-4

FOR
POUR Transport Canada, Transportation Development Centre, Montreal, Canada and Association of American Railroads, Technical Research Centre, Chicago, U.S.A.

REFERENCE
RÉFÉRENCE

LTR- WE-36

ESTABLISHMENT OF QUANTITATIVE WEAR AND FATIGUE MODEL FOR RAILWAY RAIL 1981/82 PROGRESS REPORT

TP 4347E

SUBMITTED BY
PRÉSENTÉ PAR C. Dayson
SECTION HEAD
CHEF DE SECTION

AUTHOR S
AUTEUR J. Kalousek, NRC
H. Ghonem, URI

APPROVED
APPROUVÉ E.H. Dudgeon
DIRECTOR
DIRECTEUR

THIS REPORT MAY NOT BE PUBLISHED WHOLLY OR IN PART WITHOUT THE WRITTEN CONSENT OF THE DIRECTOR OF MECHANICAL ENGINEERING

CE RAPPORT NE DOIT PAS ÊTRE REPRODUIT, NI EN ENTIER NI EN PARTIE, SANS UNE AUTORISATION ÉCRITE DE LA DIVISION DE GÉNIE MÉCANIQUE

Library and Information Centre / Centre de Documentation
RECEIVED – REÇU
AUG 19 1983
Transport Canada / Transports Canada

FORM NRC 539
FORMULAIRE NRC 539

COPY NO.
COPIE NR.

REPORT DOCUMENTATION FORM

1 Transport Canada Report No	2 TDC Project No	3 Recipient's Catalogue No
TP 4347E	4522	

4 Title and Subtitle	5 Report Date
Establishment of Quantitative Wear and Fatigue Model for Railway Rail - 1981/82 Progress Report	APRIL 1983
	6 Performing Organization Report No: LTR-WE-38
7 Author(s): J. Kalousek, H. Ghonem	8 Transport Canada File No: D1465-366
9 Performing Organization Name and Address: National Research Council of Canada/University of Rhode Island, Western Laboratory, 3904 West 4th Avenue, Vancouver, B.C. V6R 1P5	10 DSS File No 11 DSS or Transport Canada Contract No
12 Sponsoring Agency Name and Address: Transportation Development Centre (TDC), 1000 Sherbrooke Street West, Suite 2421, Montreal, Quebec H3A 2R3	13 Type of Report and Period Covered: Progress October 1981 - September 1982 14 Sponsoring Agency Code: TDC 4522
15 Supplementary Notes: This is a cooperative project between the Transportation Development Centre (TDC) and the Association of American Railroads	16 TDC Project Officer: D.W. Dibble

17 Abstract

This report summarizes the research efforts accomplished during the 1981/82 period of a joint Canadian/U.S. research program aimed at developing a wear and fatigue model for railway rail. The report consists of a collection of five papers previously published in open literature:

"Observations of Rail Wear on Heavy Haul Railway Lines"
"Aspects of Plastic Deformation and Fatigue Damage in Pearlitic Rail Steels"
"Lubrication: Its Various Types and Effects on Rail/Wheel Forces and Wear"
"Lateral Creepage and Its Effect on Wear in Rail Wheel Interface"
"On the Fracture and Wear Characteristics of Chromium - Molybdenum Bainitic Steels"

The first two papers deal primarily with the identification of significant parameters in the rail/wheel tribosystem and with a theoretical analysis of the fatigue nature of wear processes. The third paper analyzes the effect of rheological variables on rail/wheel forces and wear. The fourth paper reports the experimental results from the initial tests carried out on rail/wheel wear apparatus and the last one reports on an experimental work concerned with the fracture toughness properties of conventional and nonconventional rail-steel materials.

18 Key Words	19 Distribution Statement
Wheel/Rail Wear, Fatigue, Interaction, Lubrication, Tribology, Metallurgy	Limited number of copies available from Sponsoring Agency

20 Security Classification (of this report)	21 Security Classification (of this page)	22 No of Pages	23 Price
Unclassified	Unclassified		--

FORMULE DE DOCUMENTATION POUR RAPPORT

1 N° du rapport Transports Canada	2 N° de l'étude — CDT	3 N° de catalogue du destinataire
TP 4347E	4522	

4 Titre et sous-titre	5 Date du rapport
Establishment of Quantitative Wear and Fatigue Model for Railway Rail - 1981/82 Progress Report	avril 1983
	6 N° du rapport de l'organisme exécutant: LTR-WE-38

7 Auteur(s)	8 N° de dossier Transports Canada
J. Kalousek, H. Ghonem	D1465-366

9 Nom et adresse de l'organisme exécutant	10 N° de dossier — ASC
Conseil national de recherches Canada/Université de Rhode Island Laboratoire de l'ouest 3904 4ième avenue ouest Vancouver, B.C. V6R 1P5	11 N° de contrat — ASC ou Transports Canada

12 Nom et adresse de l'organisme parrain	13 Genre de rapport et période visée
Centre de développement des transports (CDT) 1000 ouest, rue Sherbrooke Suite 2421 Montréal, Québec H3A 2R3	état périodique octobre 1981 - septembre 1982 14 Code de l'organisme parrain: CDT 4522

15 Remarques additionnelles	16 Agent de projet — CDT
Ceci est un programme de recherche conjoint, parrainé par le CDT et Association of American Railroads.	D.W. Dibble

17 Résumé

Ce rapport récapitule les travaux de recherche faits en 1981/82 dans le cadre d'un programme canado-américain visant à élaborer un modèle mathématique représentant le processus d'usure et de fatigue des rails de chemins de fer. Il comporte cinq mémoires déjà publiées, dont voici les titres:

"Observations of Rail Wear on Heavy Haul Railway Lines"
"Aspects of Plastic Deformation and Fatigue Damage in Pearlitic Rail Steels"
"Lubrication: Its Various Types and Effects on Rail/Wheel Forces and Wear"
"Lateral Creepage and Its Effect on Wear in Rail Wheel Interface"
"On the Fracture and Wear Characteristics of Chromium - Molybdenum Bainitic Steels"

Les deux premiers donnent une large part à la mise en évidence des paramètres tribologiques significatifs liés au contact roue-rail, et à l'analyse du processus d'usure par fatigue. Le troisième analyse l'effet que les paramètres rhéologiques ont sur les forces d'usure en jeu. Le quatrième rend compte des premières expérimentations faites à l'aide d'un appareil de mesure de l'usure roue-rail et, enfin, le cinquième traite des expérimentations sur la ténacité des aciers ordinaires et spéciaux pour rails.

18 Mots-clés	19 Diffusion
Usure roue-rail, fatigue, interaction, lubrification, tribologie, métallurgie	Le CDT dispose d'un nombre limité d'exemplaires

20 Classification de sécurité (de ce rapport)	21 Classification de sécurité (de cette page)	22 Nombre de pages	23 Prix
Non-classifié	Non-classifiée		--

CONTENTS

		Page
Foreward		2
Avant-propos		4
Paper 1	"OBSERVATIONS OF RAIL WEAR ON HEAVY HAUL RAILWAY LINES", by: H. Ghonem, J. Kalousek, D.H. Stone, D. Dibble; Proceedings of the International Symposium on Contact Mechanics and Wear of Rail/Wheel Systems, University of Waterloo - Solid Mechanics Division, 1983.	6
Paper 2	"ASPECTS OF PLASTIC DEFORMATION AND FATIGUE DAMAGE IN PEARLITIC RAIL STEELS", by: H. Ghonem, J. Kalousek, D.H. Stone, E.E. Laufer; Proceedings of the Second International Heavy Haul Conference, ASME 82 - HH - 31.	27
Paper 3	"LUBRICATION: ITS VARIOUS TYPES AND EFFECTS ON RAIL/WHEEL FORCES AND WEAR", by: J. Kalousek; Proceedings of the Rail and Wheel Lubrication Symposium, Railway Systems and Management Association, 1982.	38
Paper 4	"LATERAL CREEPAGE AND ITS EFFECT ON WEAR IN RAIL WHEEL INTERFACE", by: J. Kalousek, G. Rosval, H. Ghonem; Proceedings of the International Symposium on Contact Mechanics and Wear of Rail/Wheel Systems, University of Waterloo - Solid Mechanics Division, 1983.	52
Paper 5	"ON THE FRACTURE AND WEAR CHARACTERISTICS OF CHROMIUM - MOLYBDENUM BAINITIC STEELS", by: H. Ghonem, J. Kalousek, D.H. Stone; Proceedings of the International Conference on Recent Developments in Specialty Steels and Hard Materials.	73

Foreword

This is the first annual progress report on the research program carried out jointly at the National Research Council of Canada and the University of Rhode Island, U.S.A., and sponsored by the Transportation Development Centre of Transport Canada and the Association of American Railroads. The program is concerned with the development of a wear and fatigue model for railway rail that would provide more accurate and reliable relationships for track maintenance models than the currently used wear indices.

Due to the complexity of rail/wheel interaction and the extensiveness of experimental investigations this complexity calls for, it is envisaged that the proposed research program could be completed in four years. During this time, several key variables affecting wear and contact fatigue life of rails will be thoroughly investigated, namely: fatigue properties of selected rail materials, load, angle-of-attack and lubrication. In addition to these variables, three distinctive but interrelated sets of parameters are identified as an integral part of the wear and fatigue model. These are: mechanical, metallurgical and rheological parameters. The mechanical parameters include geometry of contact, external and creepage forces acting at the rail/wheel interface, and contact stresses. Grain size, lamella spacings, dislocation density, inclusions and chemical composition fall into the group of metallurgical parameters. The rheological parameters help to define the regime of lubrication, which may be dry (no lubrication), elastohydrodynamic, or intermittent. An analysis of those parameters includes the surface topology, viscosity and composition of lubricant and tribo-chemical reactions between lubricant and rail material.

The development of such a model consists of both theoretical and experimental work. In the theoretical analysis, existing computer models in conjunction with the most recently developed concepts in the area of wear and contact fatigue will be utilized. The two main cornerstones of experimental work are biaxial fatigue testing of several rail materials carried out at the University of Rhode Island and wear testing of the same materials on rail/wheel wear apparatus at the National Research Council.

A number of complementary tests are considered, such as SEM (Scanning Electron Microscope), EDAX (Energy Dispersive X-ray Analysis), and chemical analysis of used up rail lubricants, to name a few. To establish the level of shear stress in rail/wheel interface under a variety of mechanical and rheological parameters, an instrument called a tribometer is being developed at the National Research Council. This instrument will enable researchers to establish the traction-creepage relationship for various lubrication regimes and combinations of longitudinal, lateral and spin creepages. The tribometer will be fully microprocessor-operated and should become fully operational by fall 1984.

Despite the broad scope of the proposed research, a number of sub-tasks have been completed in the first year of this program. All of these were reported in open literature. To make the information contained in these publications more accessible to industry and avoiding at the same time the duplication of our efforts by writing a separate report on the same subject, we selected five papers to form the main body of our report. As can be seen from the content page, the papers of more general interest are reprinted first, while the most specific one is reprinted last. The first two papers deal primarily with the identification of significant parameters in the rail/wheel tribosystem and with a theoretical analysis of the fatigue nature of wear processes. The third paper analyzes the effect of rheological variables on rail/wheel forces and wear. The fourth paper reports the experimental results from the initial tests carried out on rail/wheel wear apparatus and the last one reports on an experimental work concerned with the fracture toughness properties of conventional and nonconventional rail-steel materials.

Laboratory technical report LTR-WE-29, which documents our efforts carried out in the area of computer programming, is not attached herewith since it is bulky and solely concerned with computer programming. It is entitled "Modelling of Roller Rig Contact Forces for Three Point Contact - Based on Kalker's Simplified Non-Linear Creep Theory for Single Point Contact", and is available on request to anyone interested from NRC - Western Laboratory.

Avant-propos

Ceci est le premier rapport annuel sur l'avancement du programme de recherche conjoint parrainé par le Centre de développement des transports et l'Association of American Railroads et pris en charge par le Conseil national de recherches du Canada et l'université de Rhode Island. Il s'agit du programme pour l'élaboration d'un modèle mathématique représentant le processus d'usure et de fatigue des rails, et permettant de corréler entre eux les paramètres utilisés pour programmer l'entretien des voies, tout en étant plus fidèle et plus fiable que les indices d'usure couramment utilisés.

Ce programme de recherche devra s'étaler sur quatre ans, étant donné la complexité du problème posé par l'interaction roue-rail et l'ampleur des expérimentations à prévoir. Dans ce laps de temps, les principaux paramètres reliés à l'usure et à la fatigue des rails seront étudiés, notamment: la résistance à la fatigue de certains métaux entrant dans la fabrication des rails, la charge dynamique, l'angle d'attaque et la lubrification des rails. En outre, trois groupes de paramètres, distincts mais corrélatifs entre eux, seront pris en compte par le modèle envisagé. Ces trois groups rassemblent les paramètres mécaniques, métallurgiques et rhéologiques. Le premier de ces groupes de paramètres concerne la géométrie d'inscription des essieux, les forces extérieurs de frottement de glissement s'exerçant au point de contact roue-rail et les forces d'appui de roulement. Font partie du deuxième groupe, ou groupe métallurgique, la grosseur des grains, les espacements lamellaires, la concentration des dislocations, les impuretés et la composition chimique. Quant aux paramètres rhéologiques, ils participent à la définition du coefficient de frottement en cas de frottement pur (aucune lubrification), élastohydrodynamique ou intermittent. Les paramètres pris en compte sont la topologie des surfaces, la viscosité, la nature du lubrifiant et les réactions tribo-chimiques entre le lubrifiant et le rail.

Les travaux de modélisation seront tant théoriques que pratiques. Les premiers utiliseront les modèles déjà établis, de pair avec les concepts les plus récents touchant le phénomène de l'usure et de la fatigue. Les deuxièmes s'appuieront sur les essais biaxiaux de résistance à la fatigue d'un certain nombre de métaux, faits par l'université de Rhode Island, et aussi sur les essais de résistance à l'usure de ces mêmes métaux faits par le Centre national de recherches à l'aide de l'appareillage de mesure de l'usure roue-rail.

Des travaux complémentaires sont envisagées, utilisant le microscope électronique à balayage, les rayons X et l'analyse chimique des lubrifiants usés, pour n'en citer que quelques-uns. Le CNR du Canada étudie un appareil appelé tribomètre qui permettra de mesurer les efforts de cisaillement aux points de contact roue-rail, dans des conditions mécaniques et rhéologiques variables. Il servira aussi à établir le rapport traction-glissement aux différents régimes de lubrification utilisés et sous l'influence des composantes axiale, transversale et torsionnelle des forces de frottement. Ce tribomètre, à commande entièrement informatisée, devrait être opérationnel d'ici l'automne 1984.

Malgré l'ampleur des travaux prévus au programme, un certain nombre de sous-programmes ont pu être achevés dès la première année. Ils ont été entre-temps publiés. Avant de les rendre plus accessibles aux intéressés, et pour éviter d'avoir à rédiger un deuxième rapport sur le même sujet, nous avons sélectionné cinq mémoires qui formeront le gros de notre rapport à nous. Comme on peut le constater dans la table des matières, les mémoires offrant un intérêt plutôt général apparaissent en tête de liste, suivis de ceux qui traitent d'un sujet en particulier. Les deux premiers donnent une large part à la mise en évidence des paramètres tribologiques significatifs liés au contact roue-rail, et à l'analyse du processus d'usure par fatigue. Le troisième analyse l'effet que les paramètres rhéologiques ont sur les forces en jeu dans le phénomène de l'usure roue-rail. Le quatrième mémoire rend compte des premières expérimentations faites à l'aide de l'appareil de mesure de l'usure roue-rail, et le cinquième traite des expérimentations sur la ténacité des aciers ordinaires et spéciaux pour rails.

Le procès-verbal LTR-WE-29, qui rend compte des travaux de laboratoire faits par nous dans le domaine de la programmation informatique, n'est pas annexé au présent rapport parce qu'il est volumineux et qu'il traite uniquement de cet aspect. Il est intitulé "Modelling of Roller Rig Contact Forces for Three Point Contact - Based on Kalker's Simplified Non-Linear Creep Theory for Single Pointe Contact". Il s'obtient sur demande adressée au CNR - Laboratoires de l'ouest.

CONTACT MECHANICS AND WEAR OF
RAIL/WHEEL SYSTEMS
University of Waterloo Press, 1982

Vancouver
British Columbia
July 6-9, 1982

OBSERVATIONS OF RAIL WEAR ON HEAVY HAUL RAILWAY LINES

H. Ghonem
Department of Mechanical Engineering
University of Rhode Island
Kingston, Rhode Island, U.S.A.

J. Kalousek
Western Laboratory
National Research Council of Canada
Vancouver, British Columbia, Canada

D.H. Stone
Association of American Railroads
Chicago, Illinois, U.S.A.

D.W. Dibble
Transport Canada
Research and Development Centre
Montreal, Quebec, Canada

ABSTRACT: The rail-wheel tribosystem is a complex system in which output parameters in the form of wear and fatigue related problems are closely associated with and governed by the nature of the tribosystem input. This input is classified, in this paper, in groups that include operational, contact mechanics, material and rheological parameters. These parameters are discussed and their contribution to rail wear mechanisms is detailed.

RÉSUMÉ: Le tribosystème rail/roue est un système complexe dans lequel les paramètres de sortie, soit les problemes rattachés a l'usure et à la fatigue, sone étroitement liés à la nature des paramètres d'entrée et en dépendent. L'article divise les paramètres d'entrée en paramètres opérationnels, mécaniques (relatifs aux contacts), matériels et rhéologiques. On discute de ces paramétres et on précise leur contribution aux mécanismes d'usure des rails.

INTRODUCTION

The survival of any high capacity freight railroad as a competitive means of transportation depends, among other factors, upon its ability to minimize costs of rail inspection, maintenance and rerailing programs. A significant portion of expenditure in these costly programs is due to rail wear and associated problems, see Figure 1. For this reason extensive, but uncoordinated, research has been carried out in the U.S.A. and in Canada during the last two decades with the objective of achieving a basic understanding of the

rail-wheel wear process in order to improve the capability of quantitatively predicting wear effect on rail life. This is a complex task; rail wear is a multidimensional process governed by a wide spectrum of interdependent parameters. The ideal approach in which to study these parameters is through field tests on service revenue railway lines, or on an exclusive test site similar to the Facility for Accelerated Service Testing (FAST) in the U.S.A. where field conditions could be duplicated. This approach which is not possible all the time, in addition to the difficulty in interpreting its data output, is a slow and extremely expensive one. The estimated operation budget of FAST in 1981 was 6 million dollars. The alternative is small scale rigs or laboratory tests. However, the deficiency inherent in this relative inexpensive approach is that the wear process could only examine one, or a set of the influencing parameters, at a time, thereby either neglecting the effect of other parameters or assuming them to be constant during the cycle of the test period. An obvious gap therefore exists between results of small scale tests and field observations. The depth of this gap depends primarily on the accuracy in selecting the parameters and the nature of the assumption made in laboratory tests. This accuracy could only be improved by utilizing field observations to identify critical parameters and determine their interactive roles in the overall rail wear process. This study is an attempt to describe these parameters.

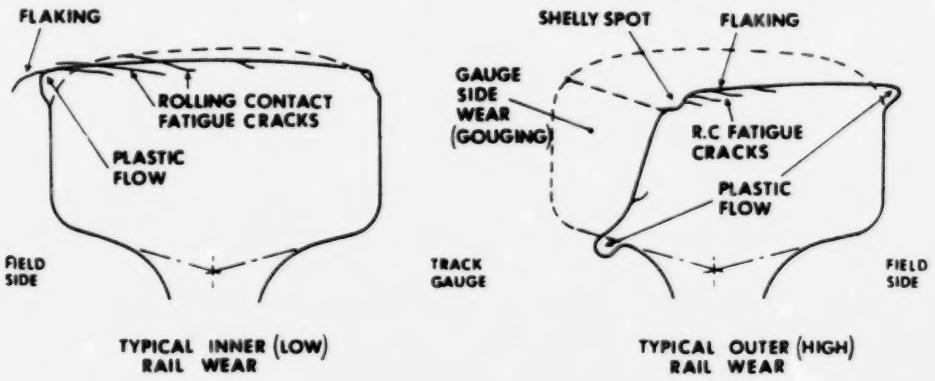

Figure 1 - Wear on High and Low Rails

RAIL-WHEEL TRIBOSYSTEM

The structure of any tribosystem is generally described by the elements or components of the system, their properties and interrelations with other components. In the case of rail-wheel tribosystem the basic elements as shown in Figure 2 consists of a wheelset as a base body, a pair of rails as a counter body and a lubricant film as an intermediate matter separating rail and wheel surfaces. The interaction of these elements is governed by a set of input variables that are determined by the operational conditions of the system, the mechanics of contact between the wheel and the rail, their material characteristics and the rheological nature of the intermediate matter. Based on the nature of this input, the wheel-rail system would then yield, in addition to the required motion

an inevitable set of output. This includes different forms of wear, fatigue related problems, surface and matrix plastic deformation and surface corrugation. Each of these variables are closely associated with the input variables which in turn cannot be separated or isolated in the study of any of the output variables.

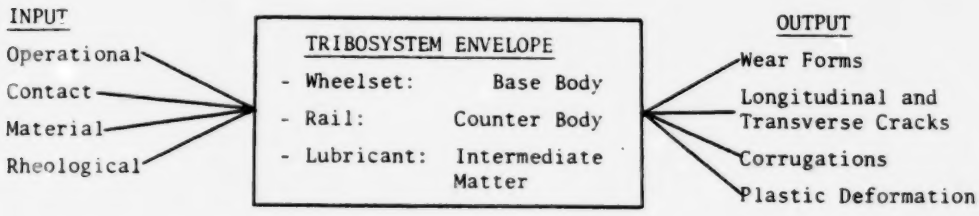

Figure 2 - Rail-Wheel Tribosystem

Each of the input variables, as has been arranged above in four main groups - see references [1,2] for different arrangements of input variables - includes a very long list of individual parameters. Carrying out an extensive description of field observations on each of these parameters is beyond the scope of this paper; instead, however, critical parameters of each group have been selected for this study.

INPUT PARAMETERS

Operational Parameters

The combination of these parameters, which is unique for every individual railway line, is the most influential factor in determining the magnitude of the externally applied load on the rail head. They consist of:

(i) Axle Load: It represents the vertical load acting on the wheel/rail contact areas and controls the magnitudes of the external tangential force in these zones. In the early 1960's the loading capacity of the freight car in heavy haul railway lines increased from 50-70 tons to 100 tons. The present world trend, however, is towards capacity loads as high as 125 tons. The effect of these increases has been examined by several authors [3,4,5]. In the work of Stone [5] a comparison is made between wear data from Waynesburg Southern Railway using cars of 318,000 lbs. versus data from Quebec North Shore and Labrador Railway which carried iron ore in cars of 254,000 to 264,000 lbs. Results of this comparison show that by increasing the car load 25 percent, wear rates of standard carbon rail have increased 5.5 times on tangent tracks and 1.2 times on 4° curves. This effect stabilises as the degree of curvature increases. At sharp curves, while the axle load is still an effective parameter, wear is more sensitive to the lateral and creep forces exerted on the rail head due to wheel position and orientation.

(ii) Traffic Characteristics: In addition to the type of traffic, i.e., passenger, freight or combined, the important parameters describing the traffic characteristics are

the frequency and the density measured in million growth tons per annum (MGT). Work of Dearden [6] has shown that rail wear decreases exponentially with the increase of traffic frequency as illustrated in Figure 3. The influence on this condition is attributed to the fact that an increase in time between wheel passages increases the effect of atmospheric corrosion on the rail surface. This phenomenon can be noted when comparing wear on branch lines versus that on main lines.

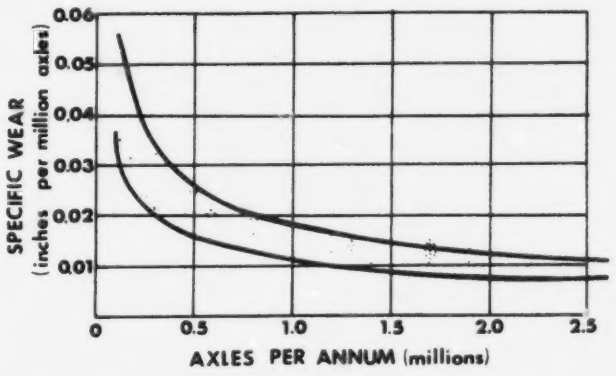

Figure 3 - Effect of Traffic Frequency on Wear of Rural Lines [6]

Wear rate increases with the increase in hauled tonnage. This relationship is shown in Figure 4 based on data from Mount Newman Railway [7]. Accelerated metal loss is observed in the range of 0-50 MGT followed by moderate loss. Same observations were made on CN Railway [8] and on FAST as shown in Figure 5.

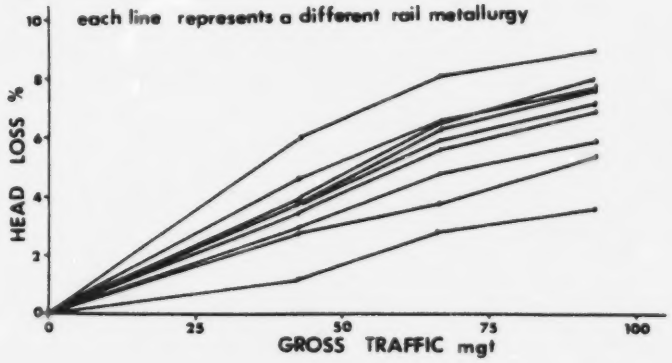

Figure 4 - Effect of Traffic Density on Rail Wear [7]

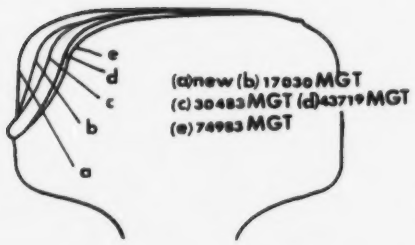

Figure 5 - Rail Wear Pattern on FAST

(iii) Travelling Speed: Field tests carried out on a 5° curve [9] indicated that a reduction in angle-of-attack occurs as the travelling speed exceeds the equilibrium speed of the test curve as shown in Figure 6. This observation is interpreted in terms of the wheelset tendency to assume a more radial position as the speed increases. A reduction in the lateral creep forces could then be achieved by increasing the travelling speed. High speeds, however, give rise to the role of the centrifugal force acting against the truck and could result in the wheel being pushed towards the high rail. This action produces high flange forces and high vertical forces as shown in Figure 7, thus increasing wear on high rails. At speeds below the equilibrium speed the loading conditions, described above, are reversed and the wear process becomes more active on the low rail of a curve.

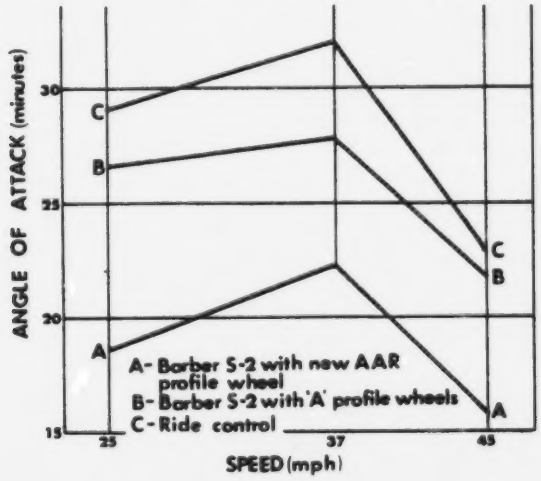

Figure 6 - Angle-of-Attack versus Speed

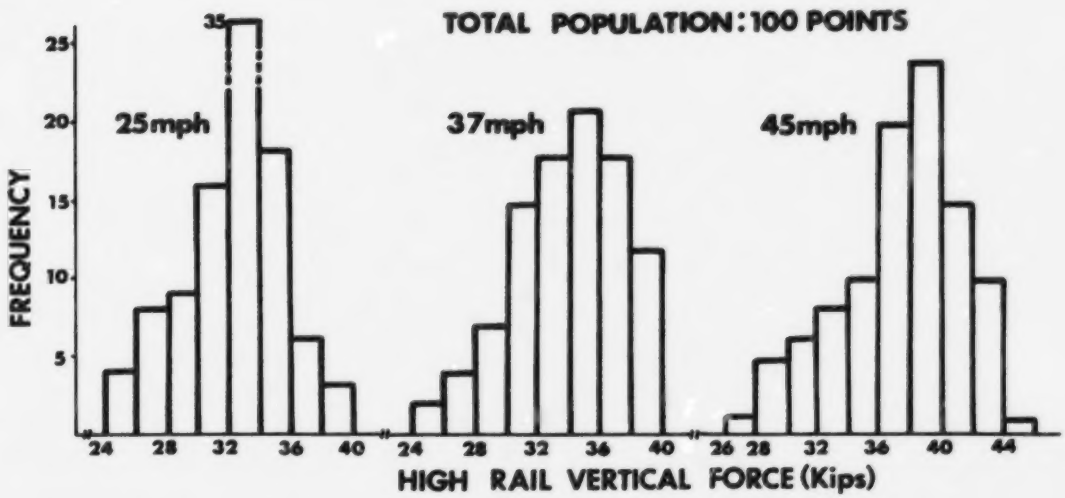

Figure 7 - Effect of Speed on Vertical Force Distribution on the High Rail. (Wheel Static Load: 32.5 kips)

(iv) Truck Design: Freight trucks can generally be split into two basic categories; the first is the type similar to and including the conventional Barber S-2, three piece truck. In this type of curve steering ability depends on a guide lateral force resulting from hard contact conditions between the upper wheel of the leading wheelset and the gauge corner of the high rail. Furthermore, the orientation of the axles of this truck type, during traversing of a curve, dictate a large angle of attack at the leading wheelset which could produce saturated lateral creep forces within the contact zone. The combination of high flange force and high creep force results in an increase in the loss of rail surface metal.

The second category of truck design is labelled type II or self steering trucks and aims at improving the curving performance by accommodating the difference between the length of the outer and inner rail on a curve. This is done by an appropriate combination of lateral and yaw stiffness between the two axles of a truck, permitting the wheelsets to take up an approximate radial alignment with the rail. This results in a reduction of the lateral creep force and, subsequently, the rail surface wear [9].

Mechanics of Contact

The importance of this set of parameters is the fact that wheel/rail contact conditions dictate (a) the geometry of the contact zone on which the shape of the wheel pressure distribution and consequently the state of contact stresses depend, and (b) positions of contact zones and associated creep forces which govern and contribute to the severity of the wear process. The critical parameters in this group are:

(i) Wheel/Rail Contact Profile: For the same track gauge and the same wheel/rail adhesion level, the steering moment, which is responsible for the self-excited oscilla-

tion of a wheelset on tangent tracks, could be reduced by selecting a wheel profile with low conicity, such as the coned AAR profile. On curves, however, this profile assumes two contact positions due to lack of conformity with the rail head. This results, in addition to high contact stresses, in high lateral forces and a high angle-of-attack.

Regardless of the initial profile there is a tendency for a wheel profile to wear into a concave or worn wheel profile accompanied by a change in the coning angle. This results in an increase in the effective conicity. Worn wheels, or wheels with worn profiles, with high conicity, such as, Heumann and CN 'A' profiles, require more energy to generate an oscillation on tangent tracks. When traversing a curve, however, a wheel with worn profile produces small angle-of-attack and a large area of contact due to conformity with the worn rail head profile. This in turn reduces both the lateral creep forces and the maximum wheel/rail contact pressure and results in reduced rail wear. If wheel wear data can be used to project rail performance under the worn and coned wheel profiles, the above observations are confirmed in Figure 8. On this subject, reference should be made to the excellent work of CN Rail Research Centre [11,12].

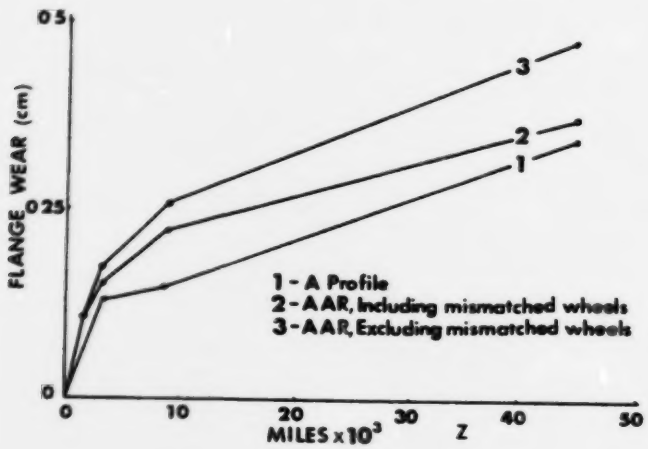

Figure 8 - Average Leading Axles Flange Wear [10]

(ii) Creep Forces: The measure of microslip within the zone of wheel/rail contact is termed creepage and consists of longitudinal and lateral components and spin creepage; their mathematical definitions are shown in Figure 9.

The way in which creepage and spin arise in a wheelset is detailed by many authors, see for example references [13,14], and can be understood by referring to Figure 10 in which a wheelset is assumed to be moving freely along a track with a constant velocity V in a steady state displaced position with a fixed yaw angle ψ. The angular velocity of the wheelset rotation is given by Ω with components $(0,\Omega,0)$ in the wheelset axis system C_{123}. Following an analysis detailed by Gilchrist and Brickle [13], the lateral, longitudinal and spin creep could, respectively, be calculated as:

$$\gamma_1 = \cos\psi - 1 \ , \tag{1}$$

$$\psi_2 = \sec\alpha \sin\psi \ , \tag{2}$$

and

$$\omega_3 = \sin\alpha / r_c \ . \tag{3}$$

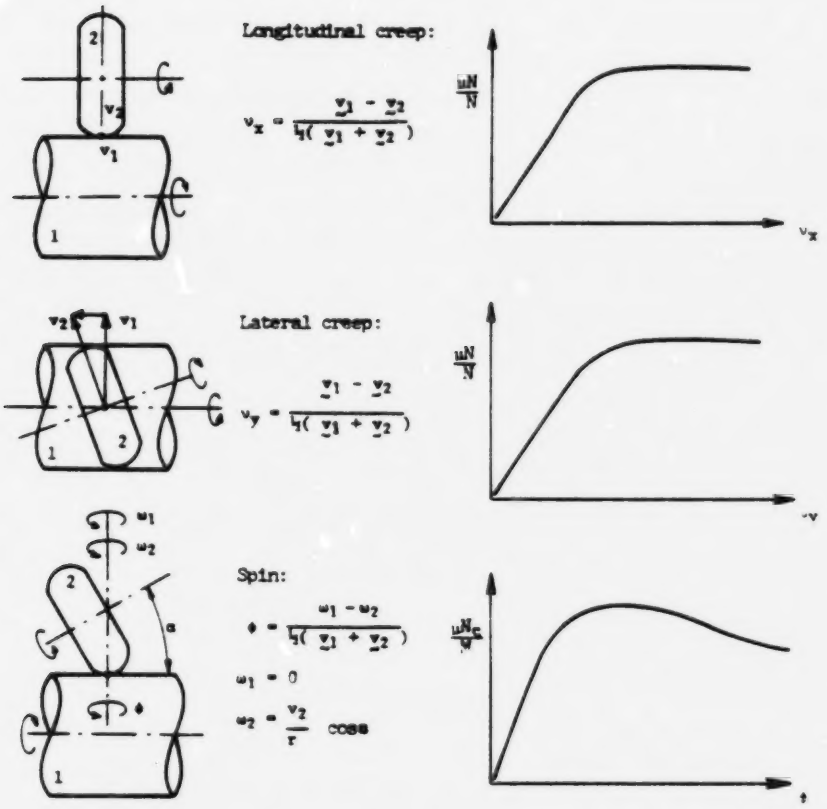

Figure 9 - Definition of Creep Components

These equations are applied at the wheel tread contact point as well as at the flange contact point for both left and right wheels. They indicate the dependency of the longitudinal and lateral creepages on the angle ψ while spin slippage is determined by the cone angle α. For small angle-of-attack the previous set of equations indicates that the only dominant creepage on the upper portion of the rail surface, which is contacting a wheel tread zone having a small cone angle, is the lateral creepage which would be equal to the angle-of-attack, ψ. At the point of flange the effect of both lateral and spin creepage will be present. The gross sliding condition in this zone, however, indicates the minimum effect of the spin component. These observations are substantiated by field data, [15] results of which are described in Figure 12. This shows replicas of nine locations of the wheel surface topography. The markings shown in these

locations are the local deformations in the area of contact caused by rail asperities on both tangent and curved tracks over which the wheel has passed prior to obtaining its surface replica. The rubbing marks of these asperities are indicative of the magnitude of the surface layer deformation and the type of creepage the wheel surface is subjected to at each location.

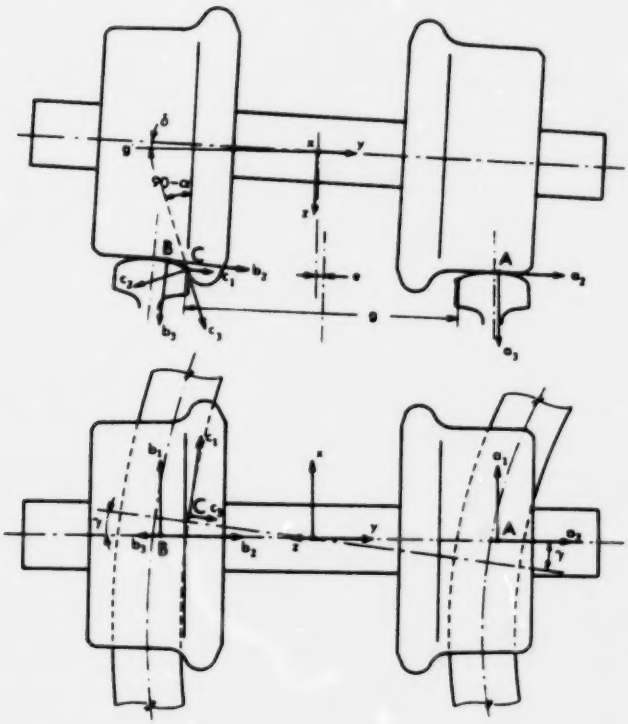

Figure 10 - Kinematics of a Wheelset

The outer portion of the tread at locations 1, 2 and 3 in Figure 11 represents a contact area with low rails and exhibits rubbing marks perpendicular to the direction of the motion. This can be deducted from the long brake marks, clearly shown in locations 1 and 2, which are parallel to the direction of travel. The direction of these rubbing marks, therefore, proposes a prevalence of the lateral creep force which agrees with the conclusions obtained from equation (2). Locations 5, 6 and 7 represent the area of the wheel surface contacting the gauge corner of outer rails in curves. Rubbing marks in these locations indicate the existence of longitudinal, lateral and spin creepages. The appearance of the lateral/creep component in these locations may be due to the fact that

these locations come in contact with the rail only in cases of conformal interaction. In these locations the plane of contact has a non-zero conicity, thus allowing spin moment to have an effect on the direction of the 'smearing' of the rail or wheel material. In locations 8 and 9, however, where the 'hard' flange condition occurs and wear of rail gauge and of wheel flange material is at its maximum, rubbing marks of asperities are dominated, in a practical sense, by lateral and transverse slippage. Angle-of-attack is a measure of this slippage which in turn determines the magnitude of the lateral creep force as shown in Figure 12. This force contributes heavily to rail wear.

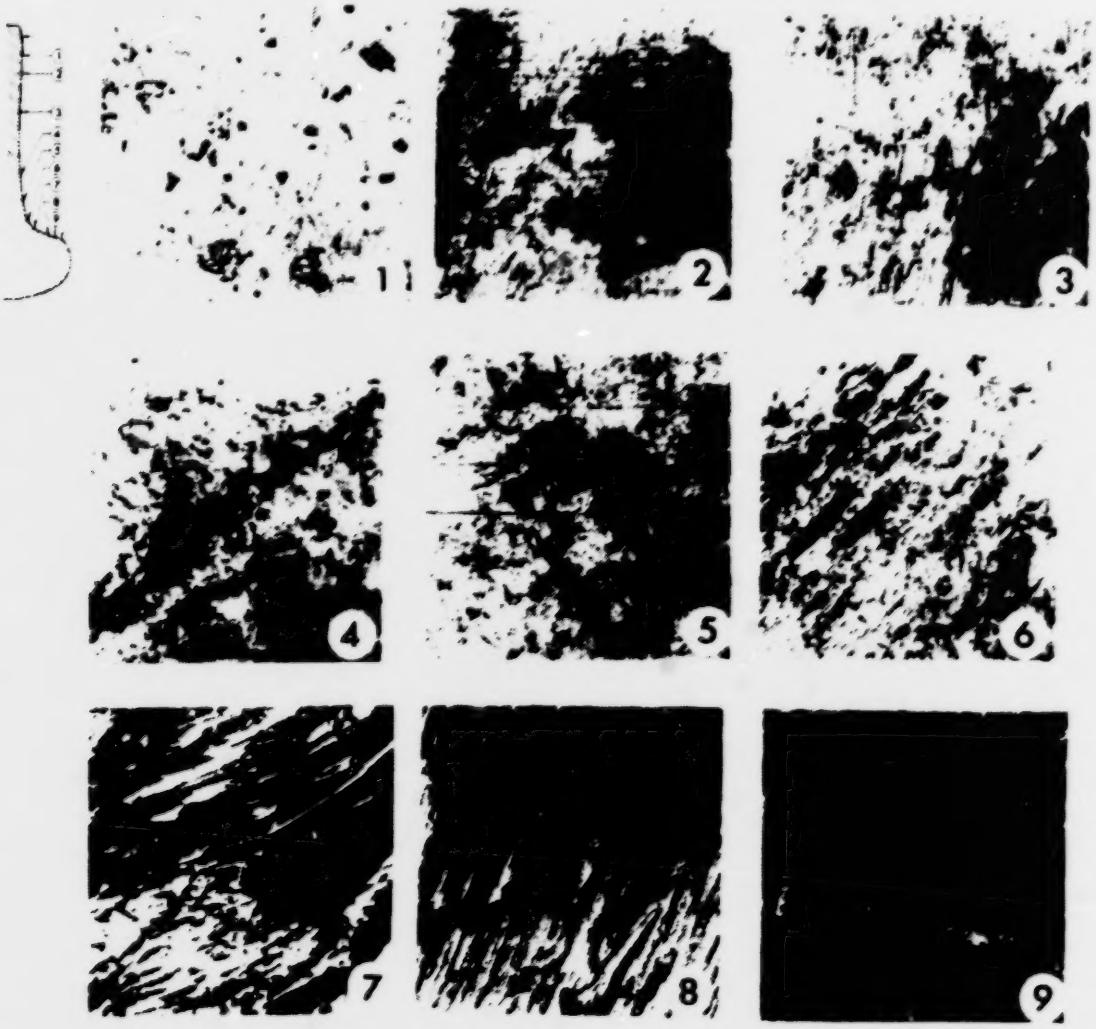

Figure 11 - Surface Topography of a Wheel Subjected to Runs Over Tangent and Curves Tracks [15]

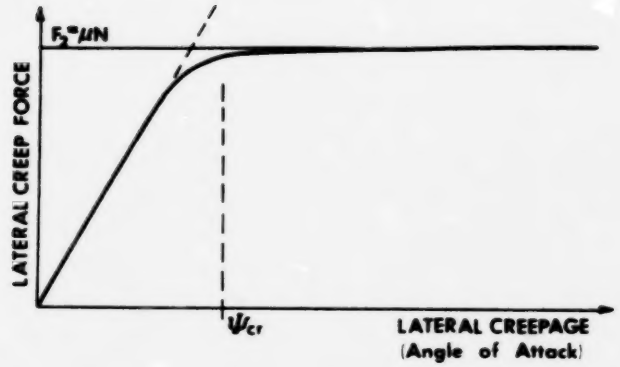

Figure 11 - Relationship Between Angle-of-Attack and Lateral Creep Force

Material Parameters

This set of parameters includes:

- Rail Composition: the role of carbon content and other alloying elements,
- Microstructure: the response of pearlite, tempered martensite and bainite to wear process, effect of lamella size and spacing and grain size,
- Mechanical Properties,
- Residual Stress Pattern,
- Inclusion Content.

This set of parameters is by far the most researched and is detailed in a large number of excellent references, see for example [16,17,18]. Hence this set will not be reviewed here.

Rheological Parameters

This set of parameters is concerned with the third body in the rail-wheel tribosystem, i.e., the lubricant layer. The purpose of injecting such a layer between wheel and rail surfaces is to utilize its viscous nature to reduce the maximum pressure between the individual asperities and to minimize the sliding friction throughout the entire zone of contact. Its beneficial effect in reducing rail curve adhesive wear is recognized by the fact that a track side mounted lubricator is a permanent element in the track structure of Heavy Haul Railway Lines in North America.

The rail lubricant is usually Calcium or Lithium soap based grease containing up to 12 percent Graphite or 3 percent MoS_2. The lubricant composition, thickness and location on the rail head are dependent on lubricator location, type of traffic, climate

conditions and other operational parameters. An analysis of lubricant samples taken from several curves in Western Canada showed that the lubricant is concentrated on the field side of the inner rail and on the gauge corner of the outer rail as shown in Table 1. Its thickness is ≈20 μm and could reach 30 μm in the absence of water mixture. When it is mixed with water a "slick" with a thickness of 200-300 μm may be formed.

Table 1 - Chemical Analysis of the Rail Lubricant on Several Locations [19]

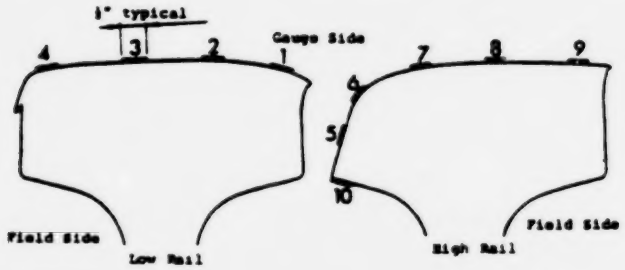

Location of 1/4" x 8" Areas		Total Impurities (mg)	MoS_2 (mg)	Fe_2O_3 (mg)	Other Impurities (mg)
Rail	Position				
Low	1	41.27	20.60	2.26	18.41
	2	16.75	trace	trace	16.75
	3	36.71	.24	.46	36.01
	4	287.23	141.20	22.19	123.84
High	5	114.18	73.58	11.52	29.08
	6	199.47	122.05	11.51	76.31
	7	79.34	32.20	6.40	40.74
	8	38.72	.43	.20	38.09
	9	40.12	3.62	1.73	35.13

The lubricant cannot be found in a clean form on the rail surface; it is always mixed with different forms of contaminants, possible sources of which are, for example, oil from wheelset bearings and locomotive traction gears, atmospheric pollution, terrain and freight materials. Sand particles with high Quartz content used by locomotives to improve adhesion are usually crushed to fine particles with an average size 1 μm and could become mixed as contaminants with rail grease.

The variation in the thickness and the rheological properties of the lubricant contaminated layer determine the type of wheel/rail lubrication regime. As shown in Figure 13 they are divided into two types: (i) elasto-hydrodynamic - in which wheel and rail asperities in the area of contact are completely separated with a relatively thick layer of lubricant, and (ii) boundary or partial elasto-hydrodynamic - in which the lubricant layer is thin in relation to the height of the wheel and rail asperities. In this most frequently encountered regime in the field, the wheel load is shared by the surface asperities in contact and dispersed lubricant film locations.

High pressures and temperatures reached at wheel/rail asperities in the contact zone could effect the rheological properties of the contaminant-lubricant mixtures and the surface-lubricant physical and chemical interactions. They also degrade the chemical characteristics of oily fluid contaminants and affect their reaction with the basic lubricants. The complex nature of these interactions and their effect on adhesive wear and rolling contact are not well researched.

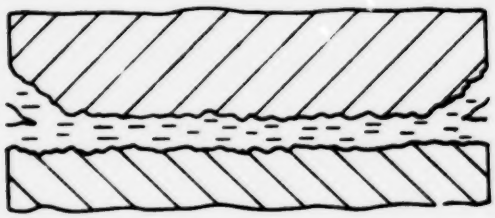

(a)

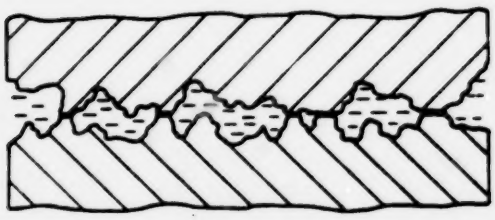

(b)

Figure 13 - Rail/Wheel Lubrication Regimes
(a) elasto-hydrodynamic lubrication
(b) boundary lubrication

OUTPUT PARAMETERS

As previously mentioned, output of the rail-wheel tribosystem as well as the input, is multiple and closely interrelated. This output includes many modes of wear phenomena which are developed by different mechanisms and vary in their surface appearances. One,

or a combination of these wear modes depending on the nature of the input parameters, could dominate and set the limits for rail removal, transposing or further grinding to restore the rail profile.

The critical modes of rail wear include wear by adhesion, abrasion, fretting and corrosion and surface fatigue wear. Additional output associated with and progress dependent upon the state of the rail head wear are surface corrugations, longitudinal cracks, which are known in the railway industry as shellings and transverse cracks which, when combined with shellings, result in what is known as detail fracture. In the following sections an attempt is made to describe field observations concerning individual output.

Wear Forms

Each form of rail wear is a result of a process in which the wheel surface applies a set of normal and tangential forces on the rail surface layer, thereby deforming it elastically or plastically and generating wear particles. Metal loss can be caused by a number of wear mechanisms which may occur independently or simultaneously. They all, however, depend on the surface structure, the time-dependent triaxial state of stress and plastic flow in highly lubricated regions. These mechanisms are:

(i) Adhesive Wear (or Mild Wear): Occurs on the top surface and gauge corner of the rail as a result of wheel-rail sliding. In this mechanism, as in the case of any sliding bodies, wheel and rail surface asperities come into contact and adhere strongly to form asperity junctions. Subsequent separation of wheel and rail surfaces break these junctions generating particles in the form shown in Figure 14. The average size of adhesive wear particles was observed to be ≈ 200 μm.

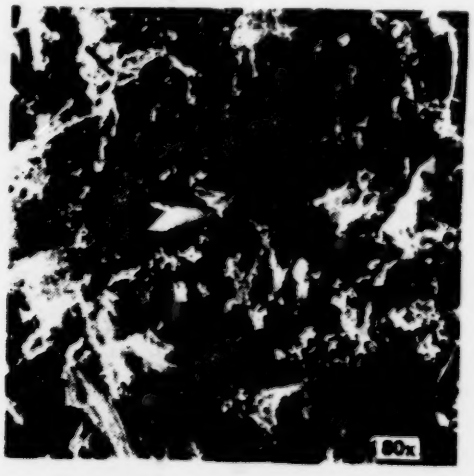

Figure 14 - Adhesive Wear Particles

The mechanism of their separation from adherent asperities, however, is not clearly understood. One explanation could be that the stored elastic energy in the particles becomes greater than the adhesion energy of the particle to the rail surface and the separation may then occur by fracture.

This mode of wear occurs most frequently on tangent tracks and curved regions with starved lubrication conditions. The presence of lubricant or contaminants on the rail retards the adhesion process and, while it may not be eliminated, it is not the dominant factor in the overall wear process of a lubricated curved rail.

(ii) Abrasive Wear: As in any sliding surfaces when hard materials, such as adhesive wear particles or uncrushed sand grains, are held between the wheel and rail sliding surfaces these hard particles slide on the rail surface and are able to deform the rail outer surface by plowing as shown in Figure 15.

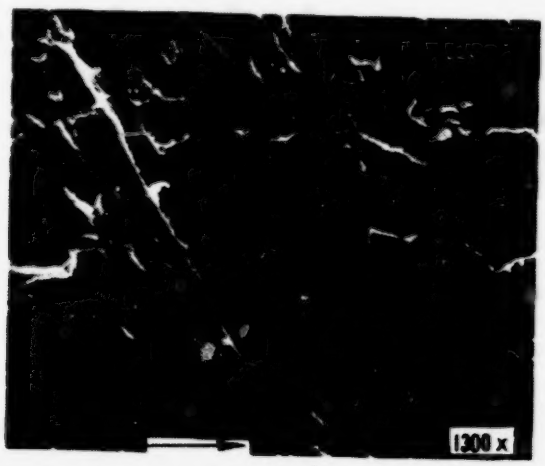

Figure 15 - Rail Surface Topography showing Plowing Marks (arrow indicated direction of travelling)

The accumulation of plastic strain in surface layers during plowing produces singular changes in the microstructure and chemistry of the surface giving rise to subsurface deformation. This process of damaging the surface layers is what permits, on subsequent passages of hard particles, a micro-cutting to take place, generating wear product in a form of chips as shown in Figure 16.

(iii) Surface Fatigue Wear: Is the wear mechanism responsible for the formation of flake-type wear debris. It dominates wear modes in curved regions where the lubrication condition could be sufficient to diminish the role of adhesive or abrasive wear.

Field observations show the dependency of this mechanism upon the degree of deformation on the rail surface. The accumulation of plastic deformation on this surface is a continuous process; the shake-down state as described, for example, in the work of Johnson [20] is not reached during the service life of the rail head. In the work of Ghonem et al [21] it has been shown, based on a microscopic study of dislocation patterns

Figure 16 - Abrasive Wear Product

and microstructure features of deformation in pearlitic rail steel, that the surface layer consists of two distinctive layers. With reference to Figure 17, they are:

- a heavily deformed outer layer with a thickness of 100 μm - 1 mm. This fragmented layer consists of deformed, broken short lamella tightly compressed, and oriented approximately parallel to the surface due to the high service tangential stress. This layer is followed by

- a plastically deformed subsurface layer which, while maintaining the integrity of its lamella structure, deforms in a pattern that coincides with the alternating shear stress. This layer has a depth of 3 - 5 mm, depending on the rail metallurgy.

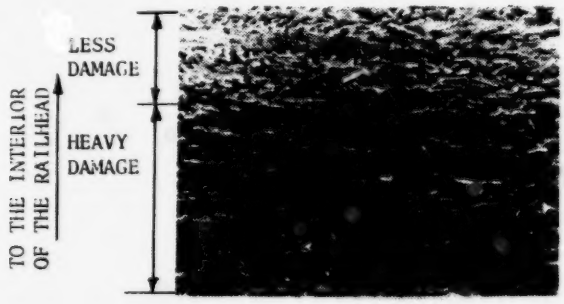

Figure 17 - Deformation Pattern of Surface Layers

It is in this first layer, and in a depth at which the magnitude of the compressive stress is relatively moderate that voids between factured lamella could nucleate and result in the formation of subsurface cracks. Under continuous deformation subsurface cracks can propagate and coalesce in a direction parallel to the rail surface. Upon

reaching a critical length, any of these cracks can become unstable and propagate to the surface producing delaminated sheets. The steps in this mechanism are illustrated in Figure 18.

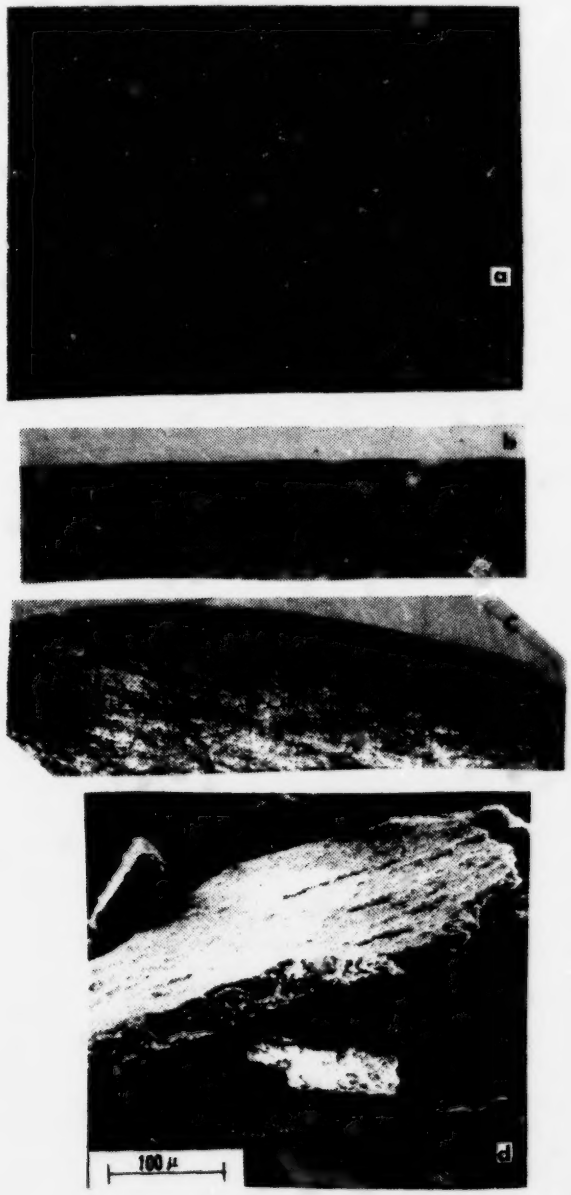

Figure 18 - Steps of Rail Surface Delamination Mechanism

(a) nucleation of voids and microcracks,
(b) propagation of subsurface cracks (500 x),
(c) appearance of subsurface crack prior to fracture (200 x),
(d) delaminated wear particle

An alternate mechanism would feature a crack propagating from the surface inward; the wear particle would be essentially the same in appearance. Field observations show the existence of these two mechanisms; but fail to determine the conditions under which either is favoured. The delaminated regions on high and low rails are shown in Figure 19 and are known in railway terminology as "shelly spots" or "flakes" depending on the size of the wear particle. Here it must be noted that there is a distinction between the terms shells and shelling. Shelling is the removal of a metal portion of the rail head gauge corner as a result of propagation and fracture of a subsurface longitudinal crack. The appearance of shelling and longitudinal crack in the gauge corner of a high rail are shown in Figure 20.

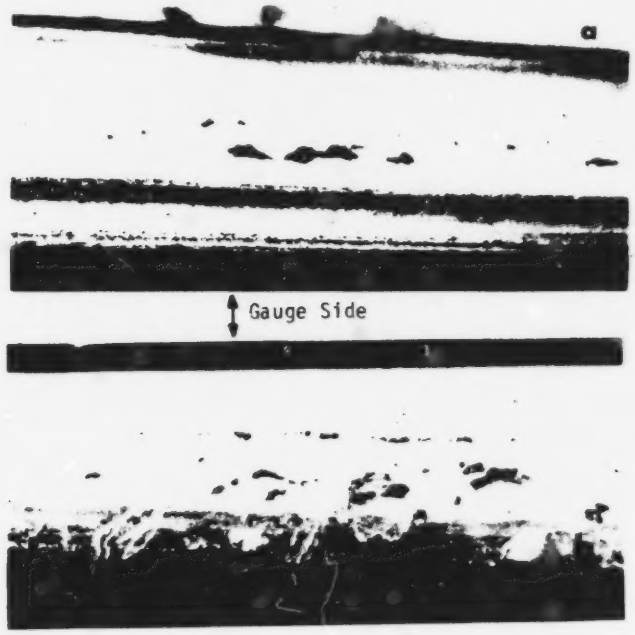

Figure 19 - Appearance of Shells (large laminated areas)
(a) Flakes on High Rail
(b) Low Rail

Hair line cracks associated with the decarburized layer on the rail surface are another form of fatigue surface cracks that could propagate into the rail head causing fracture of that layer into wear particles. This type of particle which, when entrapped into crack cavities undergoing oscillatory tangential displacement result in the production of spherical wear particles shown in Figure 21.

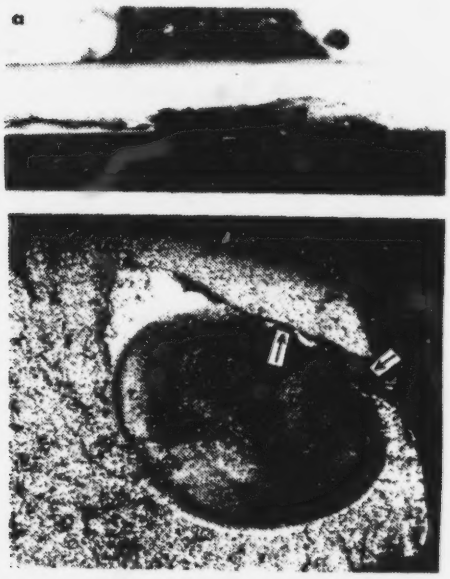

Figure 20 - Appearance of (a) Shelling and (b) Subsurface Longitudinal Crack (identified by arrows)

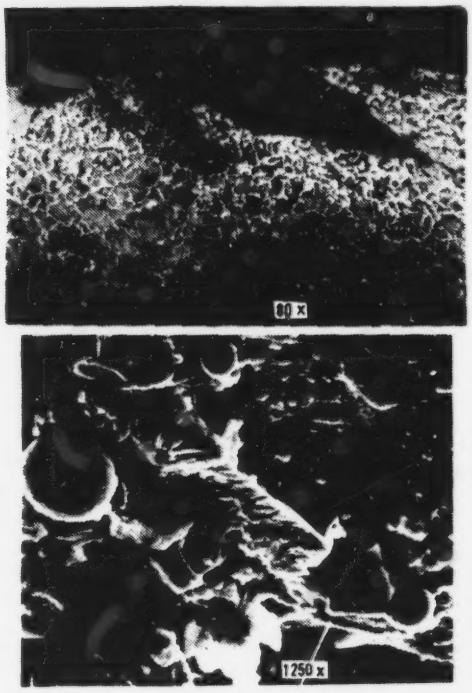

Figure 21 - Hair Line Crack and Spherical Wear Particles

CONCLUSIONS

(1) Wear phenomenon, being an output of the rail-wheel tribosystem, can quantitatively be identified only when its relationships with critical parameters simultaneously acting on the system are established. This complex form of interdependency is the reason for the lack of an acceptable rail wear formula.

(2) In all rail wear mechanisms the separation of wear particles from the surface is completed by successive steps of cyclic loading, plastic deformation and fracture.

ACKNOWLEDGEMENT

This study is part of a joint research program between National Research Council of Canada and the University of Rhode Island and is supported by Transport Canada and the Association of American Railroads.

REFERENCES

[1] KRAUSE, H., "Factor Influencing the Frictional and Wear Behavior of the Wheel/Rail - Systems", *Proc. of the Fifth Int. Wheelset Congress*, Tokyo, Japan, 1975.

[2] JAMISON, W.E., "The Wear of Railroad Freight Car Wheels and Rails", presented at the *34th Annual Meeting* in St. Louis, Missouri, April, 1979.

[3] SILVA, L. and NOBREGA, L., "A Research Trip for the Study of Axle Load", *Proc. of the Heavy Haul Railway Conference*, Perth, Australia, 1978.

[4] BRAMWELL, S. and McELROY, T.F., "Twenty-Five Years of Heavy Axle Load Unit Train Operation on the Quebec North Shore and Labrador Railway", *Proc. of the Heavy Haul Railway Conference*, Perth, Australia, 1978.

[5] STONE, D.H., "Comparison of Rail Behavior with 125-Ton and 100-Ton Cars", *AAR Report No. R-405*, January, 1980.

[6] DEARDEN, J., "The Wear of Steel Rails and Tyres in Railway Service", *Wear*, Vol. 3, 1960.

[7] CURCIO, P., MARICH, S. and NISICH, G., "Performance of High Strength Rails in Track", *Proc. of the Heavy Haul Railway Conference*, Perth, Australia, 1978.

[8] KING, F.E., "Railway Replacement Costs", *Technical Report* by Technical Research and Development, Canadian National Railways, Montreal, Quebec, 1976.

[9] GHONEM, H., GONSALVES, R. and BARTLEY, G., "Comparative Performance of Type II Trucks", *Trans. of the ASME*, 80-RT-8, 1980.

[10] IZBINSKY, G. and PAK, W., "Experimental and AAR Wheel Profile Measurement on a CP Unit Coal Train", *Canadian Pacific Technical Report*, Montreal, Quebec, 1980.

[11] MARCOTTE, P. and MATHEWSON, R., "Wheel Profile Test on Luscar Coal Service Gondolas", *Report No. 125*, Canadian National Railways, Quebec, Montreal, March, 1976.

[12] CALDWELL, W.N., "Contribution of Self Steering Trucks to Wear Reduction: CN Experience", *Int. Symposium on Contact Mechanics and Wear of Rail/Wheel Systems*, Vancouver, Canada, July, 1982.

[13] GILCHRIST, A.O. and BRICKLE, B.V., "A Re-Examination of the Proneness to Derailment of a Railway Wheel-Set", *J. of Engineering Science*, Vol. 18, No. 3, 1976.

[14] BRICKLE, B.V., "The Steady State Forces and Moments on a Railway Wheelset Including Flange Contact Conditions", *Ph. D. Thesis*, Loughborough University, 1973.

[15] GHONEM, H. and KALOUSEK, J., "The Use of Angle-of-Attack Measurements to Estimate Rail Wear under Steady State Rolling Conditions", *Proc. of the Int. Conference on Wheel/Rail Load and Displacement Measurement Technique*, Boston, 1981.

[16] CLAYTON, P., "The Wear Behavior of Pearlitic Steels with Particular Reference to Rails", *Ph. D. Thesis*, Brunel University, 1977.

[17] HELLER, W., "The Development and Further Development of the Quality and Service Properties of Modern Rail Steels", ETR - Eisenbahntechnische Rundschau, February, 1971.

[18] FOWLER, G.J. and TETELMAN, A.S., "The Effect of Grain Boundary Ferrite and their Fatigue Crack Propagation in Pearlitic Rail Steel", *ASTM Symposium on Rail Steels*, Denver, November, 1976.

[19] KALOUSEK, J., "Rail Corrugations", *Technical Report No. S488-75*, Canadian Pacific Limited, Montreal, Quebec, 1975.

[20] JOHNSON, K.L., "A Review of the Theory of Rolling Contact Stresses", *Wear*, Vol. 9, 1966.

COMMENTS

S.T. Lamson, Queen's University, Kingston, Ontario, Canada. Could you please confirm a piece of data in your presentations which shows wear rate of rails *decreases* at high tonnage level? If it does decrease, could you explain *why*, since my experience on heavy haul railways shows the contrary, for both the surface fatigue wear on the rail head and the abrasive/adhesive wear on the rail gauge face.

Authors' Reply. Figure 3 in our paper shows wear rate on tangent track versus axle frequency at low axle loads. The reduction of wear rate is due to the replacement of corrosive wear, prevailing at very low traffic densities and exhibiting high wear rates, by adhesive wear prevailing at medium traffic densities. On main line curves the situation is different; persistent conditions of high traffic densities and loads lead, as you said, to severe adhesive wear (gouging) on gauge face and surface fatigue wear (delamination, flaking, shelly spots) on top running surfaces if these are contaminated by lubricant.

* * *

H. Ghonem
Assoc. Professor
Dept. Mechanical Engr.
Univ. of Rhode Island
Kingston, Rhode Island

J. Kalousek
Assoc. Research Officer
National Research Council of Canada
Vancouver
British Columbia

D.H. Stone
Director: Metallurgy
Assoc. of American Railroads
Chicago, Illinois

E.E. Laufer
Technical University of Nova Scotia
Halifax, Canada

Aspects of Plastic Deformation and Fatigue Damage in Pearlitic Rail Steel

Increased plastic flow of rail material brought about by the introduction of 100 ton and 125 ton capacity cars in the fleets of many North American railroads has become a matter of concern to a large number of railway engineers. This problem is particularly troublesome in curves where the shakedown limit of rail material is reduced due to the presence of curving traction forces in the rail/wheel contact zone. The occurrence of shelly spots, shells and flaking, caused by the fatigue failure of rail material, is always accompanied by plastic flow. In order to establish the manner in which plastic flow affects or is affected by the cracks, two rails, removed from main line curves, were sectioned and examined under Scanning and Transmission Electron Microscopes. Electron Microscope observations of dislocations are correlated to some existing theoretical models of microcrack formation and the directionality of broken pearlite colonies is examined in view of current contact stress and residual stress theories. The field observations were confirmed by laboratory experiments with the accurately known loading histories.

INTRODUCTION

As the world trend shifts toward higher speed, longer and heavily loaded trains, plastic deformation and associated damage, in particular longitudinal and transverse cracks, as shown in Fig. 1, have been viewed as serious problems effecting the rail head operational life.

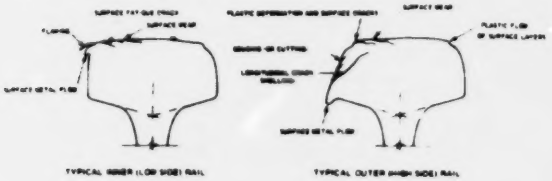

Fig. 1 Plastic deformation and associated damage in the rail head.

Considerable attention has been devoted to studying the degree of rail head deformation during service and its effect on the formation of contact fatigue cracks, changes in mechanical properties and the contact stress field (1-5). Surface topography and local changes in microstructure due to rail head deformation and the effect of metallurgical parameters in promoting subsurface cracks were studied (6-10). Other studies included the description of rail monotonic and cyclic deformation characteristics and their effect on the rail's fatigue resistance (11,12). However, beyond a preliminary study made by Stone and Marich (13), little has been contributed to the relationship between rail plastic deformation and the damage process and the contact stress field or the rail steel microstructure characteristics. This paper is a preliminary attempt to characterize such a relationship and to describe the initiation and propagation of longitudinal cracks based on the rail microstructural response to the externally induced parameters during the deformation process.

PLASTIC DEFORMATION

Introduction

While the microstructure of alloyed rail steel, in the as-rolled conditions, consists of pearlite and ferrite grains, rail steel with a tensile strength of 700-900 N/mm^2 are composed predominantly of pearlite grains with about 25 percent ferrite. Rails with tensile above 900 N/mm^2, which represents the majority of heavy section rails, have a pure pearlitic grain structure. The important variable in the microstructure of pearlite is the distance between its adjacent lamellae. The increase in yield strength and, consequently, resistance to plastic deformation, varies inversely with the interlamellar spacing of the pearlite. The early stages of plastic deformation in the pearlitic rail steel matrix, as in any polycrystalline structure subjected to external stresses, take place within individual grains or, specifically, within lamellae in highly stressed regions. As a result, a dislocation pile up occurs at the ferrite-cementite boundaries. When the density of such a pile-up is accelerated due to the increase in the level of internal stress or the increase in the loading cycles, Frank-Read sources are activated in the lamella interface, emitting dislocation loops which on the one hand neutralize the stress concentration of the original pile-up and, on the other hand, enable the slip to continue across the lamella interface or to the neighbor grain. Such a slipping process will continue with each loading cycle on the rail head causing a microscopic "monotonic" increment in deformation. When such an increment is integrated with respect to time, it results in gross plastic deformation. Another mode

of the deformation may occur when the slipping process alternate in direction causing "alternating" plasticity. Each of these deformation modes depends on the nature of the stress state that activates the dislocation multiplication process in the rail head. Such stresses while depending on the mechanical properties of the rail microstructure are a product of the stress field in the rail/wheel contact zone. Therefore, the knowledge of this stress field would enable us to characterize the mode of plastic deformation in the rail head. This will be briefly discussed in the next section.

Contact Stresses and Associated Deformation

In the rolling/sliding motion between wheel and rail, two forms of forces are transmitted to the contact zone, i.e., the normal force, N, and tangential force F. The latter may result from geometrical constraint, yaw or lateral motion of the wheelset or due to an application of external lateral forces (14). These combined forces acting on the contact zone, the geometry of which could be calculated on the basis of conformal (15,16) or counterformal constraints, produce a stress field whose three dimensional stress tensor component could be computed by using different analytical and numerical techniques (17,18). The important factor in such calculations is to recognize that the octahedral shear, and not the maximum shear component, is what controls the amount of maximum repeated plastic deformation of the stresses matrix, see Lundberg and Palmgren (19) and Greenert (20).

Under free rolling contact conditions, the subsurface octahedral shear reaches equal and opposite peak values on either side of the axis of symmetry of the contact zone. This occurs at point $x_1 = \pm 0.866a$ and $x_3 = -0.5a$ measured from the origin of that zone, where a is its major axis. When tangential force is added to the contact interface, it is found (21) to increase one of the peak values of the octahedral shear and to decrease the other. As the tangential force increases in the contact zone, the maximum subsurface octahedral shear increases in value and its location slowly decreases in depth. At the same time an additional peak of shear stress equal to $T = \mu P^*$, where μ is the coefficient of friction and P is the maximum normal pressure, is introduced on the surface at the center of the contact zone. As is known, the shake down state exists when the amount of energy dissipated in plastic flow never exceeds a finite limit so that purly elastic behavior will occur after a fixed number of load cycles. The work of K. Johnson (22) shows that, when the tangential force exceeds 0.367P, the surface shear exceeds the subsurface octahedral shear so that the shake down is controlled by the surface stress. The coefficient of friction in wheel/rail interaction ranges between 0.2 - 0.25 in a lubricating-dry condition; thus, T does not reach the 0.367P value estimated by K. Johnson. Analytical techniques exist to determine if shake down state is satisfied in structure such as rail head, see for example Ref. (23). Experimental observations indicate however that such state cannot be reached during the service life of the rail head of which the plastic deformation is an accumulative process with time. The question then concerns the depth of the plastically deformed zone and the mode of its deformation. The work of Ravitskaya (24) shows that in carbon rail the depth ranges from 8-15 mm, while in alloyed rail steel it ranges from 3-6 mm. Such depth depends on the wheel load, the microstructure of the rail head matrix and surface and the subsurface strain hardening characteristics of such structure.

As previously explained the mode of deformation in a polycrystalline structure depends on the form of the applied stress. In the deformed zone of the rail head, aside from the compressive stress resulting from the normal force, the stress applied on the surface is basically of a different character than the one acting on the interior. While the surface stress maintains a single direction following the traction force direction, the subsurface octahedral shear is an alternating stress.

In addition, the plastic flow of the subsurface layers being highly constrained in relation to that of the surface layer, these layers also possess different microstructures. The surface layer consists of a fine grain structure with a high degree of preferred orientation while the subsurface layer is a coarse structure with randomly oriented grains. Such differences manifest themselves in the degree of the severity of deformation pattern exhibited, Fig. 2(a). The subsurface, under the effect of alternating shear, deforms in an "alternating" or "zigzag" pattern, shown in Fig. 2(b), while maintaining the integrity of its lamella structure. The surface layer, measured with an 100 μm depth in Fig. 2(a), is a fragmented layer

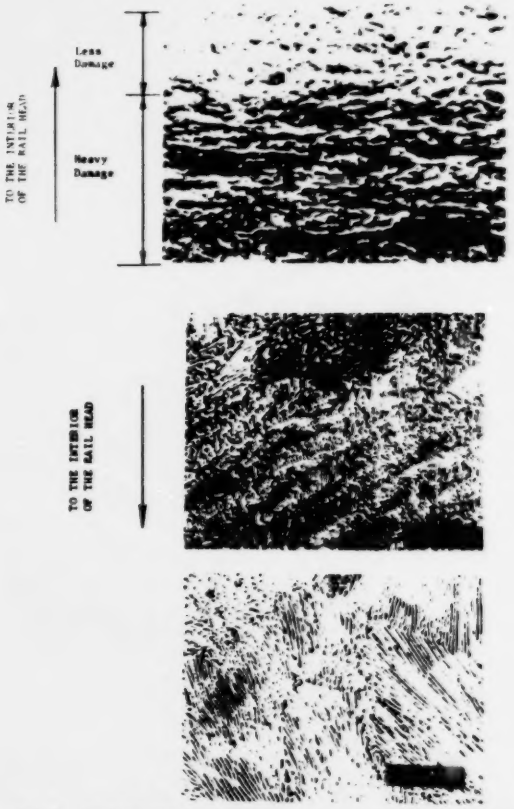

Fig. 2(a) Deformation pattern of the heavily damaged surface layers, (b) Zigzag pattern of deformed lamellae, and (c) Lamellae arrangement in undeformed grains.

*The surface shear traction does not greatly influence the subsurface distribution of strain. The subsurface plastic deformation caused by partial slip is not likely to differ significantly, therefore, from the one of complete slip, see Ref. (22).

consisting of heavily deformed broken "short" lamella. Such a structure has been shown by Rigney (25) to consist of a cellular structure which develops during an initial break-in* period of the rail surface. Indeed, when viewing the dislocation pattern in the two layers discussed, using the Transmission Electron Microscope, one can observe that at a depth of 5 mm from the surface, Fig. 3, the dislocations pile up at the ferrite-cementite boundary with no tangled dislocations in the ferrite region. The density of the tangled dislocations and consequently the cell structure increases while approaching the surface at depths of 1 mm and 500 μm shown in Fig. 3(b) and (c).

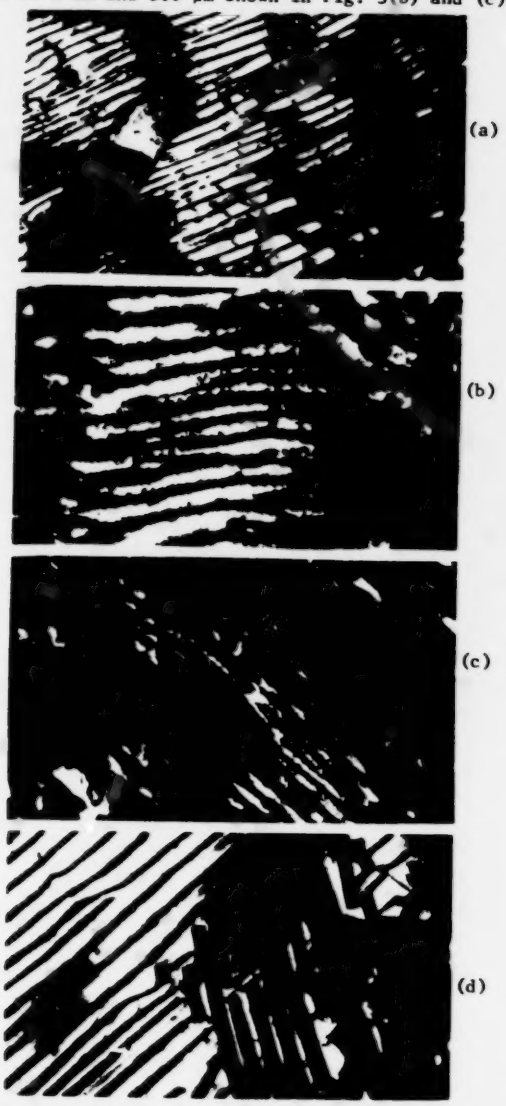

Fig. 3 Dislocation pattern in used rail at depth (a) 5 mm (b) 1 mm (c) 500 μm compared with this of new rail at depth (d) 1 mm.

*Break-in period is where the original microstructure of the surface is gradually changing to a cell structure of accommodating large strains in the sliding direction.

With this argument in mind, it should be recognized that the deformed zone in the rail head consists of two distinctive layers; i.e.:

(i) a heavily deformed surface having a thickness* of 100 μm - 1 mm followed by,

(ii) a plastically deformed subsurface layer with a thickness of 3-5 mm (depending on the rail type).

Behavior analysis of these layers or their mathematical modelling must consequently be treated independently.

While the ability to quantitatively characterize the stress and strain fields in both these two layers is equally important, the work in the following section will concentrate on developing a simple model for estimating the total strain in the surface due to the effect of the surface traction force.

Simplified Model

As described before, the critical factor in quantitatively describing the plastic flow in the outersurface layer of the rail is the surface traction force resulting from wheel/rail sliding. Such force is characterized by parameters such as the magnitude and direction of sliding in the contact zone and the position of this zone on the rail surface. Interdependence of these parameters should initially be discussed as follows:

Contact Zone Postion. In order to establish the position of the contact zone, one should consider an overall spatial orientation between a wheelset and track rather than limit such analysis to a single wheel and rail. In the case of a tangent track a wheelset is kept at the center of the track by gravitational forces. It contacts the rails at two points which are approximately symmetrical with respect to the center of the track or the wheelset. In curves, however, the situation is more complex. A wheelset may contact the rail at either two or three points, depending on its angular alignment and lateral displacement. These two variables, yaw misalignment (also referred to as skew angle or angle of attack) and lateral displacement, are interrelated. However, angle of attack is considered an independent variable.

The angle of attack may vary randomly in any given population of wheelsets in ranges from -20' to about +60' depending on the degree of curvature, location of the wheelset in a freight car and other variables affected by track irregularities. Field measurements (28) have shown that angle of attack is highest on the leading axle of a leading truck (LL) and in the vicinity of zero to slightly negative for a trailing axle on a trailing truck (TT). For example, the mean values measured in five degree curves were as follows: $\alpha_{LL} = 28'$; $\alpha_{TL} = 10'$; $\alpha_{LT} = 24'$; and $\alpha_{TT} = 5'$ (L:Leading, T:Trailing). Although lateral displacements were not measured during these tests, it has been analytically well established that with an increase in the angle of attack the wheelset displaces laterally until flange contact is established at the

*In the work of Rigney and Hirth (26) it is shown that the thickness, t, of the highly deformed layer would vary with load by some power less than unity. Tsuya (27) has estimated that the thickness for such layer (for copper) equals L^n where $n = \frac{1}{2}$.

range of α = 8' - 14'. A value of 8' is typical of a dry rail and an upper limit value of 14' is typical of a fully lubricated rail.

Since this paper is concerned with plastic flow being experienced by the outer or high rail in curves, let us analyze more closely the possible situation which may occur at this location. The left side of Fig. 4 shows three examples of contact between worn wheels and worn high rails. Case I shows a contact ellipse typical of interaction between trailing

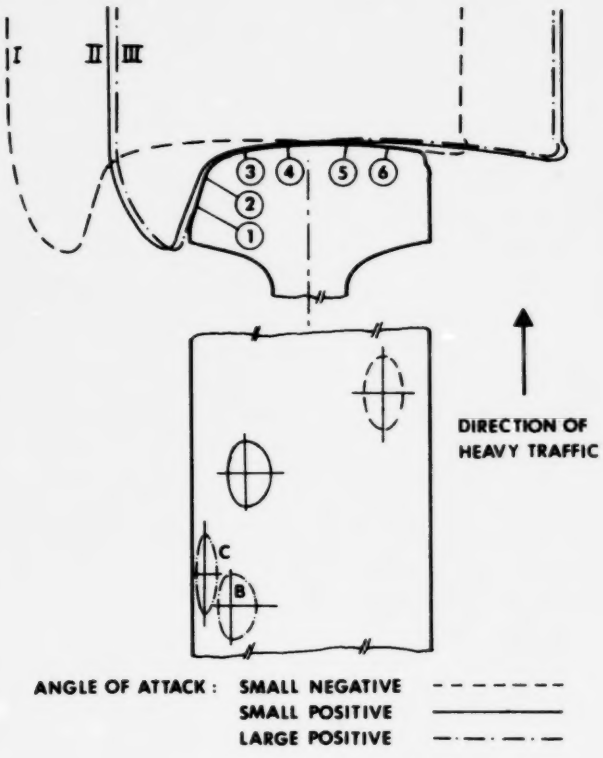

experimentally on rail or wheel surfaces. The right side of Fig. 4 shows the micrographs at six locations of the rail surface taken from an eight degree curve. Locations 1 and 2 are from the flange contact while the other four are from the tread contact. The largest amount of sliding appears at the flange contact and a trajectory of wheel asperity rubbing rail takes on a shape of extended cycloid. Therefore, if the wheel flange contacts the upper half of the gauge side of the rail, the rubbing trajectory will exhibit a large downward component. However, if the contact zone is

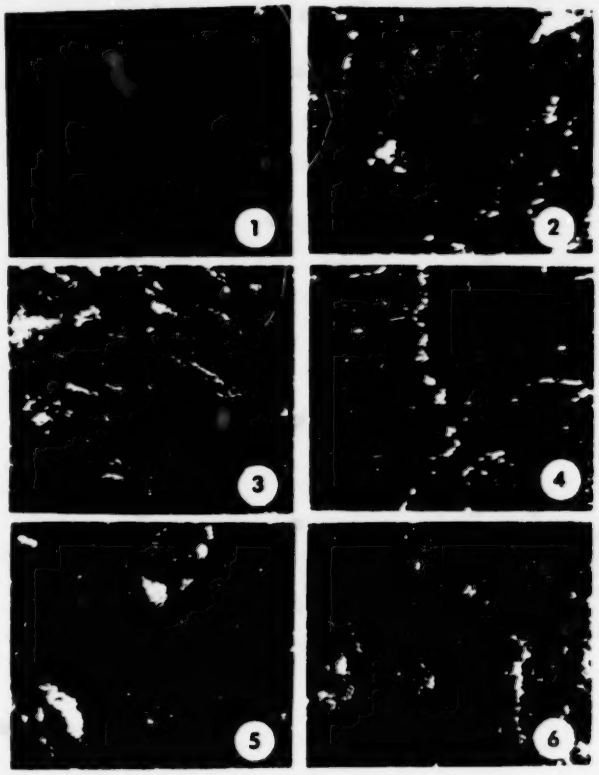

Fig. 4 Surface characteristics of contact position on the rail head.

wheelsets of trailing trucks and high rails. Both, angle of attack and lateral displacement, are slightly negative, bringing a flange of low wheels very close to the gauge corner of the low rail. Case II is typical of wheelsets with a small positive angle of attack in which hard flanging is absent and both vertical and lateral load components are supported by one contact ellipse having high conicity with respect to track center line. Case III is typical of large angles of attack where a third point of contact between a pair of rails and wheelsets is firmly established. This situation is referred to as hard flanging. As a rule, a flange contact C is located forward of tread contact B. Thus, knowledge of angle of attack, lateral displacement and tread profiles of wheels and rails has helped us establish the locality and shape of contact ellipses. These same misalignments, however, are responsible for the presence of sliding within the zone of contact during the wheelset's negotiation of curves.

Surface Tractions. The length and direction of sliding within the zone of contact could be observed located at the lower half of the gauge side of the rail, the rubbing marks will have a large longitudinal component. Wheelsets contacting the tread of the high rail with a positive angle of attack will produce surface tractions with appreciable lateral components. In fact, these tractions are almost perpendicular to the direction of travel of wheels in the case of large angles of attack.

These tractions produce significant shear stresses in the surface layer(s) of rail material causing plastic deformation and flow towards the gauge side the high rail. The fact that at Location 6 the rail material is pushed towards the field side of the rail can be attributed to a negative angle of attack which not only brings the wheelsets into contact at this location but also produces tractions with appreciable lateral components pointing in the opposite direction from tractions at Locations 3 to 5. Since these tractions have lateral and longitudinal, as well as spin components, the underlying plastic flow also appears to be in the direction of the resultant of these components, as shown in Fig. 5. This figure

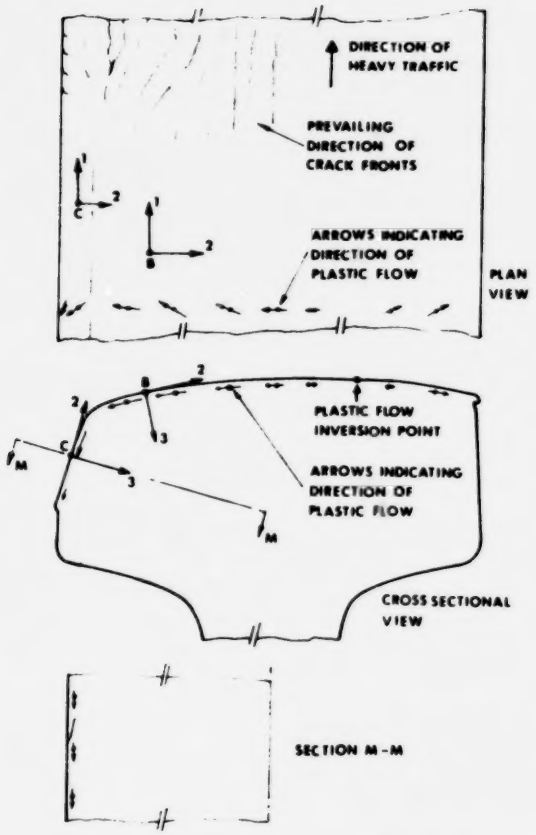
DIRECTION OF HEAVY TRAFFIC
PREVAILING DIRECTION OF CRACK FRONTS
ARROWS INDICATING DIRECTION OF PLASTIC FLOW
PLAN VIEW
PLASTIC FLOW INVERSION POINT
ARROWS INDICATING DIRECTION OF PLASTIC FLOW
CROSS SECTIONAL VIEW
SECTION M-M

Fig. 5 Configuration of surface tractions on the rail head.

also depicts the prevailing direction of surface microcracks which are, not surprisingly, perpendicular to the direction of surface tractions.

While the surface tractions and direction of plastic flow have been discussed on the basis of experimental observations, the direction and magnitude of these tractions and, therefore, the amount of slippage in the contact zone, could analytically be calculated by using, for example, a theory of Kalker's (29). A detailed analysis of such calculations is presented in Ref. (30).

Now, having characterized the surface traction, the rail surface would be assumed to have the following features during the deformation process: 1. The average surface roughness and asperities would stabilize after the passage of the first few cycles and thus the magnitude of the coefficient of friction is a constant. 2. The extent of wheel material transfer to the rail surface would be extremely limited due to the hardening and the cold working effect of the surface. Furthermore, the work function of this surface would be in a level that produces a minimal reaction to the external environment; therefore no chemistry or phase change would occur during the deformation process. When envoking these conditions, a steady state of plastic deformation is assumed to occur in the rail surface and the magnitude of strain in this surface is the same for each cycle or wheel passage.

As mentioned before, the integral amount of slippage within the area of contact can mathematically be calculated. If this amount is δa, the frictional work done in the zone of contact can then be estimated as:

$$W = F\delta a$$

$$= \mu N \delta a$$

Furthermore, the plastic work per unit volume in the area of contact could be calculated as the product of the flow stress, τ_f, in the sliding direction and the average net strain, ε_t, per cycle in the severely deformed layer. It is shown by Rigney and Hirth (26) that both τ_f and ε_t depend on the depth, d, of this layer.

The plastic work could then be written as:

$$W_p = \tau_f \, \varepsilon_t \, d \, \delta b \, \delta a$$

where δb is the width of the plastically deformed zone. It should be noted here that both δa and δb are independent of the geometry of the contact area but depend on the normal pressure distribution in such an area. Under steady state conditions which are assumed to exist, the plastic work is equal to frictional work, therefore:

$$\tau_f \, \varepsilon_t \, d \, \delta b \, \delta a = \mu \, N \, \delta a$$

which could be written as:

$$\varepsilon_t = \frac{\mu \, N}{d \delta b} \, \tau_f^{-1}$$

The flow stress τ_f for a constant value of ε_t in pearlitic structure could be approximated by:

$$\tau_f = \tau_o + K \, \ell^{-0.5}$$

where τ_o is the average frictional stress and K is the Hall-Petch slope. For pearlitic structure, these two constants are estimated as:

$$\tau_o = 76.4 \text{ MPa} ;$$

and $K = 0.5 - 0.68 \text{ MN/m}^{3/2}$

Furthermore, in the previous equation ℓ is generally considered the interlamella spacing or the average grain size. In the present analysis, however, the grain boundary and most of the bulk features are totally obliterated in the surface layer. ℓ is then taken here as an average of the cell size in the deformed surface layer.

Equation can be written, therefore, as:

$$\varepsilon_t = \frac{\mu \, N}{d \delta b} \left(\tau_o + (K/\sqrt{\ell})\right)^{-1} / \text{cycle}$$

This equation expresses the average net strain/cycle as a function of parameters that represent the load criterion on the rail surface and parameters that represent the microstructure properties of the rail material. This expression, however, suffers a major problem: in order to determine its validity, surface strain for each loading cycle in the direction of the metal flow should experimentally be measured. An X-ray diffraction method or a chemical marker technique could be used, together with Auger analysis, to measure

the variation of gross strain with depth in the near-surface region. Such experimental verification of the previous equation is part of the author's current research activities.

RAIL HEAD DAMAGE

Rail head damage is a term that covers a wide scope of defects which results from the severe conditions of wheel/rail loading and lead either to the fracture of the head section or to the early removal of the rail from service. Of the defects that have been identified and classified in several articles (31,32), the combination of subsurface longitudinal and transverse crack has been the focus of studies in the past decade (33-35). The important characteristic of such cracks is that they initiate and propagate to their critical length without surface exposure. It is estimated that they are responsible for a high percentage (90% in some cases (35)) of failure in heavy haul lines. A general view of their appearance in the head cross section is shown in Fig. 6.

In this section of the paper a model is developed to explain the initiation and propagation processes of the longitudinal crack.

The Longitudinal Crack

As described in the excellent work of Marich (33), the longitudinal crack is the crack which runs horizontally along under the inside gage corner of the high rail head at curved regions of a track. Its path as shown in Fig. 7 is inclined at an angle between 30°-60° to the vertical plane with a depth range of 3-12 mm measured from the running surface depending on the rail steel type. As this crack propagates longitudinally and laterally inside the rail, it culminates in the removal of a thick portion of the surface metal at the gage corner as illustrated in Fig. 8. This phenomenon, commonly referred to as heavy or light shelling, depending on the severity of the damage, could occur as an isolated incident on the rail curve or at several locations on the same rail length, see Fig. 9.

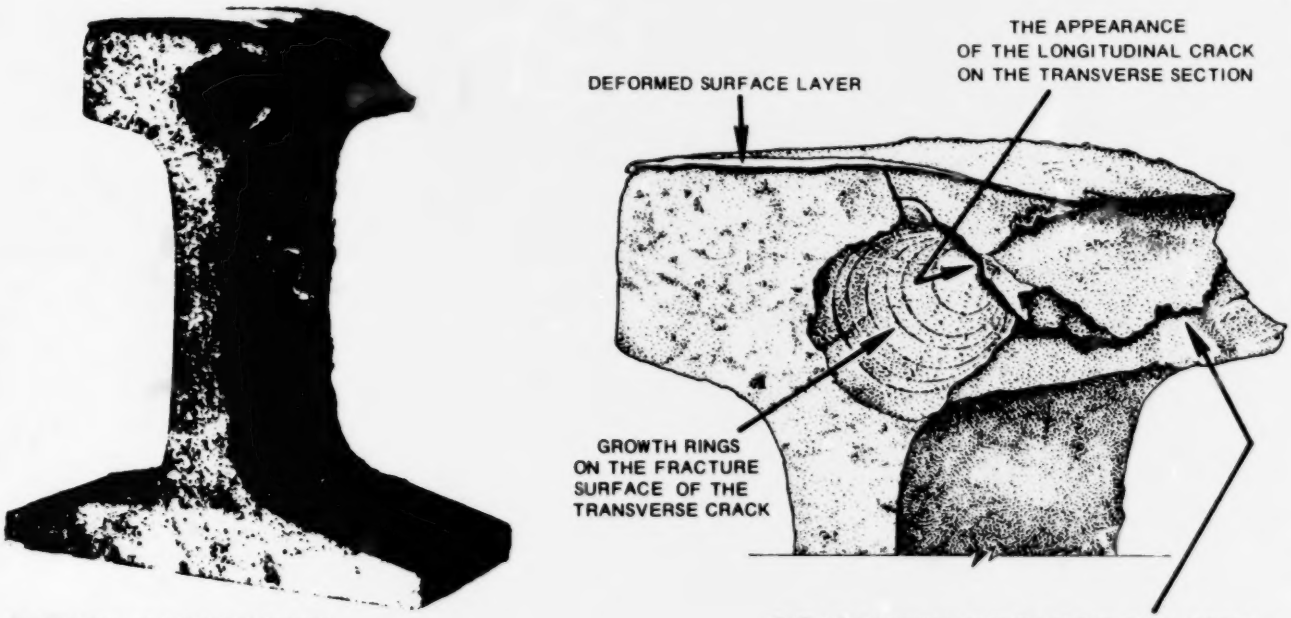

Fig. 6 General view of longitudinal transverse cracks.

It has been established that in this crack combination the longitudinal crack is formed initially and that a transverse crack is subsequently created at a location on the interface of the longitudinal crack (24).

In this concept, assuming that the general rules of the fatigue damage process apply, the fracture surface of the longitudinal crack acts as a free surface on which the transverse defect is initiated. The initiation mechanism of the longitudinal crack, however, is the least understood since it is assumed to take place in the deep layer of the rail matrix.

Models describing the initiation mechanism of this crack (33) have been proposed on the assumption that locations of random inclusions or phase transformed regions in the rail head can act as initiation sites. Keeping in mind that specimens examined in so some of these studies were manufactured a decade ago, the increase of rail steel matrix cleanliness as a result of development in steel making and rolling processes did not reduce the appearance of such cracks or alter their geometrical appearance in the rail head. Microscopic examinations, in fact, showed that longitudinal cracks can exist in regions of the rail head that are free of traces of inclusions or severe

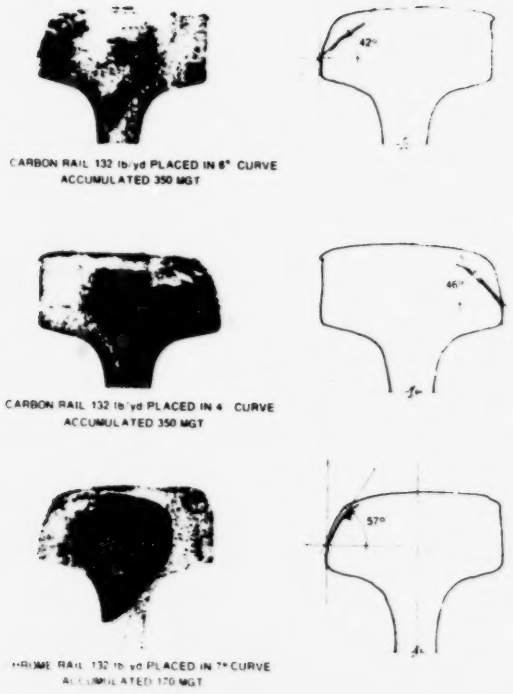
42°
CARBON RAIL 132 lb/yd PLACED IN 6° CURVE
ACCUMULATED 350 MGT
46°
CARBON RAIL 132 lb/yd PLACED IN 4° CURVE
ACCUMULATED 350 MGT
57°
CHROME RAIL 132 lb/yd PLACED IN 7° CURVE
ACCUMULATED 170 MGT

Fig. 7 Geometry of the longitudinal crack in the rail head.

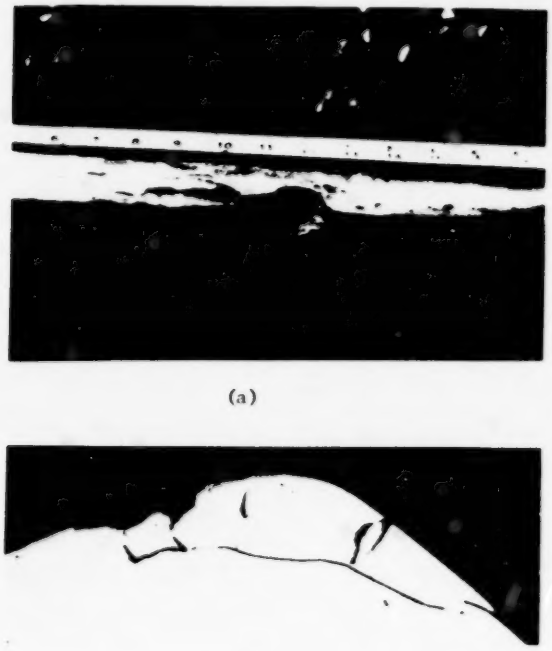

(a)

(b)

Fig. 8 Appearance of shelling; (a) surface, (b) transverse.

Fig. 9 Multiple "light" shelling on a rail length.

impurities. Such observations are consistent with the general laws of fatigue processes, one of which states that the internal fatigue cracks occur under favorable conditions in the presence of a free surface (the inclusion/matrix interface could be viewed as a free surface). It becomes reasonable then to assume that in addition to the hypothesis of inclusion, other mechanisms that include the effect of stress field and rail microstructure parameters should exist for the initiation of longitudinal cracks. In this section, a model for such mechanisms is introduced.

Initiation Mechanism

In the first part of this paper, it was shown that the outer surface layer of the rail head will experience an incremental undirectional plastic flow that continues during the operational life of the rail. As the metal flow advances along the gage corner of the rail, it terminates in a form of displaced layers accumulating along the corner. The edge of each of these displaced layers will either interact with a previous layer, having a different magnitude of deformation or with an elastic matrix that did not suffer deformation. Such interaction was observed to generate a number of surface intrusions as shown in Fig. 10.

As the rail head gage corner conforms to the wheel profile contour, the wheel/rail contact zone, in hard flanging positions, could include regions of the gage side as low as position 1 in Fig. 8. The tangential surface stresses acting in this zone create a large tensile stress in the area of its rear boundary (36). If any of the surface intrusions previously described fall into this area, it is highly probable that the cyclic repetition of this tensile stress results in such an intrusion opening into the rail matrix, see Fig. 11. Simulated work using a laboratory wheel/rail wear rig confirmed that such surface crack initiation mechanism exists.

The number of wheel cycles, N_i, necessary for this initiation process to be completed, i.e., for the surface intrusion to reach the threshold length a_{th},

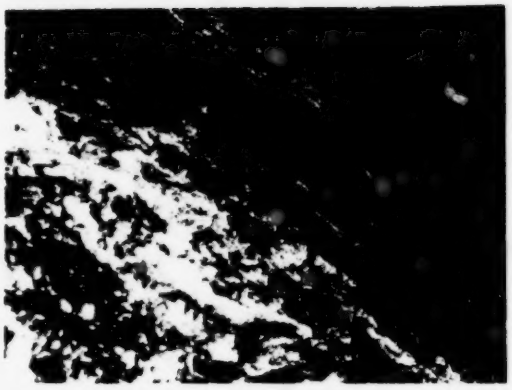

Fig. 10 Surface intrusion on the gauge side of a rail.

Fig. 11 Development of a surface into a surface crack.

can be calculated from the knowledge of the magnitude of tensile stress in the rear boundary of the contact zone, the hardening characteristics of the rail surface. a_{th} which can be evaluated by calculating the threshold stress intensity factor, K_{th}, for pearlitic rail steel. Analytical models for calculating N_i exist; they will not be detailed in this paper, see Refs. (37,38).

As the crack develops inside the rail head, it enters a plastically deformed region. The orientation of the crack propagation plane or plateau within this zone is governed, in addition to the active shear stress component, by the magnitude and orientation of residual stresses and hardening characteristics of the matrix in this zone.

Residual stresses and hardness values were measured in the corner gauge of an unfailed portion of a rail that had developed a longitudinal crack. Fig. 12 shows hardness contours connecting points of equal hardness in the deformed gauge corner. Each of the

Fig. 12 Hardness contours in the gauge corner.

contours separates a layer (or layers) of different deformation or hardening level and Figs. 13 and 14* indicate the pattern of radial and transverse stresses in this region. While radial stresses, below 3 mm of the running surface of the rail, are in a form of tensile stress,** thus aiding a crack to propagate in a direction parallel to the surface of the rail head corner, all other stresses, Fig. 14, are in compression, preventing any crack from propagating in a perpendicular direction to the rail surface or from linking with the heavily deformed layer of this surface.

The optimum path for a crack's propagation is, therefore, a plane of uniform hardening (parallel to the gauge corner) subjected to tensile residual stresses and passing through the transitional region between a plastically deformed structure and elastic material. This region has been shown by Marich et al. (13) to be, in fact, work softened. The geometry of this path is similar to what observed in the large portion of failing rail cross sections.

In the model described above the propagation process is achieved through combined propagation modes; Mode I governed by the influence of the tensile radial residual stresses and Mode II (in-plane shear) due to the shear stress component of the externally applied wheel/rail contact stresses. In this latter mode of propagation, the fracture surface is subjected to a fretting fatigue process that leads to the appearance of spherical particles as shown in Fig. 16.

The effective stress intensity factor, therefore, as reported by Shah (39) and utilized by Marich (33), is the sum of the stress intensity factor associated with each mode, i.e.,

$$K_{ef} = K_I + K_{II}$$

$$= 2\sigma \sqrt{a_{th}\pi} + 0.8\ \tau \sqrt{a_{th}\pi}$$

*Mitchell, C.M. and Laufer, E.E., AIME Meeting, Las Vegas, 1980.

**Radial residual stresses of an average of 200 MPa, shown in Fig. 13 could actually be capable of opening grain boundaries inside the microstructure. These openings could act as crack initiation sites. Such phenomenon is observed to occur in the rail head, see Fig. 15.

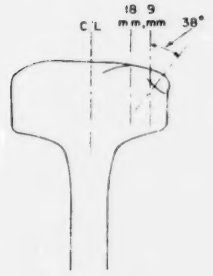

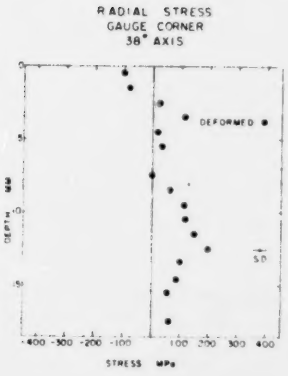

Fig. 13 Radial residual stress pattern in the gauge corner.

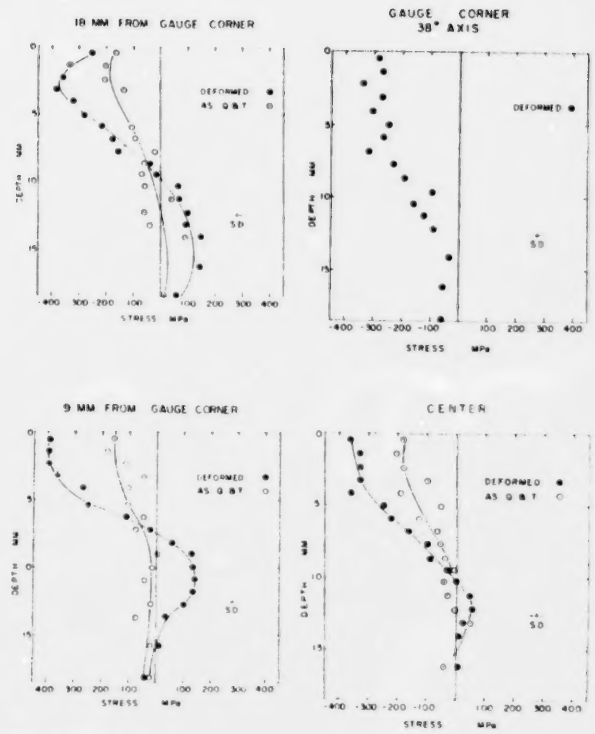

Fig. 14 Transverse residual stress pattern.

Fig. 15 Grain boundary openings on the fracture surface 11,000x.

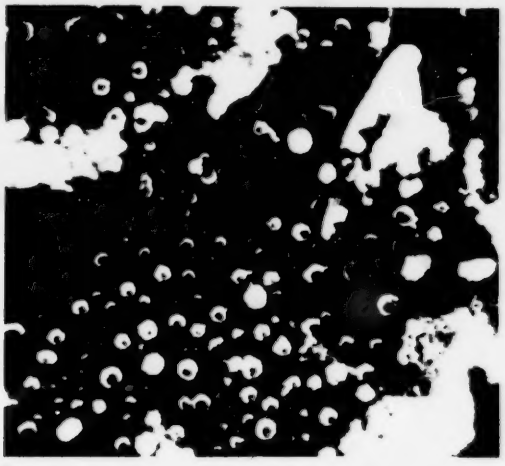

Fig. 16 Spherical particles on the fracture surface of the longitudinal crack 1,000x.

where K_{ef} is taken to be the maximum threshold stress intensity factor determined by Broek and Rice (40) and utilized by Marich. It equals 14.8 MPa$\sqrt{m}$ for fully eutectoid steel.

a_{th} is the threshold crack length, i.e., the minimum length of a crack which will lead to

fatigue crack propagation.

τ is the shear stress component along the fracture surface = 530 MPa (33).

σ is the tensile residual stresses (the effect of thermal contraction of the rail and vertical and bending are negligible) σ is taken as 200 MPa, see Fig. 13.

From the above equation a_{th} is shown to be 300 μm. This value is much larger than the diameter of a typical inclusion or inclusion/matrix diameter of any cluster of inclusion which are normally observed in the rail head microstructure. It has to be acknowledged, however, that inclusions larger than 300 μm - although not typical - exist in the rail head and could lead to the appearance of internal cracks.

CONCLUSIONS

1. The deformed zone in the rail head consist of two distinct layers, I, a heavily deformed surface having a thickness of 100 μm - 1 mm followed by, II, a plastically deformed subsurface layer with a thickness of 3-5 mm depending on the rail type.

2. A new model is proposed to explain the phenomenon of initiation of a longitudinal crack in the rail head. In this model service intrusions on the gage face of the high rail are considered the initiation sites of these cracks.

REFERENCES

1. Tamazaki, T. and Sugiyama, T., "Experiments on Horizontal Crack Propagation in Rail Head," Quarterly Report, Railway Tech. Res. Inst., Vol. 22, 1981.

2. Akaoka, J. and Hirasawa, K., "Fatigue Phenomenon under Rolling Contact Accompanied with Sliding," Bulletin of JSME, Vol. 2, 1959.

3. Allmen, N.J., "The Effect of the Ratio of Wheel Diameter to Wheel Load on Extent of Rail Damage," Proc. 45th Conv. AREA, Vol. 47, 1946.

4. Toth, L. "Fatigue-Wear Testing of Rails Under Rolling Load," Acta Tech. Acad. Sci. Hung., 70: 445, 1971.

5. Marich, S., "Research on Rail Metallurgy," AREA Bulletin 78, 1977.

6. Fastenrath, F., ed. "Railroad Track, Theory and Practice," Frederick Ungar Pub. Co., N.T., 1977.

7. Park, Y.J. and Bernstein, I.M., "Effective Grain Size for Cleavage Fracture in Pearlitic Eutectoid Steel," Int. Fracture, Waterloo, Canada, 1974.

8. Parsons, D.E., "Chemical Composition and Impact Transition Temperature of Carbon and Alloy Rail Steels (1951-1977)," CANMET, Report MRP/PMRL 77-4(R), 1977.

9. Marich, S., "Development of Improved Rail and Wheel Materials," Proc. of Seminar on Vanadium in Rail Steels, Chicago, Nov., 1979.

10. Leis, B.N. and Laflen, J.H., "Cyclic Inelastic Deformation and Fatigue Resistance of Rail Steels-Experimental Results and Mathematical Models," DOT-TSC-1076, 1977.

11. Leis, B.N., "Cyclic Inelastic Deformation and Fatigue Resistance Characteristics of a Rail Steel," ASTM, STP 644, 1976.

12. Stone, D.H. and Steele, R.K., "The Effect of Mechanical Properties Upon the Performance of Railroad Rails," ASTM, STP 644, 1976.

13. Stone, D.H. and Marich, S., "Deformation Behavior of Rail Steels," Transportation Research Record 744.

14. Brickle, B.V., "The Steady State Forces and Moments on a Railway Wheelset Including Flange Contact Conditions," Ph.D thesis, The Loughborough University, 1973.

15. Paul, B. and Hashemi, J., "An Improved Numerical Method for Counterformal Contact Stress Problem," Department of Transportation, Report No. FRA-ORD-78-26, 1977.

16. Hashemi, J. and Paul, B., "Contact Stresses on Bodies with Arbitrary Geometry, Application to Wheels and Rails," Department of Transportation, Report No. FRA-ORD-79-23, 1979.

17. Johnson, K.L. and Jefferis, J.A., "Plastic Flow and Residual Stresses in Rolling and Sliding Contact," Proc. Symp. Fatigue in Rolling Contact, London, 1963.

18. Martin, G.C. and Hay, W.W., "The Influence of Wheel-Rail Contact Forces on the Formation of Rail Shell," University of Illinois, 1970.

19. Lundberg, G. and Palmgren, A., "The Dynamic Capacity of Roller Bearings," Acta Polyt., Stockholm, No. 7, 1947.

20. Greenert, W.J., "The Toroid Contact Roller Test as Applied to the Study of Bearing Materials," J. Basic Engng., Trans. Amer. Soc. Mech. Engrs., 84, 1962.

21. Smith, J.O. and Liu, C.K., "Stresses Due to Tangential and Normal Loads on An Elastic Solid with Application to Some Contact Stress Problems," ASME, J. of Applied Mechanics, Trans. ASME, 75, 1953.

22. Merwin, J.E. and Johnson, K.L., "An Analysis of Plastic Deformation in Rolling Contact," Proc. Inst. Mech. Engrs., 177, No. 25, 1963.

23. Hodge, Jr., P.G., "Plastic Analysis of Structure," McGraw-Hill, N.T., 1959.

24. Ravitskaya, T.M., "Features of the Initiation and Development of Internal Fatigue Cracks Considered on the Examples of Rail Failure," Problemy Prochnosti, No. 11, 1974.

25. Rigney, D.A., and Glasser, W.A., "The Significance of Near Surface Microstructure in the Wear Process," Wear, 46, 1978.

26. Rigney, D.A. and Hirth, J.P., "Plastic Deformation and Sliding Friction of Metals," Wear, 53, 1979.

27. Tsuya, T., "Microstructures of Wear, Friction and Solid Lubrication," Tech. Rep. No. 81, Mech. Eng. Lab., Igusa Suginami-Ku, Tokyo, 1976.

28. Ghonem, H., Gonsalues, R. and Bartley, G., "Comparative Performance of Type II and Premium Trucks," Trans. of ASME, 80-RT-8, 1980.

29. Kalker, J.J., "Rolling with Slip and Spin in the Presence of Dry Friction," Wear, 1966.

30. Kalousek, J., Rosval, G. and Ghonem, H., "Lateral Creepage and Its Effect on Wear in Rail/Wheel Interfaces," Proc. of Int. Symp. on Contact Mechanics and Wear of Rail Wheel Systems, University of Waterloo, Canada, 1982.

31. Schoeneberg, K.W., "Rail and Research - Problem Definition," Association of American Railroads, Tech. Report No. R-120, 1973.

32. Monaghan, B.M., "Rail Life Study and Recommendations," Quebec North Shore and Labrader Railway, Quebec, 1961.

33. Marich, S., Cottam, J.W. and Curcio, P., "Laboratory Investigation of Transverse Defects in Rails," Heavy Haul Railway Conference, Perth, Austra Australia, 1978.

34. Ito, A. and Kurihara, R., "Shelling of Rails Experienced in Japanese Railways," Bulletin of Permanent Way Soc. of Japan, Vol. 13, 1965.

35. Skinner, D.H. and Judd, P.A., "A Metallurgical Study of Fatigue Defects in Rails," Aust. Inst. Mining, 34th Annual Conference, Queenland, 1981.

36. Masumoto, H., et al, "Some Features and Metallurgical Considerations of Surface Defects in Rail Due to Contact Fatigue," STP 644, 1978.

37. Ghonem, H. and Provan, J.W., "Micromechanics Theory of Fatigue Crack Initiation and Propagation," Int. J. of Fracture Mechanics, Vol. 13, No. 4, 1981.

38. Ghonem, H., "Longitudinal and Transverse Cracks in the Rail Head," Proc. of CANCAM, Vol. 1, 1981.

39. Shah, R.G., "Fracture under Combined Modes in 4340 Steel," ASTM STP 560, 1974.

40. Broek, D. and Rice, R.G., "Fatigue Crack Growth Properties of Rail Steels," Battelle, Report No. DOT-TSC-1076, 1977.

Proceedings

RAIL & WHEEL LUBRICATION SYMPOSIUM

DECEMBER 1-2, 1981 PEABODY HOTEL, MEMPHIS

"THE LUBRICATION SOLUTION"

Lubrication: Its Various Types and Effects On Rail/Wheel Forces and Wear

*by Dr. Joseph Kalousek**

Thank you, Mr. Glavin. I would also like to thank and express my appreciation to the organizing committee for bringing about this symposium. We have had symposia on rail metallurgy, vehicle dynamics, wheelsets and other subjects, but never on lubrication. In view of its significance, I am happy such a thing has happened.

Let me start with a little bit of history and go back into that time in railroading which even precedes the time in which Claude Monnett painted the Old St. Lazare Station (Exhibit 1). One of the big concerns of the first railway engineers was adhesion. They were afraid that the trains would not be able to climb the slightest hill because of lack of traction. For this reason the early locomotive designs provided for a pinion wheel on a driving wheelset which engaged into the rack rail located in the centre of the track. They didn't realize that on rail and wheel surfaces there are little protrusions called asperities, which under the load come into a contact. If a slippage is applied to the zone of contact these asperities move over each other and are able to transmit a substantial traction force.

A hundred and fifty years later, we tend to fall into the opposite pit. We believe the asperities are always in contact and underestimate the presence of intermediate matter in rail/wheel interface (Exhibit 2). It forms a third body which is as significant, from the point of view of traction forces and wear, as wheel and rail. It also significantly affects the steering behaviour of car and locomotive trucks.

Since the intermediate matter received insufficient attention in the past, I will try to correct this situation and will devote the first half of my presentation to the description of its composition and properties. In the second half, I will try to correlate how the lubrication affects lateral forces and wear in curves.

Depending on the amount and viscosity of the intermediate matter

* *National Research Council, Canada.*

and the surface roughnesses the rail wheel interface can sustain an elasto-hydrodynamic lubrication. If the surface roughnesses are very very large or the contamination is inadequate we can get boundary lubrication. If there is no intermediate matter present, meaning the surface is absolutely clean and therefore not lubricated, the term "dry" lubrication is colloquially used to describe this very rare situation. This situation occasionally occurs in curves within the zone of flange contact and is characterized by severe form of adhesive wear referred to as gouging.

2.0 BODY 3: THE INTERMEDIATE MATTER

To make this presentation about intermediate matter easier, I have divided it into four groups (Exhibit 3). The first two groups typically occur in the laboratory. The other two groups deal with the field lubrication. The only difference in the latter two is that in one case the lubricant is introduced deliberately and in the other it sneaks in unintentionally. It should be noted that an important lubricating agent in the field is water, which is introduced in the form of adsorption, dew, rain or snow.

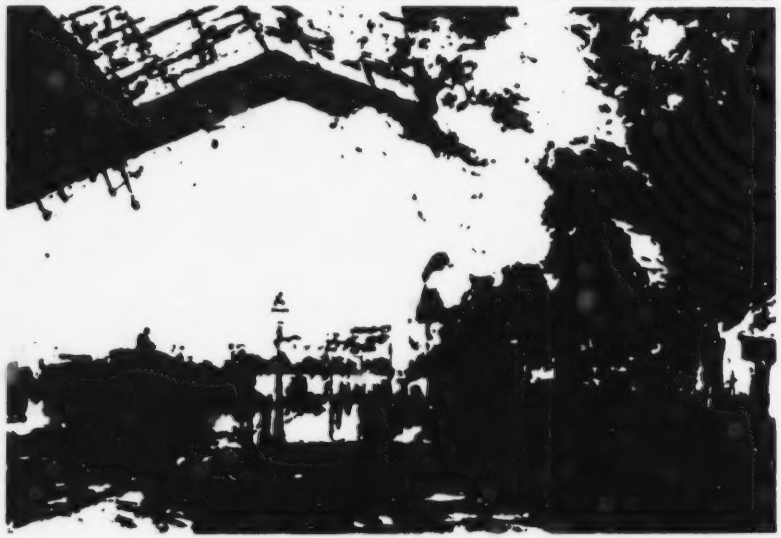

EXHIBIT 1

"Old St. Lazare Station" by Claude Monet
(Courtesy of the Art Institute of Chicago)

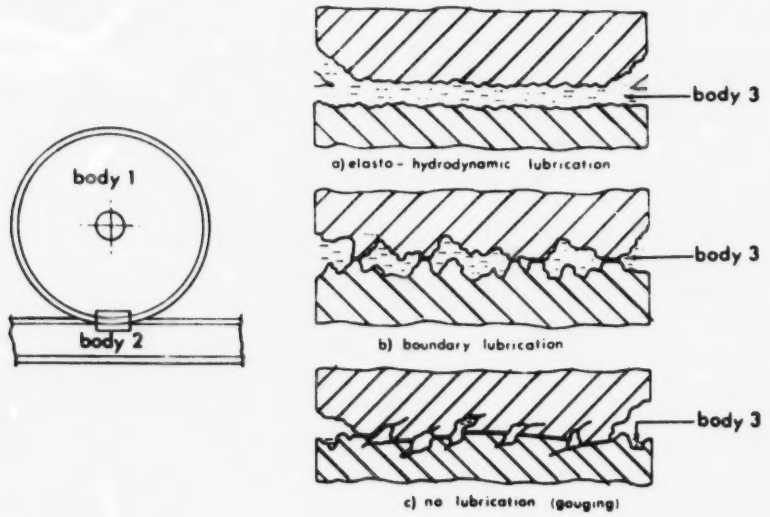

RAIL - WHEEL TRIBOSYSTEM

EXHIBIT 2

2.1 *Lubrication by oxidized wear debris* (*Exhibit* 4).

The wear debris generated in the laboratory experiments does not resemble rust. If this debris is smeared on a white sheet of paper, it has the consistency of black paste. It contains a multitude of oxides and the individual particles are 5 to 20 μm in size. These particles can lubricate in a similar manner as solid lubricants and bring the coefficient of friction into the range of .2 to .3. If the surfaces were kept absolutely clean, the coefficient of friction would be around .6 to .7.

There are two schools of thought which attempt to explain lubricity of wear debris. One is based on the fact that these particles have a tremendous surface area (in the range of 20 to 40 m^2 g) which is able to adsorb contaminants (Exhibit 5). The typical thickness of these particles ranges from 5 to 15 μm. Regardless of the type of oxide from which each particle is made, their surfaces adsorb the water or hydrocarbon molecules from the atmosphere or some other sources and enhance the ability of these particles to slide over each other.

BODY 3: INTERMEDIATE MATTER

LABORATORY

a) OXYDIZED WEAR DEBRIS

b) GREASE OR LUBRICANT ONLY

"DRY" RAIL

c) WEAR DEBRIS, HYDROCARBONS CONTAMINANTS: BRAKE SHOE DEBRIS, SAND, ORGANIC DEBRIS, COAL, MINERALS, WATER (ADSORPTION, DEW, RAIN, SNOW).

LUB RAIL

d) GREASE, WEAR DEBRIS, CONTAMINANTS (SAME AS ABOVE) WATER.

EXHIBIT 3

OXIDIZED WEAR DEBRIS

FeO, Fe_3O_4, FeC

α-FeOOH α-Fe_2O_3

β-FeOOH β-Fe_2O_3

c.f. $\approx$ .2 to .3

EXHIBIT 4

EXHIBIT 5

Scanning Electron Micrograph of Oxidised Wear Debris

The other school of thought says that lubricity of wear debris is affected by the type of tribooxydation process, which is greatly affected by humidity. Each process can produce different types of oxides which simply have different lubrication properties. I think a well controlled experiment is needed to establish the degree of validity for either school.

2.2 *Lubrication by grease.*

Grease is the most common lubricant used in North America to alleviate flange wear in curves (Exhibit 6). The grease typically used has either calcium or lithium soap base to which mineral oils are added as lubricating agents. Extreme pressure additives such as graphite or molybdenum disulfide are almost always added. The oxidation inhibitors and adhesive agents are optional. The viscosity of a lubricant is usually known, and if the wheel and rail roughnesses are also known the type of lubrication regime can be established.

This can best be achieved by calculating the specific film thickness, λ, which is the ratio of the film thickness, h, and the composite roughness, σ, of the two surfaces (Exhibit 7). The composite roughness is defined as the square root of the sum of squares of the individual surface roughnesses. If the specific film thickness is larger than three, then

SPECIFIC FILM THICKNESS

$$\lambda = \frac{h}{\sigma} \quad , \quad \sigma = \sqrt{\sigma_1^2 + \sigma_2^2} \quad , \quad \sigma_{RMS} = 1.3\,\sigma_{CLA} \quad , \quad \lambda > 3$$

FILM THICKNESS FOR V-E REGIME
(HAMROCK-DAWSON)

$$H_{min} = 3.63\ U^{0.68}\ G^{0.49}\ W^{-0.073}\ (1 - e^{-0.68k})$$

$H_{min} = \frac{h_{min}}{R_x}$, h_{min} = min. film thickness, R_x = effective radius

$U = \frac{\mu_e u}{2E'R}$, μ_e - eff. viscosity, $u = \frac{1}{2}(u_1 + u_2)$, $E' = \frac{E}{1-\nu}$

$G = \alpha E'$, $\alpha = \frac{1}{\mu}\frac{\delta \mu}{\delta p}$ = pressure viscosity coefficient

$W = \frac{F}{E'R_x}$, F - load; $k = \frac{a}{b}$

EXHIBIT 7

an elasto-hydrodynamic lubrication regime is fully established. At lower values a partial elasto-hydrodynamic lubrication may prevail and for λ values at the vicinity of two, the lubrication regime may be termed boundary. However to calculate the value of λ we must first establish the actual film thickness. For this purpose the Hamrock-Dawson formula for V-E regime [1] may be adopted since it is applicable to the variable (v) viscosity lubricant grease) squeezed by elastically (E) deformable bodies (wheel and rail). The formula contains four dimensionless terms. The "v" term accounts for initial viscosity of lubricant and elastic properties of materials in contact. To establish the "G" term one has to know how much the viscosity of lubricant increases with increasing pressure once it enters the zone of contact. The "W" term takes into account load and some geometry parameters.

Although this equation was originally developed for the ellipticity parameter of one, Koye has experimentally shown that it is valid for ellipticity ratios from about .12 to 3.7 [2]. Also Koye and Winer [3], based on additional experimental work, concluded that this equation conservatively estimates the film thickness, since the film thickness which they measured was about twenty or thirty per cent higher than the one theoretically calculated from this relationship. The only problem in applying this equation to rail/wheel interface is caused by non-availability of data pertaining to the pressure viscosity coefficient for railway greases. I searched for it but I could not find it.

2.3.1 *Contamination by oily fluids ("dry" rail).*

Some excellent work on contamination of "dry" rail was done by Beagley of British Rail about 10 years ago [4]. Beagley collected and analyzed the contaminants found on the rail surfaces in main line track. These contaminants are inadvertently introduced and originate from leakages of bunker fuel, or as dripping from gear or bearing boxes.

When subjected to high pressures and temperatures occurring at rail/wheel interfaces these hydrocarbons become more complex in their consistency than they originally were (Exhibit 8). The most significant group from the lubricity point of view is the one containing naphtenic acids, esters and ketones. When chemically separated it is dark in color and has a very strong adhesion to the surfaces. The typical oil coverage of rail surfaces was found to be in a range of .2 to 2.7 x 10^{-6} g/cm² range which may form films several molecular layers thick.

2.3.2 *Contamination by debris-water mixtures ("dry" rail).*

Another type of "dry" rail contamination, frequently encountered

GREASE - REGULAR TYPE
SOAP BASE: Calcium or Lithium
LUBRICATING OIL: Mineral Type
ADDITIVES: Graphite - up to 12% MoS_2 - up to 3%
OXIDATION INHIBITORS AND ADHESIVE AGENTS ARE OPTIONAL
VISCOSITY: Known
C.F. ≈ 03 to 15

EXHIBIT 6

"DRY" RAIL: OLEIC CONTAMINATION	
Aliphatic Hydrocarbons (C_{14}):	30-65%
Hydrocarbons (C_{20} - C_{36}):	2-6%
Naphtenic Acids, Esters, Ketons:	20-60%
Oil Coverage: 0.2 to 2.7 x 10^{-6} g/cm² (After T. M. Beagley)	
C.F. ≈ .1 to .3 (Boundary)	

EXHIBIT 8

in rainy weather, is by rust/water mixtures. These mixtures form slurries which severely affect the available adhesion to locomotives. As shown in Exhibit 9 the tangential force transmitted by these mixtures is a function of yield shear stress (σ_y) and rate of shear 1/2 ($u_1 + u_2$) [5].

For high concentration of solids (90 – 100% by weight) the coefficient of friction μ is primarily a function of yield shear stress. For dry wear debris it is in the vicinity of 0.2 and drops very rapidly to a low value of 0.001 for paste-like mixture containing 10% water. At lower concentrations of solids, the shear rate term takes over and the coefficient of friction is a function of flow properties of water-debris mixtures. Since water is an isoviscous fluid of low viscosity, it is able to sustain an outward flow from zone of contact during each loading cycle and a dewatering occurs. Generally, the slower the train, the smaller number of wheelsets are needed to accomplish a complete dewatering of these mixtures and bring up adhesion to desirable levels.

2.4 *Lubricated rail.*

The composition of intermediate matter becomes more complex if the rail is lubricated by track or vehicle borne lubricators (Exhibit 10). As soon as the lubricant leaves these lubricators, its performance is affected not only by rail/wheel interaction (high pressures and temperatures) but also by intake of contaminants which are either terrain or traffic generated. The viscosity of the intermediate matter on the rail surface is usually unknown but greasy, slurry, or paste-like consistency

DEPENDENCE OF COEFFICIENT OF FRICTION ON YIELD SHEAR STRESS AND FLOW PROPERTIES OF IRON-OXIDE/WATER MIXTURES

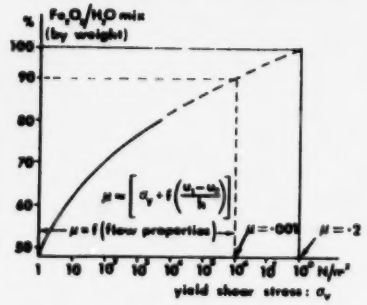

EXHIBIT 9

LUBRICATED RAIL

Composition of "Lubricant": (Locality, Traffic)

Viscosity of "Lubricant": Unknown

"Lubricant" consistency: Greasy; Slurry; Paste; Caking

Distribution of "Lubricant": Uneven

Sanding: Necessary

C.F. .03 to .2 (EHL, boundary, solid)

EXHIBIT 10

may be identified. In some extreme cases it may cake. The intermediate matter is not distributed across the railhead profile evenly (Exhibit 11) [6]. The highest concentration of lubricant can be found at the field side of the low rail and gauge corner of the high rail (locations 4 and 6 in Exhibit 11). However the remaining locations typically contain more hydrocarbons than the "dry" rail contaminated by oily fluids. Not surprisingly, coefficient of limiting friction can be very low, down to .03.

The presence of solid contaminants in "grease" is demonstrated in Exhibit 12. These contaminants were separated by dissolving the grease by various solvents. In addition to metal wear particles (flat and spherical in share) we have identified coal particles, quartz, chalcopyrite and wood fibres in appreciable quantities.

The solvents were then processed through the ferroanalyzer and again yielded large quantities of sand particles (Exhibit 13). These particles are very small ($\cong 2\mu m$) and originate from larger sand particles powderized by the action of the wheels. Together with wear and molybdenum disulfide particles, they adhere to surfaces of the composition brake shoes, and very effectively, polish the wheels (Exhibit 14).

The brakeshoe surface roughness is correspondingly low, which under adverse climatic conditions, may lead to the loss of braking ability due to hydroplaning. This represents a serious safety hazard specifically for loaded unit trains operated in mountainous territories.

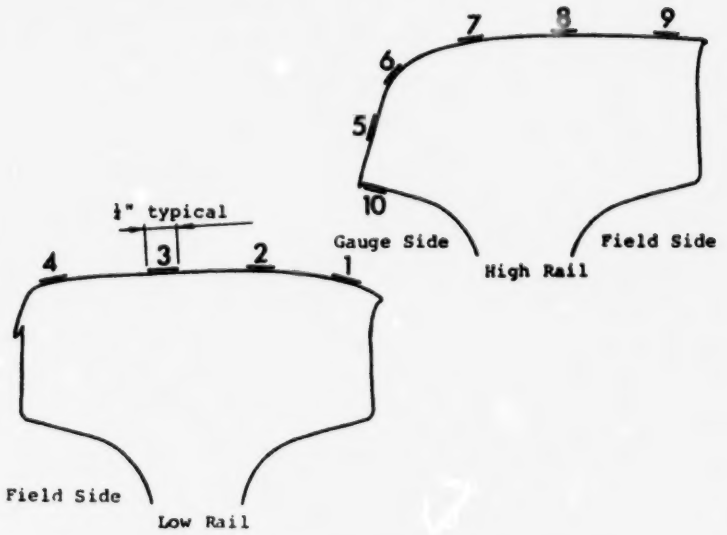

Location of 1" x 8" Areas		Total Impurities (mg)	MoS_2 (mg)	Fe_2O_3 (mg)	Other Impurities (mg)
Rail	Position				
LOW	1	41.27	20.60	2.26	18.41
	2	16.75	Trace	Trace	16.75
	3	36.71	.24	.46	36.01
	4	287.23	141.20	22.19	123.84
HIGH	5	114.18	73.58	11.52	29.08
	6	199.47	112.05	11.51	76.31
	7	79.34	32.20	6.40	40.74
	8	38.72	.43	.20	38.09
	9	40.12	3.62	1.73	35.13

EXHIBIT 11

Representative grease distribution pattern and chemical composition across rail heads.

42

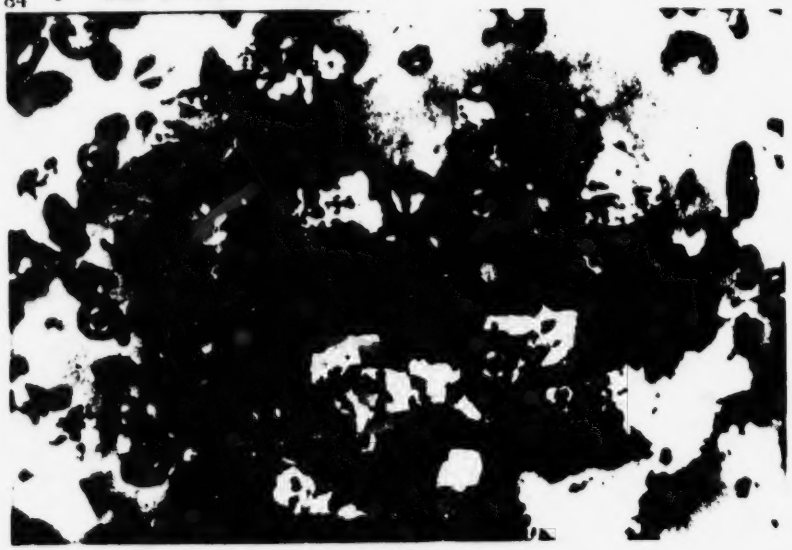

EXHIBIT 12

Solid Contaminants Extracted From Rail Grease Deposits (Mag. 200x)

EXHIBIT 13

Sand Particles Extracted From Rail Grease Deposits (Mag. 1000x)

EXHIBIT 14

Polished Wheel Tread of a 100t Coal Car

3.0 *Mechanical aspects of rail wheel interaction.*

One of the pivotal variables from the curving mechanics point of view is the angle of attack. For an absolutely rigid truck, the angle of attack would equal half of the wheelbase, divided by the radius of the curvature. For the three-piece North American truck we can add to this value an angle by which such truck is able to lozenge. Thus the leading wheelset may attack the rail at an angle of 45 minutes in a five degree

curve. Based on measurements done by CP [7] an average angle of attack for the leading wheelset of the leading truck (LL) in a five degree curve is about 28 minutes, for the trailing wheelset of the leading truck (TL) it is about 12 minutes and for the TL and TT combinations the angle of attack values are 18 and 6 minutes respectively.

Angle of attack can be used as a direct measure of lateral creepage (Exhibit 15b). This creepage gives rise to lateral traction force which brings the wheelset into the flange contact with the high rail. Similarly two other creepages, longitudinal and spin (Exhibit 15a, c), may occur in rail wheel interface.

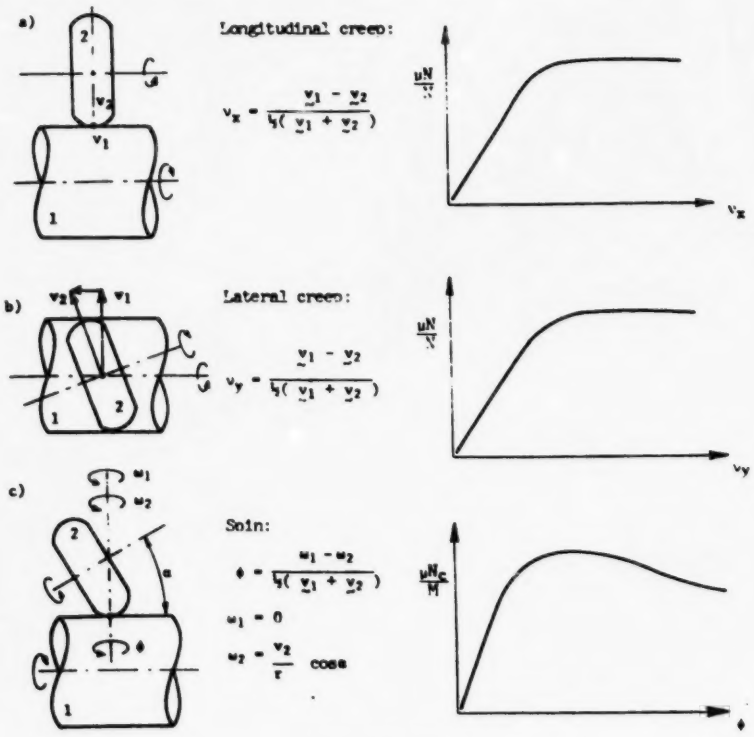

EXHIBIT 15

Definition of a) Longitudinal, b) Lateral and c) Spin Creepages and Their Effect on Traction Forces.

The manifestations of these three forms of creepages are directly observable on the surfaces of rails and wheels. Exhibit 16 shows nine locations of the wheel surface topography (magnified 200 times) obtained by the use of the replica technique from a leading wheelset on a leading truck of 100 ton capacity coal car. The markings shown in each location are the local deformations in the area of contact caused by rail asperities on tangent and curved tracks over which the wheel has just passed. The orientation of the individual photographs is apparent from locations 2 and 5 where the horizontal brake shoe rubbing marks indicate the longitudinal direction of rolling. At locations 1, 2, and 3 which represents the contact area with low rails, the prevailing direction of rubbing marks is in lateral direction. Locations 5 to 7 represents the contact areas between wheel and high rail prior to the occurrence of hard flange contact. All three, longitudinal, lateral, and spin components of creepage are observable on the rubbing marks in varying proportions. Spin creepage is attributable to the curving of these rubbing marks. In locations 8 and 9 which represents that of a hard flange contact, no curving of the rubbing marks occur. This is indicative of the fact that no appreciable spin occurs in the flange contact zone during hard flange conditions.

From the field observations of this type it has been concluded that the sliding distance in a lateral direction does not exceed 2mm in the zones of contact supporting the vertical load and is in the range of 5 to 25mm in the flange contact supporting the lateral load. Thus the flange contact zone experiences, on the average, ten times more sliding than the contact zone supporting the vertical load.

To study the effect of lubrication on the forces and wear rates in curves, let us limit our attention to distribution of lateral tread and flange forces. For large angles of attack (neglecting the unbalanced speed force) the distribution of these forces is shown in Exhibit 17. It should be noted that the horizontal component of the flange force is approximately equal to the sum of lateral tread forces. The lateral tread force on each rail is taken as a product of vertical load and friction coefficient which is determined by the degree of contamination and magnitude of the angle of attack.

4.0 EFFECTS OF MECHANICAL AND LUBRICATION ENVIRONMENT ON WEAR

Although the vertical and lateral forces as well as angle of attack could be measured in the field, the control of lubrication, evaluation of the wear rates or maintenance of any specific angle of attack in the

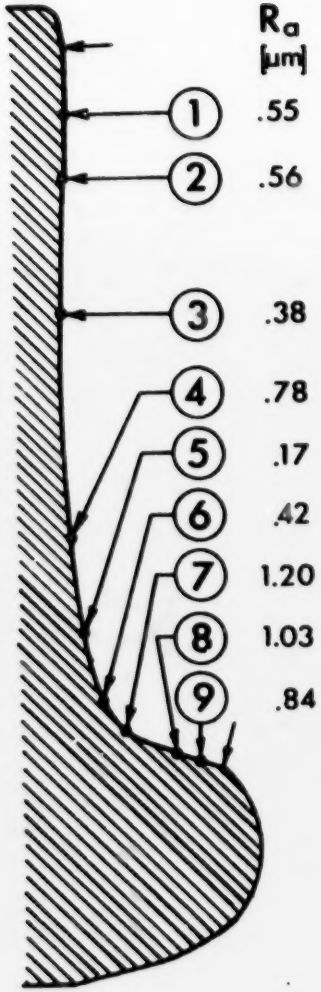

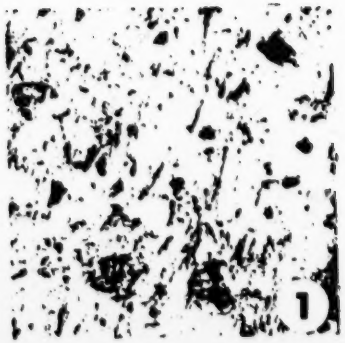

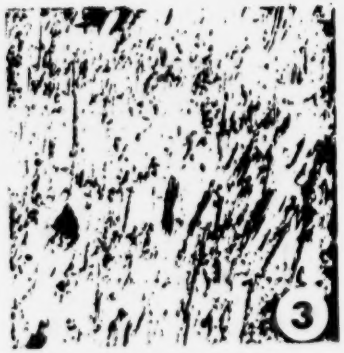

EXHIBIT 16

Wheel Surface Replicas of a 100t Coal Car (Mag. 200x)

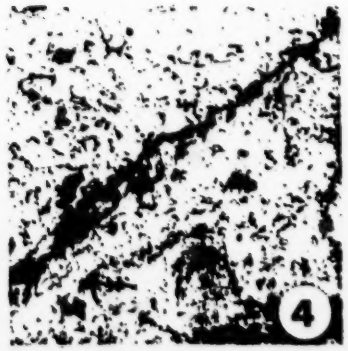

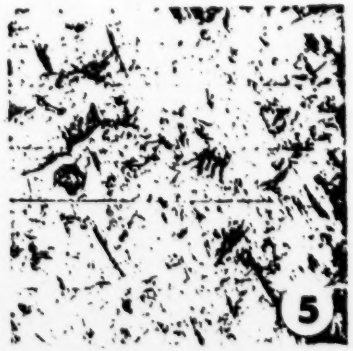

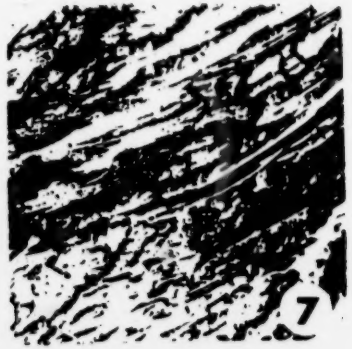

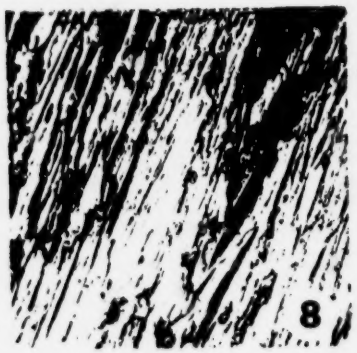

EXHIBIT 16 (continued)

LATERAL TREAD AND FLANGE FORCES FOR LARGE ANGLES OF ATTACK

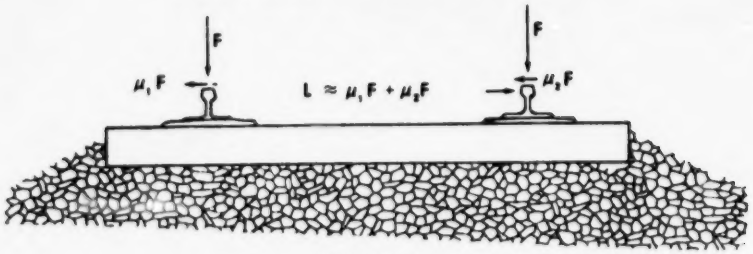

EXHIBIT 17

field, is difficult and impractical. For this reason, the following measurements were carried out on the rail/wheel wear apparatus located in the Western Laboratory of the National Research Council of Canada. Although the description of this apparatus can be found elsewhere [8] several relevant features of the apparatus are mentioned here for the benefit of a better understanding of the obtained results. The design concept of this apparatus is apparent from Exhibit 18. The apparatus simulates a wheelset riding on a pair of rail discs in a tangent track or curve. The simulation of curve negotiation is achieved by yawing the wheelset discs with respect to rail discs. (The yaw angle and angle of attack are synonymous.) This yawing is achieved by the rotation of three flexure pivots (which also hold the wheelset on top of the rail discs) above the vertical axis of the wheelset. The lateral and vertical softness of these flexure pivots enable the wheelset to move laterally into a flange contact and to move downwards to compensate for wear and plastic flow. Although the flexure pivots resistance increases with lateral or vertical deflections, for small movements or deflections it is negligible.

The adoption of disc on disc concept in a design of this machine allows the specimens to be machined from commercial railway wheels and rails. This ensures a good representation, with the exception of residual stress patterns, of the original metallurgical properties of the full-size wheels and rails. The crown of each rail disc is machined to a new 132 or 136 lbs. AREA rail profile and the wheel discs are profiled to worn Heumann type profile designated "CN profile A." Both rail and wheel profiles are reduced 10 times in their cross-section.

The load is applied through 1 to 20 ratio lever system coupled with another set of flexure pivots which only transmit a vertical component of load for any lateral position of the wheelset. Each rail disc shaft is supported by biaxial load cell enabling the measurement of vertical and lateral load between both pairs of rail wheel discs. The load is scaled down to yield the same Hertzian contact stresses as experienced in the field. A photograph of this apparatus is shown in Exhibit 19.

SCHEMATICS OF RAIL WHEEL WEAR TEST APPARATUS

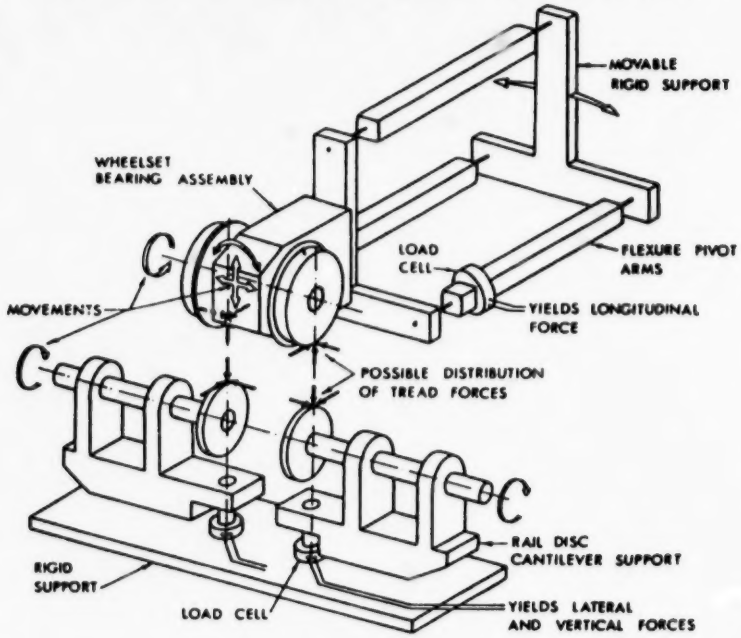

EXHIBIT 18

Using this wear apparatus, the external lateral force was measured and plotted as a function of angle-of-attack and lubrication regime (Exhibit 20). From this diagram it is apparent that the external lateral force in the range of angle-of-attack from 0 - 12' is very low for both unlubricated cases. Although the lateral traction force in fact increases with the angle-of-attack it is probably negated by the gravitational stiffness and spin creepage [9]. The wheelset linearly deflects towards the high rail until a 'hard' flange contact is firmly established at the angle-

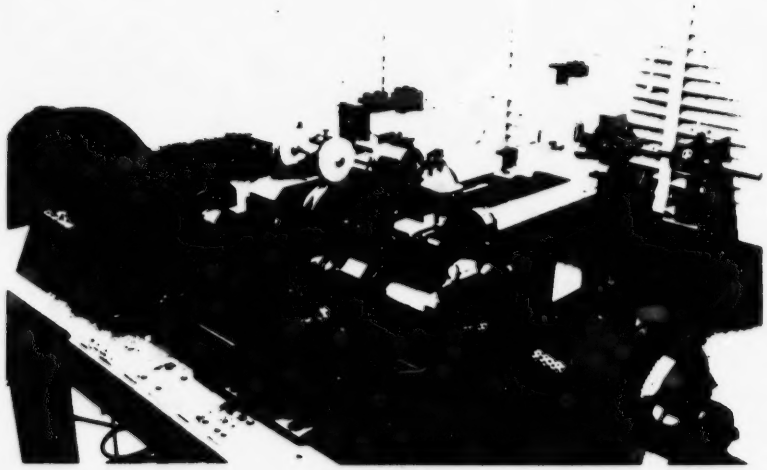

EXHIBIT 19

Photograph of Rail/Wheel Wear Apparatus

of-attack value of 12′ and 16′ for the unlubricated and lubricated case respectively. In the range of 12′ to 25′ of angle-of-attack the external lateral force increased linearly and for the angles-of-attack of 30 minutes and larger, it reached its maximum value. This value is determined by the coefficient of limiting friction and is unaffected by further increases of angle-of-attack. As apparent from Exhibit 20, the maximum lateral force for lubricated case is approximately one-third of that for the unlubricated one.

Using the results from these measurements and assuming that the lateral force generated by the vertical contact on the high rail is the same, the magnitude of flange force was established for various lubrication conditions on top running surfaces of high and low rails. As shown in Exhibit 21 the magnitude of flange force is again a function of angle-of-attack and lubrication conditions on running surfaces of high and low rails. When both rails are lubricated, the maximum flange force attainable is quite low, approximately 20% of the vertical wheel load. However, if one rail is unlubricated, the flange force may increase to 40% and if both rails are dry it may reach 60% of vertical wheel load. Thus, the flange wear is affected not only by lubrication conditions in

EXTERNAL LATERAL LOAD ON 'LOW' RAIL DISC
UNDER LUBRICATED AND UNLUBRICATED CONDITIONS

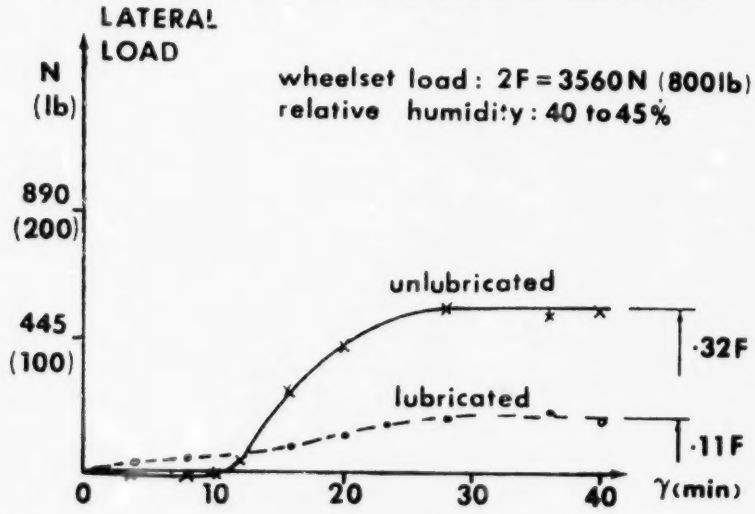

EXHIBIT 20

the flange contact itself but also by lubrication on the top running surfaces of rails.

The effect of lubrication on wear rates was established, using the rail wheel wear apparatus, for different lubrication combinations at three points of contacts, one on low and two on high rail. The lubrication separation between the flange and running surfaces was achieved by machining a groove in a gauge corner of the high rail disc. The wear was measured by weighing the discs. The difference between the weight at the beginning and end of test period divided by the number of revolutions is reported as wear rate in μg cycle in Exhibit 22. Six cases marked A to E were investigated.

Case A: The highest wear rates were experienced, as expected, in the case of unlubricated rails. The high rail had about 20 times larger wear rate than the low rail. It may be assumed that most of this wear had been generated by a flange contact. Although the flange force is smaller than the vertical force the flange contact experiences about 10 to 15 times more slippage than the vertical one. The smaller size wear debris of high velocity generated on top running surfaces contribute to

CALCULATED HORIZONTAL COMPONENT OF FLANGE FORCE FOR VARIOUS LUBRICATING CONDITIONS

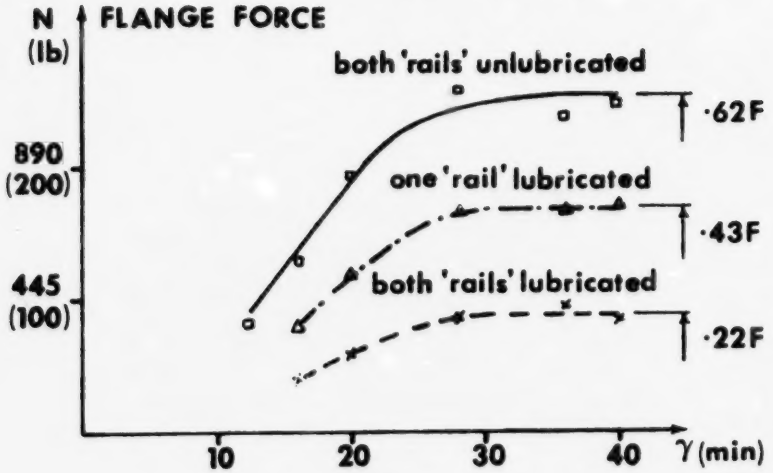

EXHIBIT 21

KEY	LUBRICATION STATUS			RAIL DISC WEAR RATES	
	LOW (INNER) RAIL DISC	HIGH (OUTER) FLANGE	RAIL DISC TOP	LOW (INNER) μg/CYCLE	HIGH (OUTER) μg/CYCLE
A	NONE	NONE	NONE	6.7	110
B	GREASE	NONE	NONE	.06	62
C	NONE	GREASE	NONE	2.8	7.4
D	NONE	GREASE	GREASE	3.5	.2
E	GREASE	GREASE	GREASE	.07	.1
F	GREASE + 20% SAND	GREASE + 20% SAND	GREASE + 20% SAND	.6	1.5

TEST CONDITIONS: ANGLE OF ATTACK: 40'
WHEELSET VERTICAL LOAD: 3560N (800 lb)
RAIL DISC MATERIAL: PLAIN CARBON
WHEEL DISC MATERIAL: CLASS "C" STEEL
RELATIVE HUMIDITY: 40 to 45%

EXHIBIT 22

Effect of Rail/Wheel Lubrication on Wear Rates

the reduction of wear at these surfaces, further increasing the difference between flange and rail top wear.

Case B: For lubricated low and dry high rail the wear rate on the low rail dropped drastically. The wear rate on the high rail was also reduced, which can be attributed to the reduction of flange force.

Case C: When grease was applied to the flange only it reduced drastically the flange wear despite the existence of large flange force and sliding distances at this location. Such a situation (flange contact lubricated, running surfaces dry) may perhaps be the most desired form of rail wear in curves.

Case D: Wear rates on high rail are reduced even further if the entire high rail is lubricated. In this case the wear rate on low rail remains approximately constant.

Case E: The least wear rates are achieved when all three points of contact between wheelset and a pair of rails are lubricated. The wear rates on high and low rails are reduced by the factor 1000 and 100 as compared to the unlubricated rail discs (Case A). It, however, does not mean that the lubricated high rail will last a thousand times longer than the unlubricated one. In fact the rail fails, unless ground, in rolling contact fatigue after several months in service, depending on traffic density and quality of rail material. Early development of long-wave length corrugations are associated with this form of rolling contact fatigue.

Case F: The last simulated case included lubrication with a mixture of grease and sand (20% sand by weight). With the exception of other contaminants, this form of lubrication is much closer to the field conditions than the case of lubrication by plain grease. The sand in grease at this concentration is able to increase the wear rates by a factor of 10.

5.0 DISCUSSION AND CONCLUSIONS

Based on the analysis of the lubricant contaminant mixtures in the field and the experimental analysis of forces and creepages in rail wheel interface we are allowed to formulate the desired features of the rail wheel tribo-system from the lubrication point of view. These are: high adhesion capabilities, a balanced adhesive and contact fatigue wear modes and, of course, elimination of flange wear (Exhibit 24). The simplest way to maintain high adhesion levels, which provide good traction on the front units of the train, is to keep the rails clean (Exhibit 25). Although this occurs after grinding, the rails may be cleaned by plas-

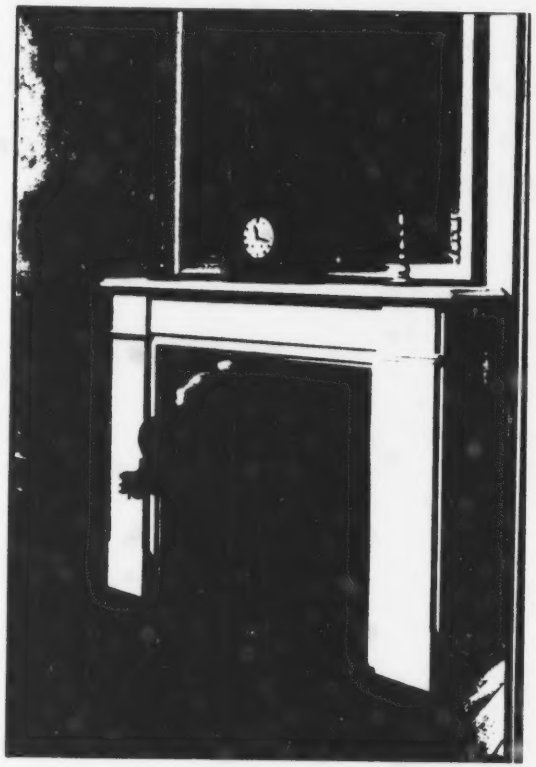

EXHIBIT 23

The Ultimate Solution to Rail Wear (No Rail): "Time Transfixed" by Reene Magritte. (Courtesy of the Art Institute of Chicago)

ma treatment or chemical treatment where warranted. However, the most common method to increase adhesion between rail and wheel is by sanding. All these methods to increase adhesion are either being used or have been tried out. A novel approach would be to try out high traction fluids, the ones typically used in traction drives as a rail wheel lubricant.

It is highly desirable and also feasible to combine high adhesion and balanced adhesive and contact fatigue wear (Exhibit 26). This may most simply be achieved by keeping the rail wheel running surfaces clean. Another, less conventional approach, may aim at appreciable increases in the amount of sliding on rail running surfaces. Thus, the use of high adhesion locomotives utilizing the longitudinal creepage values of 5 to 15% may not only cleanse the rail and thus provide the higher adhesion but also wear the top running surfaces of rail leading to the reduction of rolling contact fatigue. Since most of the tread wear on railway wheels is caused by braking shoes (especially in the case of freight car wheels) one may consider using specially designed wear blocks which could be dragged over the running surfaces of rails in curves. In this manner the rail contact fatigue may be alleviated and the need for rail grinding considerably reduced.

To eliminate the flange wear (Exhibit 27) one should primarily aim at the reduction of the angle of attack on the leading wheelsets of freight car trucks. This could either be achieved by the straightening of the curves which is not always feasible or by using the self-steering trucks. Several types of these trucks are now available on the market. The lubrication alternative would be to apply the lubricant to the flange contact only. Since the grease cannot be prevented from migrating to the top running surfaces of rails, solid lubricants may be less migratory and should be considered for this purpose.

The implementation of some of the recommendations mentioned above require, in many cases, appreciable capital investments. Some other suggestions require further research to prove their validity. However, one very simple method which could be implemented without any delay by each railroad concerned about rail wheel wear and lubrication simply consists of a judicious use of flange lubrication (Exhibit 28). Under- and over-lubrication of track has a negative effect on the rail

MECHANICAL AND RHEOLOGICAL ASPECTS OF WEAR AND ADHESION
DESIRED FEATURES:
A) High Adhesion
B) Balanced Adhesive and Contact Fatigue Wear
C) No Flange Wear

EXHIBIT 24

POSSIBLE REMEDIAL MEASURES
HIGH ADHESION:
a) Clean Surfaces:—Grinding —Chemical Treatment —Other: Plasma, Sanding
b) Lubricate With High Traction Fluids

EXHIBIT 25

POSSIBLE REMEDIAL MEASURES (CONT'D)

HIGH ADHESION COMBINED WITH BALANCED ADHESIVE AND CONTACT FATIGUE WEAR:

a) CLEAN SURFACES

b) INCREASE SLIDING DISTANCE ON RAIL SURFACES

— USE HIGH ADHESION LOCOMOTIVES

— DRAG WEAR BLOCKS OVER RAILS

— APPLY BRAKES TO RAIL SURFACES

EXHIBIT 26

life. Under-lubrication leads to excessive gauge face wear and over-lubrication leads to the early occurrence of rail corrugations. Since it takes time to develop an ability to "judiciously" operate the lubricators, it is recommended that one person on each subdivision with lubrication problems of one kind or another be assigned to take care of nothing else but lubricators. His responsibility would be to keep the lubricators filled with grease and take care of their proper adjustment so that they do not over or under discharge the lubricant. Some railroads may already have such a person. I am sure that his salary is an investment which yields an appreciable return in the form of longer rail life and less maintenance.

QUESTIONS TO DR. KALOUSEK:

MR. GLAVIN: Thank you, Dr. Kalousek. One thing, your last slide, I think there are probably many maintenance of way people here who have been trying to accomplish that for many years, and maybe what they need to do is take the slide back. We might get the message across.

One thing I noticed that you talked about the use of drag blocks, and it reminded me of Dr. Rabinowicz statement, I think, that if you took a loaded train of a hundred cars and ran it from coast to coast, from Chicago to Los Angeles and back, you would have three-quarters of a ton of lost metals. I would dare say that if you used drag blocks that it would probably be 1.3 times of lost metal.

Now, are there any questions of Dr. Kalousek?

Q. In one of the slides at the start of your presentation, you showed the contaminants on the rail that had been cleaned by your department, etc. To what do you attribute those little metal spheres and what was their composition?

POSSIBLE REMEDIAL MEASURES (CONT'D)

NONE OR REDUCED FLANGE WEAR

a) Reduce Angle-of-Attack: Self-Steering Trucks

b) Apply Lubricant to Flange Contact Only: Solid Lubricant

EXHIBIT 27

WHAT CAN BE DONE TOMORROW?

a) Fill-in Your Lubricators

b) Prevent Over-Discharge of Lubricant

c) Assign a Tribo-Superintendent on each Subdivision

EXHIBIT 28

A. There are three sources of spherical particles in the rail/wheel interface. Many of them are generated by grinding. On the sides of the rail, there are always deposits of grease and as the sparks hit the grease they quench and form spheres. Some fretting wear particles may roll into spheres and sometimes they just resemble doughnuts. These are formed within the subsurface cracks. The third kind of spherical particles consists of metal or other debris and grease residue. These particles are formed like spitballs within the subsurface cracks due to the minute circular motion of overlay material caused by passing wheels.

Q. You mentioned the laboratory measurement of film thickness. Now, that is under ideal conditions, with, I assume, pure grease. Have you thought of a way of measuring the thickness collected in the field?

A. Yes, I did. I can only describe the way in which we did these tests. In the field we outlined the rail surface area with masking tape and cleaned it thoroughly using tampons soaked in solvents. In the laboratory the contaminants were extracted from the tampons, weighed, analyzed chemically, and looked at under the microscope, etc. The ratio of weight of various fractions over the area cleaned, then gives either the concentration of solids or grease thickness. Usually the deposits are very thick next to the lubricators. Half a mile down the track these are much thinner.

Q. One of your tables showed lubrications at various combination points, A, B, and C. One of the combinations you did not measure was grease on top of the low rail, plus flange of the high rail. I just wonder why not and what do you speculate those coefficients would be?

A. You are referring to this table? (Exhibit 22.)

Q. Yes. In other words, grease, grease, none.

A. One reason why I didn't do that was lack of time. The other reason is the fact that the wear rate on low rail in such a combination would be very similar to the case grease, none, none. The high rail conditions would be the same as in the case none, grease, none.

MR. GLAVIN: Any other questions?

Q. Joe, could you return to your table of your results to about the fourth line, none, grease, grease.

A. Yes.

Q. Looking at the low rail, where you have 3.5 (combination D) and above it (combination C) you just have grease on the flange, and it is 2.8. Did you give us an explanation of that? If you did, I must have missed it.

A. No, I did not give you any explanation because it is one thing I cannot explain. So many factors affect the wear rates, that even in laboratory tests it is possible to miss some.

Q. Forgive me for asking. I do have one last question that maybe you can answer, which is not related to the table there. If you have debris produced on dry running surfaces they resemble flakes. What is the thickness of those?

A. The thickness is typically 5 to 15 microns. The thickness in the field is somewhat larger, 10 to 25 microns.

ACKNOWLEDGEMENT

Experimental work reported in this presentation represents a portion of a cooperative rail wheel research program undertaken by Western Laboratory (NRCC) and University of Rhode Island. The financial support of Transportation Development Centre (Canada) and Association of American Railroads toward this program is greatly appreciated.

REFERENCES

1. Hamrock, B. J. and Dawson, D., "Isothermal Elastohydrodynamic Lubrication of Point Contacts, Part III — Fully Flooded Results," J. of Lubrication Technology, 99, No. 2, 1977, p. 26.
2. Koye, K. A., "Experimental Evaluation of the Hamrock and Dawson Elastohydrodynamic Point Contact Theory," M.S. Thesis, Georgia Institute of Technology, December 1979.
3. Koye, K. A. and Winer, W. O., "An Experimental Evaluation of the Hamrock and Dawson Minimum Film Thickness Equation for Fully Flooded EHD Point Contacts," ASME Trans., Vol. 103, April 1981, p. 284.
4. Beagley, T. M., McEwen, I. J. and Pritchard, C., "Wheel/Rail Adhesion—the Influence of Railhead Debris," Wear, Vol. 33, 1975, p. 147
5. Beagley, T. M., "The Rheological Properties of Solid Rail Contaminants and their Effect on Wheel/Rail Adhesion," Proc. Inst. Mech. Engrs., Vol. 190, 33/76, p. 419.
6. Kalousek, J., "Track/Train Dynamics Report #4: Rail Corrugations," Canadian Pacific Dept. of Research Report No. S488-75, Feb. 1975.
7. Ghonem, H. and Gonzalves, R., "Comparative Performance of Type II Trucks," Canadian Pacific Dept. of Research, Report No. S576-78, Nov. 1978.
8. Kalousek, J., "Rail/Wheel Wear Testing Facility," NRCC-DME Newsletter, Vol. 13, No. 1, July 1981.
9. Marcotte, P. P., Mathewson, K. J. R. and Caldwell, W. N., "Improved Wheel Tread Profiles for Heavy Freight Vehicles," ASME J. Eng. for Ind., Vol. 102, Aug. 1980, p. 263.

CONTACT MECHANICS AND WEAR OF RAIL/WHEEL SYSTEMS
University of Waterloo Press, 1982

Vancouver
British Colbumia
July 6-9, 1982

LATERAL CREEPAGE AND ITS EFFECT ON WEAR IN RAIL WHEEL INTERFACE

J. Kalousek

Western Laboratory
National Research Council
Vancouver, British Columbia, Canada

G. Rosval

Department of Research
CP Rail
Montreal, Quebec, Canada

H. Ghonem

Department of Mechanical Engineering
University of Rhode Island
Kingston, Rhode Island, U.S.A.

ABSTRACT: Reduction of high rail and wheel replacement costs due to wear requires a better understanding of the complex processes taking place at the wheel/rail interface. These processes were studied as a function of yaw angle on a 1 : 10 scale apparatus modelling a wheelset riding on a pair of rail discs. Eight tests simulating straight and curved track were carried out at four values of yaw angles of 0', 8', 20' and 32', under lubricated and unlubricated conditions. The tests revealed a marked difference in wear mechanism and material response between lubricated and unlubricated cases as well as between high (outer) and low (inner) rails in the unlubricated cases.

RÉSUMÉ: Le souci de réduire les coûts de remplacement des rails et des roues dûs à l'usure exige une meilleure compréhension des phénomènes complexes d'interactions entre les roues et les rails. Des études de ces phénomènes, fonction de l'angle d'attaque des roues sur les rails, ont été faites, sur un appareil model réduit à l'échelle 1 : 10 représentant un ensemble de roues roulant sur une paire de rails à disque. Huit essais en laboratoire simulant les attaques des roues sur les rails en ligne droite et sur les courbes, avec et sans lubrification des matériaux, one été effectués pour quatre valeurs différentes d'angle d'attaque: 0', 8', 20' et 32'. Ces essais ont révéle une différence marquée des mécanismes d'usures et de la réponse des matériaux dépendant de la lubrification ou de la non lubrification des matériuax et aussi, dans le cas de la "non lubrification" des matériaux, en courbe, cette différence dépend de l'attaque des roues "sur le rail externe" ou "le rail interne".

INTRODUCTION

A rail/wheel tribosystem becomes fully defined if all of its input and output variables are quantitatively determined. Input variables in this system include operational, contact mechanics, material and rheological parameters. The interaction of these parameters within the tribosystem envelope, which occurs in a unique pattern for each individual railway, yields a set of output variables (see Figure 1), one of which is wear. The significance of this phenomenon is the large maintenance budget that is required to overcome problems associated with rail wear in curves [10].

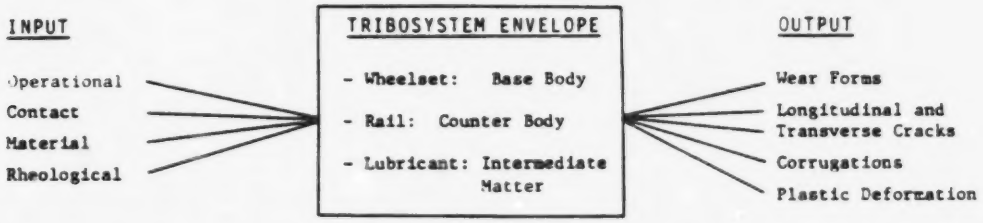

Figure 1 - Rail/Wheel Tribosystem

Wear performance of high (outer) and low (inner) rails in curves differ. Although the mode of wear on the top running surfaces of both rails is similar, the main difference comes from gauge side wear occurring on the high rail due to frequent flange contacts from passing wheels. The establishment of the flange contact is governed by the equilibrium between external forces transmitted to a wheelset by vehicle suspension, and rail/wheel forces. If a wheelset is in hard flange contact with the high rail then three sets of forces, one on the low rail and two on the high rail, balance the suspension forces. For any such force and moment equilibrium the spatial orientation between the wheelset and the track can be characterized by a particular lateral displacement, e, and angle-of-attack or yaw angle ψ.

It is the value of this angle that controls the magnitude of lateral creepage acting on the wheel/rail contact zone which consequently determines the severity of rail wear. The relationship between angle-of-attack and wear should then be recognized as an important element in the basic understanding of rail wear. It is this relationship that is the subject of this paper.

ANGLE-OF-ATTACK RELATED FIELD OBSERVATIONS

The conventional North American three-piece truck design normally yields an angle-of-attack that ranges from -20° to about +60° depending on the degree of curvature, wheel and rail profiles, location of the wheelset in a railway car and other variables affected by track irregularities. Field measurements [2] have shown that this angle is highest on the

leading wheelset and zero or slightly negative for a trailing wheelset. The magnitude of this angle, which is difficult to ascertain from field tests, affects the orientation and position of the wheel/rail contact zone. A wheel flange root could contact the gauge side in one position as shown in location 3 of Figure 2. A two point contact on this rail may however occur as a combination of locations 1 and 2 with either locations 4 and/or 5 as shown in the same figure. The latter case is referred to as "hard flanging" and leads to higher values of ψ.

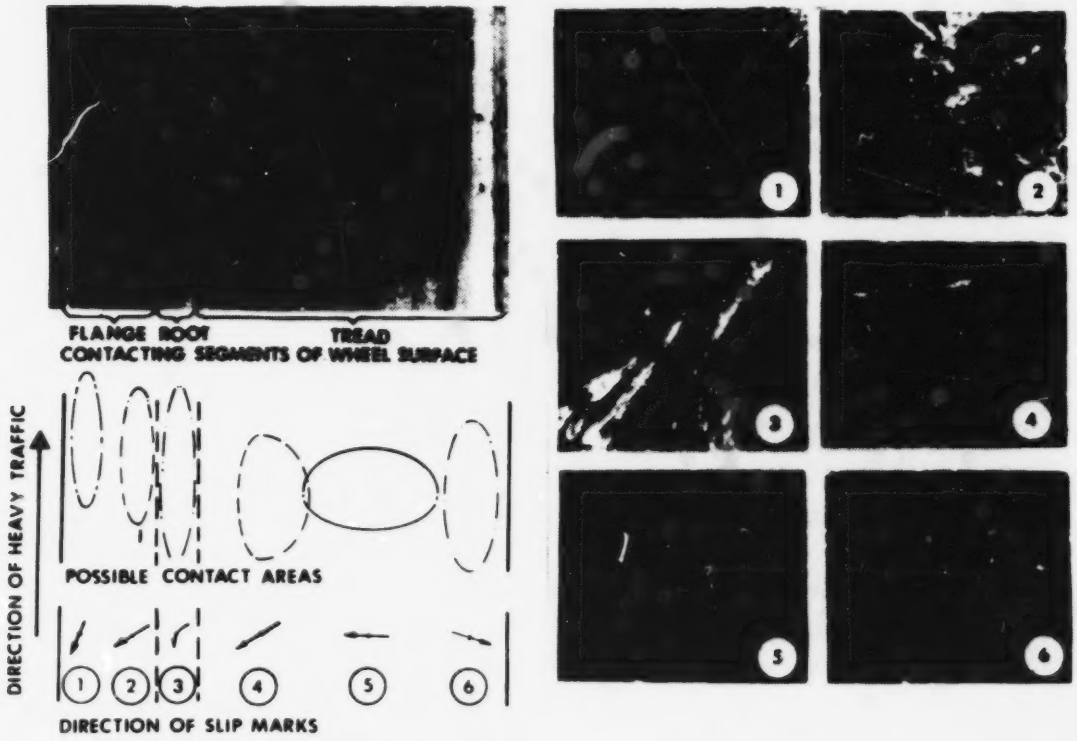

Figure 2 - High Rail Surface Showing Possible Contact Areas and Observed Slip Marks

The angle-of-attack significantly affects the amount of sliding in the rail/wheel interface. If this angle, the magnitude of e and rail and wheel profiles are known the slip could be calculated using, for example, the theory of Kalker [4]. On the other hand, by being familiar with this theory one can make judgements as to the values of ψ and e from the experimental observations of surface sliding marks. The right portion of Figure 2 shows the direction of such marks taken at six locations on the worn rail surface shown in the left portion of this figure. The lateral component and length of these marks at locations 4 and 5 indicate a positive ψ which could range from 20' - 40'. However, at position 6 these marks point in opposite directions, i.e., towards the

field side of the rail. These marks are due to wheelsets which were displaced towards the low rail and have a slightly negative ψ.

At a flange contact, where the largest amount of sliding takes place, the marks follow the trajectories of wheel flange asperities which, from a geometric point of view, are extended cycloids [7]. Depending on the flange angle of a worn wheelset, which in the field may vary between 70° and 76°, the flange can be contacted at either upper or lower portion (shown in Figure 2) or the entire height (not shown in Figure 2) of the gauge side of the rail. Therefore, the wheel flanges contacting the upper section of the rails exhibit a large downward component (location 2) and those contacting the lower half of the gauge side of the rail have a large longitudinal component (location 1). For positive ψ the flange contact is located in front of the top surface contact area.

Figure 2 also depicts a large number of surface microcracks. Field observation indicate that the growth of these cracks as well as the severity of gauge face wear are significantly affected by the degree of lubrication. Therefore, lubrication, in addition to angle-of-attack, is also considered as an independent variable in the laboratory test program described next.

LABORATORY SIMULATION OF CURVE WEAR

This experimental study has been carried out on a 1 : 10 scale apparatus simulating a wheelset riding on a pair of rails. The rails are represented by two discs (see Figure 3) manufactured from the head of actual rails. Both of these rail discs are driven at the same angular speed whilst the wheelset rolling is, with the exception of possible brake application, unrestrained. This ensures that the apparatus models the freight car wheelset rather than a locomotive wheelset. The simulation of creepages and tread forces for two or three point contact is achieved by restraining the wheelset yaw movement but allowing for lateral positioning with respect to the disc centre line. This is achieved by a flexure pivot assembly which is stiff in longitudinal but soft in lateral or vertical directions. By rotating this assembly around a vertical axis intersecting the centre of the wheelset a desired angle-of-attack can permanently be set or periodically altered during the test with an accuracy of 1'. The apparatus is instrumented to yield the three-dimensional components of forces, the displacement of the wheelset, the angular velocities of both shafts and the vibration characteristic of the apparatus. All test manipulations including data acquisition are computer controlled. A detailed description of this apparatus can be found in reference [6].

Although great care has been taken to simulate the complexity of rail/wheel interaction in the field, the reproduction of the contact stresses between test discs similar to those experienced by rail and wheel in the field appears difficult for the following reasons. A rail in the field is subjected to wheels of different cross-sectional profiles and diameters yielding either conformal or counterformal contacts. Such an "open" system results in a wide range of shapes of contact ellipses (see Figure 2). This, combined with a wide range of contact forces occurring on high capacity railway lines, does not permit the shakedown state to be satisfied, thereby causing severe plastic

deformation and wear. In a "closed" system, such as a laboratory test, the mating discs over a period of time always wear into conformal contacts that minimize the level of contact stresses. If wear occurring in the field is to be reproduced in the laboratory a high level of contact stresses must be achieved. This is only possible by an adequate increase in normal load since to reproduce the irregularities in the wheel/rail contact geometry, typical of the "open" system, is difficult in a laboratory experiment.

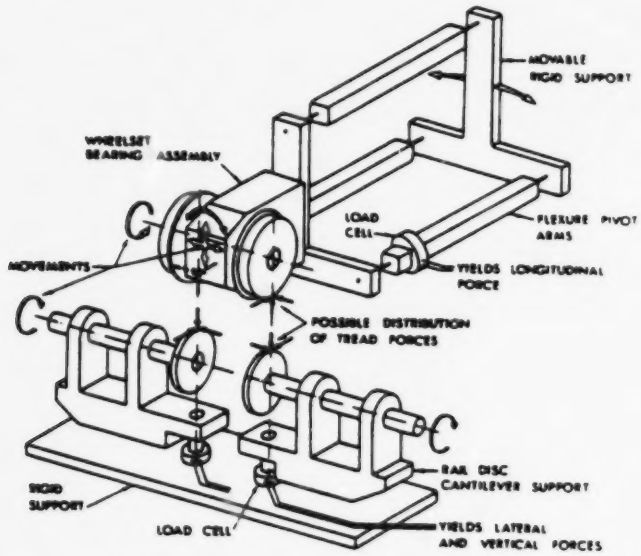

Figure 3 - Schematics of Rail Wheel Wear Apparatus

It may be appropriate to add that the system with a captive rolling stock, often of identical design, such as FAST or some mining railway lines can be termed "semi-closed". These systems develop high conformity of wheel and rail profiles leading to lower levels of contact stresses than those characteristic of the "open" systems. The "semi-closed" systems are easier to simulate in the laboratory because the contact stresses in the field can be more accurately estimated.

TEST PROCEDURES

A series of eight tests were carried out to establish the relationship between wear, angle-of-attack and lubrication conditions. Each individual test was run for specific load and angle-of-attack which were maintained constant during the test period. Tests were run unidirectionally for a pre-determined number of revolutions.

A pair of test runs, one lubricated and one unlubricated, were carried out for the following angles-of-attack: 0', 8', 20' and 32'. These angles were selected so that a spectrum of flange forces and consequently variations in flange wear could be produced. As a first approximation, the flange force is taken in this analysis as the

sum of the tread lateral forces on both running surfaces. Such a force could be easily measured, as a function of angle-of-attack using the wheel acting on a low rail of the test apparatus. This relationship, which is shown in Figure 4, has three distinctive regions. At ψ = 0' - 12', the wheelset linearly deflects with increasing ψ towards the high rail until a hard flange contact is established. Because the lateral force includes spin and gravitational stiffness effects in addition to lateral creepage, it can, for a small angle-of-attack, become slightly negative. Once a hard flange contact is established the lateral force gradually increases at ψ = 12' to 30' until the tread creepage becomes fully saturated at ψ = 30' and unaffected by further increases in yaw angle. Therefore the selected yaw angle 0' corresponds to the tangent track, 8' stands for the onset of flanging (region I), 20' lies in about the middle of region II and 32' represents a high level of flange force.

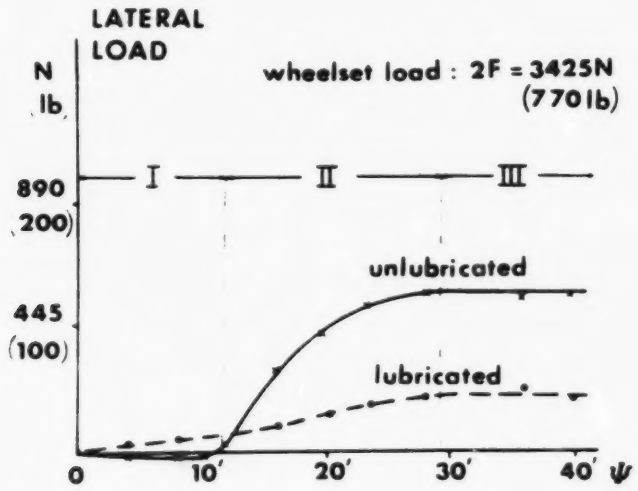

Figure 4 - External Lateral Load on Low Rail Disc under Lubricated and Unlubricated Conditions

Standard railway curve grease, containing three-percent molybdenum disulfide and eleven percent graphite, was used as a lubricant in these tests. Twenty per-cent by weight of silica sand, which is normally used in lubricated territories to maintain adequate adhesion levels under locomotive wheelsets, was mixed into the grease to approximate the composition of actual lubricant on the top surfaces of rails of heavy haul lines.

Rail discs were manufactured from the head of commercially rolled chromium alloyed rail. The nominal chemical composition of this material is: 0.65-0.7C; 0.45-0.55 Mn; 0.040 P; 0.055 S; 0.1-0.25 Si; 1.2-1.3 Cr. Controlled cooling of this rail produced fully pearlitic microstructures with the mean railhead (disc) hardness of ≈ 340 VHN. The rail discs were 69.8 mm in diameter and contained NC machined new AREA profile reduced 10 times in size and tilted by a 1 : 40 ratio towards the centre of the discs simulating the track.

The wheel discs were made from Class C steel with a nominal chemical composition: 0.67-0.77 C, 0.6-0.85 Mn, 0.05 P, 0.05 S, 0.15 Si. These discs were heat treated to attain a pearlitic microstructure and hardness of ≈ 350 VNH. The discs were NC machined to CN "Profile A" (reduced 10 times) and had a tape line diameter of 119.4 mm. All discs had an initial roughness of 0.01 μm and were thoroughly cleaned before commencement of each test. Since rail and wheel disc materials were of the same microstructure, their modulus of elasticity and poison ratio were assumed to be identical, i.e., 200 GN/m^2 and 0.29 respectively.

EXPERIMENTAL RESULTS AND DISCUSSION

The well-established linear law of adhesive wear, based on numerous experiments carried out with metallic surfaces sliding over each other states that volume of worn material is directly proportional to load and distance slid and indirectly proportional to hardness of material at the surface. Similarly, for rolling-sliding contacts, knowledge of Hertzian contact stress, rather than normal load, amount of slippage and hardness is desired. Since the normal loads at surface contact B and flange contact C on the high rail cannot be measured, a computer program was used to calculate a distribution of forces between wheelset (including low rail contact A) and a pair of rail discs. These forces, oriented parallel to the frame, together with calculated contact stresses, are shown in Table 1. Details of this program are discussed in reference [1]. The following section will concentrate on the concepts of slippage with the purpose of understanding its lateral component.

Slippage

Slip, slippage or sliding distance may be physically visualized in the rail/wheel interface as follows. Let us imagine a point on a wheel and a point on a rail which are in contact at the front of the contact zone and which initially do not experience any traction force between them. Due to the tendency of these two points to move in different directions and/or at different speeds, a friction force must develop if they are to maintain the same trajectory through the contact zone. This frictional force elastically deforms each body increasing the elastic stresses at the interface to a point at which the asperities start to yield or slide over each other. Thus, the portion of the area of contact where these points maintain the same trajectory is referred to as the zone or region of adhesion. The remainder of the contact area where these points move in a specific direction is called the slippage zone or slip region.

Kalker's computer program DUVOROL [5,11], see Appendix 1, was used to compute the relative distance slipped for the steady state rolling conditions experienced by the disc specimens. Plots of slip vectors for five points within contact area B, using input data from tests 4, 6 and 8 are shown in Figure 5. It can be seen that the contact area at test 4 (ψ = 8') contains a small adhesion zone but such a zone is absent at ψ = 20'

and 32' and both contact areas are fully saturated with slip. The process of slipping is completed at the trailing edge of the contact zone where the maximum magnitude of slip vector can usually, but not always, be found in the vicinity of the minor axis. The maximum values of slip d_{max} were calculated for all cases and are shown in Table 1. Figure 6 shows numerous scratch marks left behind by sand particles at the gauge (Figure 6(b)), centre (c) and field (d) sides of the disc surface of the high rail. These micrographs were taken from test 6 after its completion. A comparison of Figures 5(b) and 6 indicate a good agreement between theory and experiment. The curving of the slip vectors across the width of the contact zone is caused by spin which is particularly significant at $\psi = 8'$.

Table 1 - Summary of Test Conditions and Results

TEST NO.	ANGLE OF ATTACK	LUB	NUMBER OF REVS.	CONTACT AREA	FRICTION COEFFIC.	FORCES [N] A,B-INERTIA FRAME COORD. C-FLANGE CONTACT COORD.			SLIDING DISTANCE PARAMETER d_{max} [μm]	CONTACT STRESS p_{max} [MN/m²]	SURFACE ROUGHNESS [μm]	WEAR RATE [μg/cycle]
						A,B-VERT C-NORMAL	A,B-LAT C-TANG.	A,B-LONG				
1	0	No	2×10^6	A	≈.02	1710	-	-	.3(edge)	1410	0.19	<0.004
				B	≈.02	1710	-	-	.3(edge)	1410	0.17	<0.004
2		Yes	2×10^6	A	≈.15	1710	-	-	.3(edge)	1410	0.30	<0.004
				B	≈.15	1710	-	-	.3(edge)	1410	0.23	<0.004
3	8'	No	9×10^5	A	≈.02	1690	22	9	2.3	1200	0.02	0.022
				B	.25	1615	380	62	2.1	860	0.23	0.700
				C	.25	235	70	-	>500	360	-	0.330
4		Yes	2×10^6	A	≈.15	1710	-	-	2.3	930	0.37	0.130
				B	≈.15	1710	-	-	2.1	930	0.52	0.120
5	20'	No	5×10^5	A	.18	1700	280	65	5.2	930	1.75	4.400
				B	.25	1510	360	80	5.5	860	2.47	5.750
				C	.25	605	150	-	>500	340	-	2.710
6		Yes	2×10^6	A	.15	1704	255	31	5.2	900	0.31	0.850
				B	.15	1660	245	27	5.5	900	0.18	0.870
				C	.15	415	60	-	>200	170	-	0.100
7	32'	No	5×10^5	A	.30	1700	495	130	9.0	930	1.28	6.940
				B	.30	1420	410	93	9.1	930	1.77	10.10
					.30	785	235	-	>500	400	-	3.50
8		Yes	2×10^6	A	.15	1705	255	27	9.0	900	0.30	1.04
				B	.15	1660	245	27	9.1	930	0.44	0.820
				C	.15	400	62	-	>200	170	-	0.11

TOTAL WHEELSET LOAD = 3425 N; TEMPERATURE 20° C; R.H. 40%

For unlubricated contacts the slip distance could not be ascertained experimentally because of the presence of wear particles. Since the distance slipped is equal or less than the thickness of these particles, it is assumed that the bulk of the slippage was accounted for by shear deformation, or by slippage between these particles. A review of d_{max} values in Table 1 nevertheless indicates that distance slipped is the same for lubricated and unlubricated contacts and varies only as a function of angle-of-attack and geometry of contact.

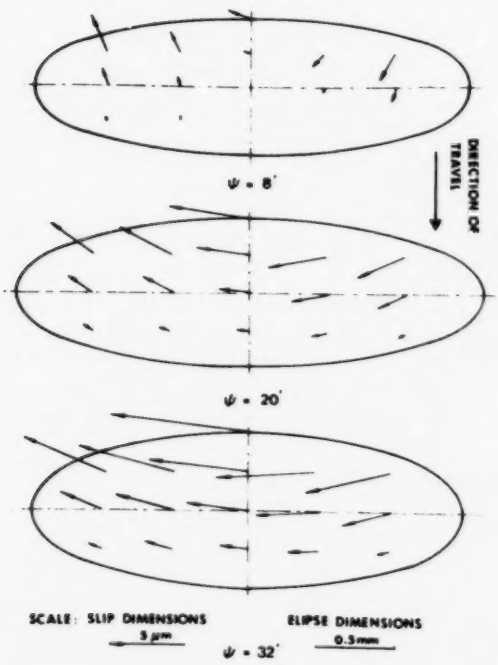

Figure 5 - Plots of Slip Vectors at Top Surface Contact Areas on High Rail Discs

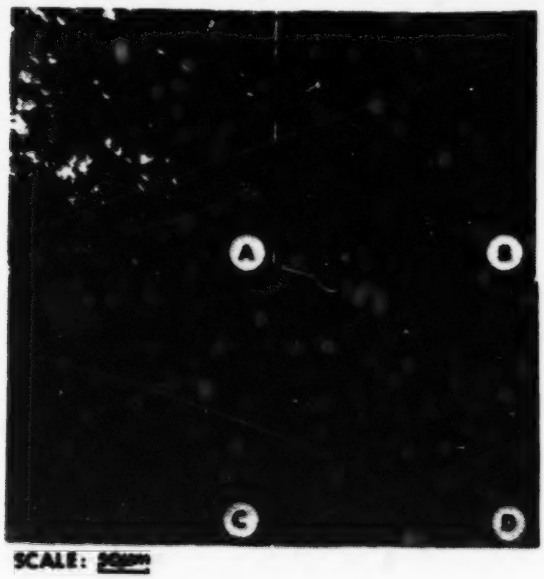

Figure 6 - Slip Marks Observed at (a) Flange, (b) Gauge Side, (c) Centre and (d) Field Side on the Surface of Lubricated High Rail Disc at ψ = 20'

Material Response

In this section we will further examine some aspects of plastic flow and wear behaviour of rail material. The rail profiles recorded at the beginning and the end of each test by an electronic instrument, utilizing stylus pick-up as a sensor, are shown in Figure 7. The polished and etched sections in the vicinity of the gauge corner of high and the field side of low rail discs are shown in Figure 8.

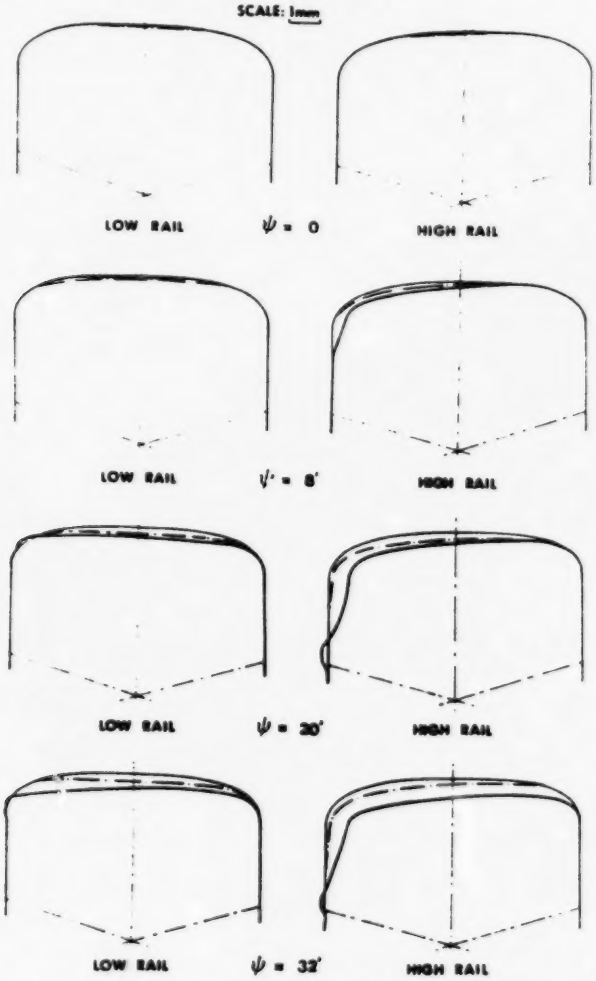

Figure 7 - New and Worn Profiles of Rail Discs

The most appreciable difference in plastic flow and wear behaviour occurred on the high rail discs between tests at ψ = 0' and tests at ψ = 8'. At ψ = 0', representing the tangent track, no plastic flow, save the fractional flow at the edges of the contact zones, and no wear, save the small amount which lies beyond the accuracy of our scales, was experienced by the discs under both lubricated and unlubricated conditions. At the value of ψ = 8', which is somewhat representative of a mild curve, an appreciable amount of plastic flow and wear occurred on the top running surface of the high rail in

both lubrication regimes. This difference could be attributed to changes in slippage. Over the tangent track (ψ = 0'), a wheelset approaches a state of pure rolling with the contact area containing a zone of adhesion at the centre of contact with two slip regions at the edges where slip is quantitatively small. At ψ = 8', the adhesion zone shrinks and the magnitude of d_{max} (see Table 1), becomes an order of magnitude larger. This is sufficient to cause appreciable plastic flow in both lateral and longitudinal directions. As the amount of slippage increases at the higher angles-of-attack of 20' and 32', the lateral component of plastic flow on the top running surfaces becomes more pronounced for both lubrication regimes.

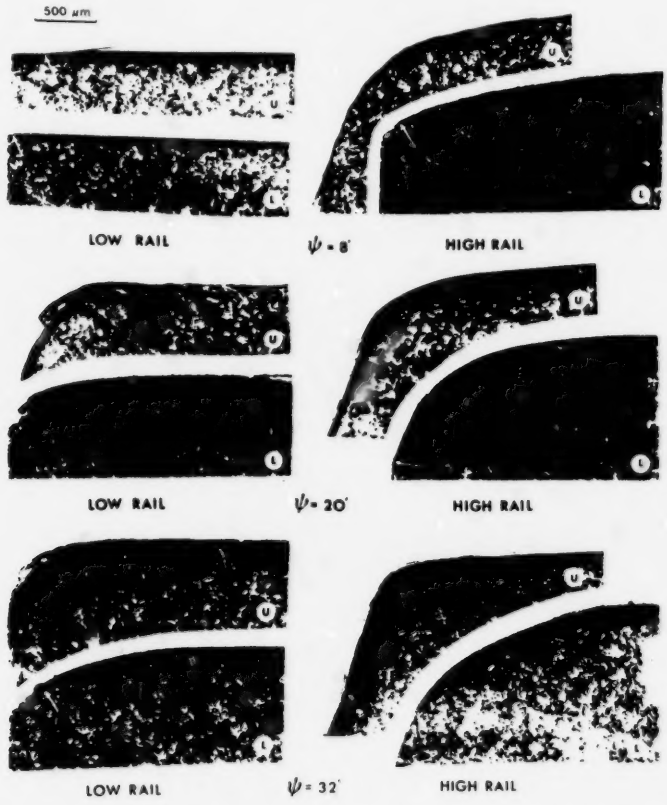

Figure 9 - Metallographical Sections of Rail Discs Showing Plastic Flow

Based on the absence or presence of plastic flow, it is apparent that the contact stresses at ψ = 0' lie below, and at ψ = 8' above, the shakedown limit. The reduction in contact pressure brought about by wear was not sufficiently large to prevent continuous plastic deformation of the surface layer of the rail material. Nor did the ability of pearlite material to strain-harden appear to prevent the continuous progression of plastic flow. The hardness profiles, shown in Figure 9, indicate that for unlubricated tests, the strain-hardening process, due to plastic flow, starts at some depth, for

example, 120 μm for ψ = 32', and reaches a maximum at the surface. Because the rate of strain-hardening and plastic flow are inversely proportional to the depth they are caused by surface rather than subsurface shear. A similar pattern is observed for lubricated surfaces with μ = 0.15 especially at the low rail discs. Based on a review of shakedown theories [3] and the experimental results presented above, it appears highly desirable to develop a theoretical model capable of predicting the shakedown limit for three-dimensional rolling contacts with arbitrary slippage.

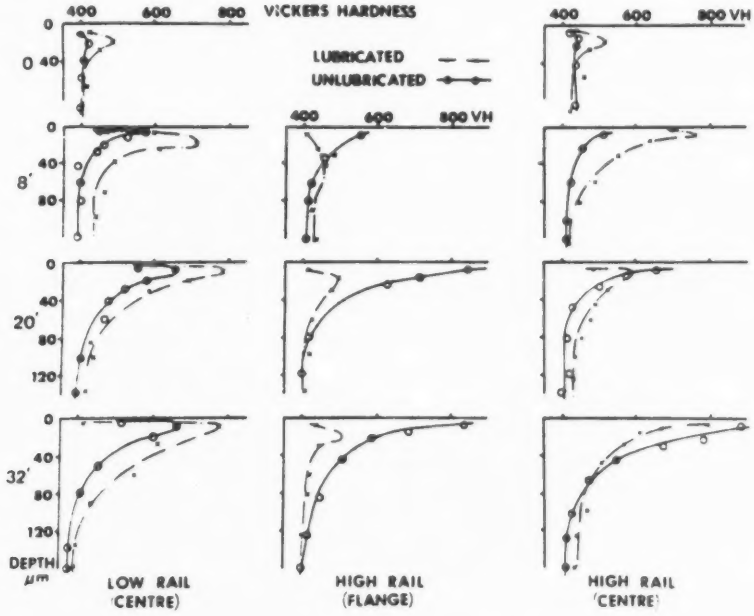

Figure 9 - Microhardness Surveys

Effect of Lubrication

The division of the test into lubricated and unlubricated only reflects the fact that in one case we did not use any lubricant but in the other we did. From the tribological point of view both cases were lubricated since the wear debris in the unlubricated case remained in the interface and behaved as a solid lubricant. It can be seen from Table 1 that while the angle-of-attack does not affect the properties of grease-sand mixtures it profoundly influences the lubricity of generated wear particles. This behaviour is most pronounced on the low rail in tests 3, 5 and 7 where the lubricity of wear particles is inversely proportional to ψ. In test 3 it exceeds the lubricity of the grease-sand mixture. Although the nature of varying lubricity of these wear particles is not fully understood it can be attributed to complex tribo-oxidation processes taking place in the rail/wheel interface [8]. In the case of the high rail, however, these particles maintained relatively low lubricity due to the intermixing of the particles between the flange and the top running surfaces.

The grease-sand mixture, on the other hand, exhibits a constant lubricity giving $\mu = 0.15$. In a true sense, the grease-sand mixture can be defined as a grinding paste rather than a lubricant. The only difference between grinding pastes and our mixture is that no control could be exercised over the size of abrasive particles. The size can nevertheless be estimated either from surface roughness measurements (shown in Table 1) or simply from the width of scratch marks seen in Figure 5. Based on these observations the size of sand grains present in the tread were in the vicinity of 1 μm while those in the flange contact retained a much larger size of approximately 25 μm. These particles can imbed into the rail and the wheel surfaces leading to the presence of abrasive wear on opposite surfaces.

It should be noted that although the type of abrasive interaction remains the same a significant difference in plastic flow can be observed in Figure 8 between the top running surfaces and the flange contact. Tests 6 and 8 show plastic flow under the top surfaces but almost no flow can be observed in the flange contact. This difference may be satisfactorily accounted for by the difference between the product of the slip and sand particle size, which for the flange contact is three orders of magnitude larger than the one typical for the top running surfaces. To explain this in a more figurative manner let us imagine the wheel flange, with imbedded sand particles, as a grinding wheel, which removed the metal from the rail gauge by a cutting action which is not conducive to appreciable plastic flow. It must be emphasized, however, that the wear rate associated with this type of abrasive interaction is about 1/30th of that typical for unlubricated flange contacts.

The microscopic dimensions of slip and particles imbedded into the top running surfaces, on the other hand, severely affect the cutting ability of such particles and an appreciable plastic flow results. This is further supported by the observation that abrasive metal loss is fractional compared to the total wear experienced by these surfaces. Most of the metal loss is accounted for by the fatigue wear mechanism further described in the next section.

Wear Rates and Wear Mechanisms

Wear data require careful interpretation since the forces, sliding distances, plastic flow, lubricity of wear particles and grease-sand mixtures all considerably affect the wear rates. The largest difference in wear can be observed between the tangent track at $\psi = 0'$ and that representing the curved track at $\psi = 32'$. The wear rates differ by a factor of 1000 if the high rails are compared (test 1B with 7B, C). Lubrication by grease-sand mixture reduces this difference by an order of magnitude. An exception to this trend can be observed on the low rail at $\psi = 8'$, where the unlubricated rail disc had worn less than the lubricated one. As pointed out previously, the lubricity of wear particles was better than that of the grease-sand mixture.

The high rails in unlubricated tests 3, 5 and 7 exhibit higher rates of metal depletion from the top surfaces than the low rails (see Figure 7). Since the loads and

surface hardnesses between contact zones A and B are comparable, it appears that some kind of synergy exists between the flange and the tread wear on the high rail discs. This could be attributed to plastic flow which feeds the deformed metal from the tread into the flange contact (see Figure 10(a)) where it is worn away. High conicity of the top surfaces found on the worn outer rails should be attributed to this wear pattern.

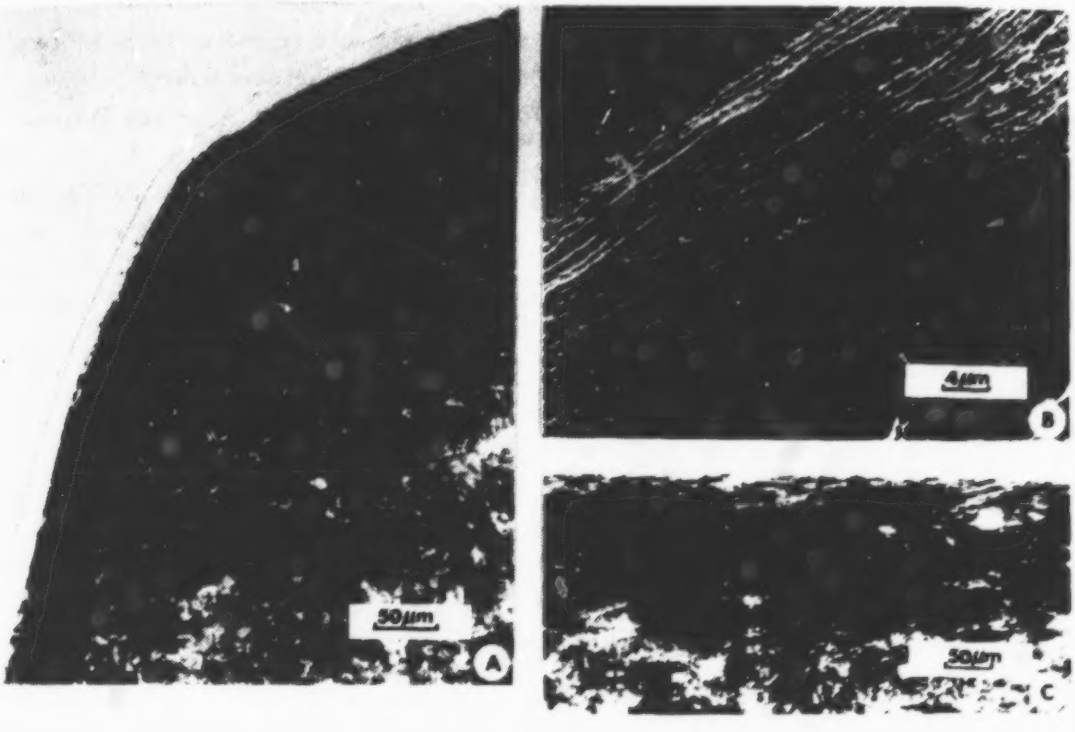

Figure 10 - (a) Detail of plastic flow at gauge corner of high rail disc in test 7.
(b) SEM photograph of a white etching wear particle generated by low rail disc in test 7.
(c) Subsurface cracks observed on high rail disc in test 7.

Another observation regarding the high rails and worth mentioning is that the wear rates at ψ = 8' (unlubricated) and ψ = 20' and 32' (lubricated) are about the same. This indicates that self-steering bogies, with low yaw angles, on the unlubricated track should be expected to yield the same amount of wear as the standard three-piece bogies on the lubricated track. However, a mixed population of both types of bogies on the lubricated track should be further examined namely from the point of view of the development of shelly spots.

Analysis of wear particles collected from the unlubricated and lubricated interfaces indicate that both populations of these particles were formed by similar mechanisms. Figures 11(a) and (b) show the cross-section of these particles from tests 7A and 8B

respectively. In both tests, two qualitatively different types of particles could be distinguished. One etched dark with a hardness ranging from 100 to 600 VHN. The other type ranges in hardness from 500 to 1200 VHN and etched white. Only ≈ 5 percent of the particles etched white in the unlubricated regime while in the lubricated regime they were far more frequent at about one third of the total population. Since the size of the particles originating from the lubricated interface is much larger than that of sand particles, their formation cannot be attributed to abrasion. Noting that in a large majority of these particles pearlite lamella are aligned parallel to the surface due to extensive plastic flow (Figure 10(b)), it is possible to visualize the particle formation by the gradual or sudden propagation of cracks in between the same pair of lamella at a depth equal to the thickness of such particles. (Numerous cracks of this type were observed in the unlubricated regime as shown in Figure 10(c) but in the lubricated regime these cracks were far less frequent.) By this mechanism, a hundred-fold longer particles, as compared to slippage length or size of sand particles, can be generated by the compression and shear stress field existing in the rail/wheel interface. This form of wear is obviously fatigue-related for both the lubricated and the unlubricated regimes and should be referred to as delamination.

Figure 11 - Wear Particles Generated by Low Rail Discs in (a) Test 7 and (b) Test 8

CONCLUDING REMARKS AND SUMMARY

This paper discusses the dependence of wear in curves on the angle-of-attack and lubrication. Since the yaw angle in any population of wheelsets, say a train or some other unit of traffic, are distributed randomly, it is not possible to correlate a degree of curvature to a unique angle-of-attack. However, as the curvature of the track increases, so do the individual values of yaw angle. The results contained in this paper help us to identify the amount of wear and plastic flow which individual wheelsets can inflict on the rails in curves. The results of our investigations can be summarized as follows.

For the unlubricated regime:

(1) the high rail discs experienced more wear than the low rail discs;

(2) at the low values of yaw angle wear particles of high lubricity may be generated which significantly reduce wear rates;

(3) the wear rate observed on the top surfaces of the high rails is higher than those observed on the low rails. Both a difference of lubricity of wear particles and synergestic interaction between the top surface plastic flow and the flange wear might be involved.

For lubrication by grease-sand mixtrues:

(1) the hard flange contact on the high rails experience predominantly abrasive wear but with much lower wear rates than those typical of unlubricated contacts;

(2) the prevailing form of wear on the top running surfaces is of a delamination type similar to the one existing in the unlubricated regime but exhibiting lower wear rates and generating harder wear particles.

ACKNOWLEDGEMENT

Experimental work reported in this paper represents a portion of a cooperative rail/wheel wear research program undertaken by the Western Laboratory of the National Research Council, Canada and the University of Rhode Island. The financial support of the Transportation Development Centre (Canada) and the Association of American Railroads towards this program is greatly appreciated. Canadian Pacific Rail and Hawker-Siddeley Canada - Canadian Steel Wheel Division are gratefully acknowledged for the supply of material and assistance in the production of rail and wheel specimens used in this investigation. And last, but not least, the support of the technical staff at the Western Laboratory, namely Messrs. H. Ackroyd and P. Bigelow whose meticulousness contributed to the quality of technical illustrations are most appreciated.

NOMENCLATURE

d - relative distance slipped
e - lateral displacement of wheelset
N - normal load
NC - numerically controlled
p_{max} - maximum Hertzian contact pressure
r - radius
s - relative slip velocity
u,v - tangential surface displacement difference in x and y directions
V - 'velocity' of contact area
VHN - Vickers hardness number
x,y - rolling and lateral directions
$\gamma_{1,2}$ - longitudinal and lateral creepage

- · - cone angle at point of contact
- μ - coefficient of friction
- · - angle-of-attack or yaw angle
- ω - spin creepage
- Ω - angular velocity
- R.W - rail and wheel
- i - grid within the contact zone

REFERENCES

[1] BRADLEY, J. and KALOUSEK, J., "Modelling of Roller Rig Contact Forces for Three Point Contact - Based on Kalker's Simplified Non-Linear Creep Theory for Single Point Contact", *NRC Report LTR-WE-29*, (in preparation).

[2] GHONEM, H. and GONSALVES, R., "Comparative Performance of Type II Trucks", Canadian Pacific Department of Research, *Report No. 5576-78*, November, 1978.

[3] JOHNSON, K.L., "Inelastic Contact: Plastic Flow and Shakedown", *Proc. of the Int. Symposium on Contact Mechanics and Wear of Rail/Wheel Systems*, held in Vancouver, British Columbia, July, 1982.

[4] KALKER, J.J., "On the Rolling Contact of Two Elastic Bodies in the Presence of Dry Friction", *Ph. D. Thesis*, Delft University of Technology, 1967.

[5] KALKER, J.J., "The Computation of Three-Dimensional Rolling Contact with Dry Friction", *Int. J. for Numerical Methods in Engineering*, Vol. 14, 1979, pp. 1239-1307.

[6] KALOUSEK, J., "Rail/Wheel Wear Testing Facility", NRCC, *DME Newsletter*, Vol. 13, No. 1, July, 1981.

[7] KALOUSEK, J. and BETHUNE, A.E., "Rail Wear Under Heavy Traffic Conditions", *Rail Steels - Developments, Processing and Use*, ASTM STP 664, D.H. Stone and G.G. Knupp, Editors, ASTM, 1978, pp. 63-79.

[8] KRAUSE, H. and DEMIRCI, A.H., "Factors Influencing the Real Trend of the Coefficient of Friction of Two Elastic Bodies Rolling Over Each Other in the Presence of Dry Friction", *The Mechanics of the Contact Between Deformable Bodies*, A.D. de Pater and J.J. Kalker, Editors, ASTM, 1975, pp. 342-358.

[9] MARCOTTE, P.P., MATHEWSON, K.J.R. and CALDWELL, W.N., "Improved Wheel Tread Profiles for Heavy Freight Vehicles", *Journal of Engineering for Industry, ASME*, Vol. 102, August, 1980, pp. 263-271.

[10] RONEY, M.D., "Economic Studies of Rail Deterioration", *Proc. of the Int. Symposium on Contact Mechanics and Wear of Rail/Wheel Systems*, held in Vancouver, British Columbia, July, 1982.

[11] TJOENG, A.S.K.S. and KALKER, J.J., *User's Manual for the Program DUVOROL in ALGOL 60 and FORTRAN for the Computation of Three-Dimensional Rolling Contact with Dry Friction*, Department of Mathematics, Delft University of Technology, The Netherlands.

APPENDIX

To indicate the manner in which the slip vectors within the zone of contact were established let us briefly mention a few relevant relationships. For steady rolling, the relative slip velocities in a nondimensional form at a point on a grid [5] are given by:

$$s_x = \gamma_1 - \omega y + \frac{\delta u}{\delta x}, \qquad s_y = \gamma_2 - \omega x + \frac{\delta v}{\delta x}, \qquad (1,2)$$

where:

$$\gamma_1 = (\Omega_W r_W - \Omega_R r_R)/V \ , \qquad \gamma_2 = \Omega_R r_R \sin\psi/V\cos\lambda \ , \tag{3,4}$$

$$\omega = \left(\frac{1}{r_W} - \frac{1}{r_R}\right)\sin\lambda \ , \qquad v = \frac{1}{2}\ (\Omega_R r_R + \Omega_W r_W) \ . \tag{5,6}$$

The exact position of a point on the wheel or rail is therefore dependent on both the velocity of the material moving through the contact zone and the relative slip velocity within this zone. In many cases of practical interest, the influence of the latter velocity is small in relation to that of the former. This enabled us, using the results of DUVOROL to approximate a relative slip distance between the rail and wheel discs in the following manner.

The time Δt_i required for a point to move a distance Δx_i in the longitudinal direction within the contact zone is given by:

$$\Delta t_i = \frac{\Delta x_i}{r_W \omega_W} \ . \tag{7}$$

If the grid distance Δx_i is small such that the relative slip velocity may be assumed to be constant over this distance, the relative distance slipped is:

$$\bar{d}_i = \bar{s}_i \frac{\Delta x_i}{r_W \omega_W} \ , \tag{8}$$

and the total relative distance slipped is:

$$\bar{d} = \Sigma \bar{d}_i \ , \tag{9}$$

where a summation is carried out over each length Δx_i along the trajectory of the point of interest. This procedure was carried out for all cases and the maximum length of slip distance d_{max} occurring at each ψ is shown in Table 1.

COMMENTS

T. Appa-Rao, Ontario Ministry of Transportation and Communications. Both angle of attack and lateral wheel/rail force are considered to have a significant effect on wheel/rail wear. Have you attempted to study the effect of lateral force in your model experiments? The rig you have may also be useful for a study of wheel squeal. Did you observe any squeal noise during your experiments?

Authors' Reply. Yes, the values of lateral forces, contact stresses and the wear rates for each rail disc are shown in Table 1 of the main paper. An appropriate modification of wheel disc design would represent the only change needed to study wheel squeal on our rig. As a rule our rig does not produce, at present, a squeal noise. However, under

very high normal load and dry conditions, the squeal noise can occur with the present rig design.

* * *

D.J.H. Corderoy, University of New South Wales, Australia. It is most interesting that you have been able to obtain discrete particles of the white etching phase. There has been considerable debate as to the nature of this phase and it would seem that you have the opportunity to do a definitive experiment to determine whether this phase results from adiabatic heating and transformation to martensite. X-ray diffraction would establish conclusively whether this phase is martensite.

Authors' Reply. Thank you for the useful suggestion. We will try to follow it up.

* * *

W. Duffek, DFVLR - Institut für Dynamik der Flugsystem, Munichner, West Germany. How do you find contact point locations? By measurement or calculations.

Authors' Reply. By measurements.

* * *

J.J. Kalker, Technical University of Delft, The Netherlands. Does not using a disc machine alter the shape of contact with regard to wheel/rail situations? Does this not have a quantitative influence?

Author's Reply. In a tread contact the major axis of a contact ellipse could be oriented in the field either parallel or perpendicular to the direction of travel, depending on the geometry. In a disc machine, the major axis for worn discs is always perpendicular to the travel direction. However, this rule does not always hold for the new discs. In flange contact, the ellipse is elongated in the travel direction for new "rail on wheel" and new "disc on disc" combinations. For worn profiles, the flange contact geometry is not at present theoretically or experimentally well-established.

Using computer programs (reference [1] of our paper) which took into account the relevant changes in contact ellipse dimensions, we calculated the traction forces for "rail on wheel" and "disc on disc" systems. For the cases considered, the difference was in general very small and did not in any case exceed 5 percent.

* * *

S.T. Lamson, Queen's University, Kingston, Ontario, Canada. Could you explain the reason for the very low lateral force in the range of small angle-of-attack (0' to 10').

Authors' Reply. In a range of angle-of-attack 0' to = 10' the wheelset displaces laterally towards high rail disc, which increases the flangeway clearance between low wheel and rail discs. The external lateral force measured on low rail disc reflects the sum of all the tread forces including those due to lateral creepage, spin creepage and gravitational stiffness which do not necessarily all act in the same direction. Thus, depending on lubrication, the net external force could take on a slightly positive or negative value for small angles-of-attack.

P.P. Marcotte, Dynamic Sciences Limited, St. Laurent, Quebec, Canada. May I add some additional comments to Mr. Lamson's question. The condition shown in Figure 4 of the paper can be explained from considerations of the opposing effects of "gravitational" forces and lateral forces resulting from spin. Depending on the contact geometry parameters (a contoured profile is used in the test) it is theoretically possible for the spin effect to overcome the gravitational effect. With lubrication however, the spin effect may decrease and let the gravitational effect dominate. This would produce a trend as shown in the experimental data.

* * *

J.J. Moyar, Moyar Technical Services Ltd., Downers Grove, Illinois, U.S.A. You made some use of the measurement of worn contact geometry in your elastic slip/adhesion calculations. How much change in contact ellipse aspect ratio, orientation and Hertz pressure from new to worn did you calculate?

Authors' Reply. For new rail and wheel discs geometry, zero yaw angle and a load of 1710 N (385 lb.), the calculated contact ellipse dimensions are 2a = 1.92 mm, 2b = 1.2 mm, given a/b = 1.61; "a" is perpendicular to direction of travel and maximum Hertz pressure p_{max} = 1410 MN/m^2. The wear tracks at the end of test 1 (unlubricated) remained about 2 mm wide, but became wider (2.8 mm) at the end of test 2 when the rail was lubricated with a mixture of grease and sand. In both these tests, we presume, the material has shaken down even under the presence of relatively high contact stresses.

For the tests 3 to 8, the 2a varied in a range of 4 to 6 mm and a/b = 4.6 to 7.2, "a" again being perpendicular to the direction of travel. The values of calculated p_{max} are shown in Table 1. Due to the presence of spin and lateral creepages, the shakedown limit was not reached in these tests in spite of the fact that wear has reduced p_{max} to 900 MN/m^2 on average.

* * *

E.E. Laufer, Technical University of Nova Scotia. You see more white etching debris particles when running with lubrication. Are there white etching particles also associated with white etching layers on the discs?

Authors' Reply. Yes, the white etching particles are associated with white etching layers present on the running surfaces of lubricated discs. These layers were found in long, sometimes circumferential bands 0.5 to 1.5 mm in tests 4, 6 and 8. Such bands could be found anywhere across the discs, but they appeared to be most frequent and widest at the field side of low rail discs and gauge side of high rail discs. A micrograph showing a portion of a white etching band is shown in Figure 12.

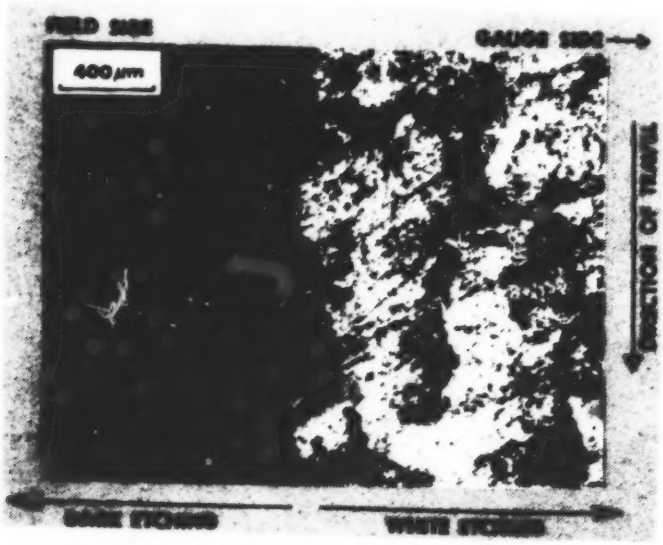

Figure 12 - Micrograph showing white and dark etching areas found at a field side of low rail disc in test 6 (L = 1%, lubricated).

* * *

Submitted to: International Conference on Recent Developments in
Specialty Steels and Hard Materials,
Pretoria, Republic of South Africa,
November 8-12, 1982.

ON THE FRACTURE AND WEAR CHARACTERISTICS OF CHROMIUM-MOLYBDENUM BAINITIC STEEL

H. Ghonem*, J. Kalousek** and D. Stone***

*Mechanical Engineering Dept., Univ. of Rhode Island,
Kingston, R.I., U.S.A.
**National Research Council, Vancouver, B.C. Canada
***Association of American Railroads, Chicago, ILL., U.S.A.

ABSTRACT

This paper summarizes the fracture toughness and wear characteristics of the first bainitic rail steel to be produced in North America.

KEYWORDS

Bainitic; Pearlite; Fracture toughness; microstructure inhomogenity; Compact tension; Wear rate.

INTRODUCTION

In the work of Kalousek and Beynon (1) it wasconcluded that rail life, all variables being constant, could be increased by refining both grain size and spacings between pearlite lamella. Several methods will achieve this - one of which is the alloying method. Out of available alloyed rail composition, reviewed in Ref. (1), the chromium-molybdenum rail appeared to be the most desirable for future premium rail.

In order to obtain an optimum pearlitic structure of such rail a three phase gradual structure refinement was suggested: first, to obtain a rail with a subsurface structure having a hardness level of 340-360 BHN; second, to reach 360-380 BHN; and third, to aim for 380-450 BHN. To carry out the first phase, a 100 ton Cr-Mo heat (identified as C5599) was ingot cast, aluminum-deoxidized and rolled to develop a microstructure of fine pearlite. During rolling of the ingot, streaks appeared in the webs in localized areas affected by microsegregation of Mn, Mo and Cr. Furthermore some of the rolled rails developed excessive curvature during cooling on the hot bed. To rectify these problems, a second strand cast heat was produced. This heat was also intended to fall into the phase I category, however, the average hardness exceeded 400 BHN with an upper-bainitic microstructure. This is considered the first bainitic rail steel to be produced in North America and this paper summarizes its fracture and wear characteristics.

II. Microstructure Properties

The hundred tons of silicon-deoxidized Cr-Mo II* (BOF) heat was produced in billets

of cross section 27x32 cm and rolled into 66 Kg/m RE rails. Ladle and spectroscopic analysis of head sections of these rails showed the steel composition to have an excess of 0.15-0.20% Mo compared to Cr-Mo I. The microstructure of the rail cross section was found to consist of 70% upper bainite and 30% transitional pearlite with interlamellar spacings of 500-800 A°.

A Scanning Electron Microscope examination of the web region of the baintic rails revealed that, while the microsegregation is reduced 50% more than in Cr-Mo I, web streaks were equally numerous, arranged in platelet form and oriented parallel to the vertical plane, see Figure 1. They consist of lower bainite and traces of tempered martensite and have a hardness of RC55. The microstructure and hardness were unchanged by subzero quenching or by stress-relief treatment, which suggests that the lower bainite is relatively stable after manufacture.

Tests reported here measured and compared fracture toughness of bainitic and pearlitic steel structures as well as the effect of the lower bainite streaks on the fracture toughness of the bainitic rail web.

III. Fracture Toughness and Impact Properties

III. 1. Effect of Bainitic Structure. Two different pearlitic rail types were compared with the bainitic Cr-Mo II and the pearlitic Cr-Mo I; namely, heat treated carbon rail steel and plain carbon steel. Out of each rail type sixteen compact tension (CT) specimens 32x25x13 mm were machined from head, web and base sections, as shown in Figure 2, with transverse starter notches cut in a direction normal to the rail surface. An electric discharge notch (0.18 mm width x0.76 mm depth) was used to locate the initial fatigue crack.

A similar number of WOL specimens (19x19x38 mm) from the same rail steels were machined with saw cut notches and similar electric discharge notches, see Figure 3. Fatigue precracking was done using tension-tension loading for CT specimens and full cycle tension-compression loading for WOL specimens.

Keeping in mind that rail steel of all types is known to violate the ASTM E399 condition of $K_{max}/K_Q \leq 1.10$ because of short cleavage bursts which occurs well below the breaking load, test results at 24°C and -50°C, see Ref. (2), are shown in Table 2. They indicate i) $K_{IC}(K_Q)$ values for pearlitic steel are 1.6 times higher than those of baintic steel, ii) the permissible defect size (d_c) of pearlitic steel calculated for σ = 196 MPa is twice that of the bainitic and plain carbon steel.

Notched and unnotched charpy impact tests were also performed on the same rail types in the transition temperature range. Figure 4 indicates that the "energy to fracture" values of Cr-Mo I is comparable to the fully heat treated rail steel while, again, the values of Cr-Mo II are the same level as the plain carbon steel.

III. 2. Effect of "Streaks". Eight miniature compact tension specimens (W = 13.5 mm) were prepared, one pair from each of four web center regions in Cr-Mo I and Cr-Mo II rails, respectively, as shown in Figure 5. In addition, eight similar specimens were obtained from similar regions of plain carbon and 1% Cr steel rails.

---

*Cr-Mo II will be used to identify the bainitic Cr-Mo steel (heat 9273B) while Cr-Mo I will identify the pearlitic one (heat C5599).

In each test specimen, the initial machined notch was oriented towards the vertical plane of the rail web while its tip was to be located in a streak region. Preparation of the electric discharge notch, the fatigue precrack and the test procedure was similar to the CT specimens described in the previous section, see Ref (3). Crack length traces were observed with an accuracy of 0.05 mm. Test results are shown in Table 2. When this table is compared to values in Table 1, it was apparent that the existence of streaks in Cr-Mo rail did not reduce its fracture toughness.

Fracture surfaces of test specimens were studied using a SEM in order to determine the features of the crack front and the induced effects on its propagation stage due to the presence of streaks. As all test specimens were fractured under a plane strain condition, their fracture surfaces were predominately transgrannular cleavages, with some of the cleavage facets containing small steps similar to these reported by Park and Bernstein (4). In the case of Carbon and 1% Cr steel, distortion of cleavage facets was observed and related to an extension ductile tearing.

IV. Wear Performance

Twenty lengths of Cr-Mo II were placed in section 3 of F.A.S.T. loop which has a 5° curvature, a 2% grade and a 1/40 cant. Seven other different rail types, in addition to Cr-Mo II, were to be tested in this section; all of these were 66 Kg/m. In this experiment, detailed in Ref. (5), rails were subjected to programmed regimes of lubricated and dry conditions so that wear and metal flow in both regimes could be studied and compared. The twenty lengths of Cr-Mo II were removed from F.A.S.T. loop after an accumulation of 115 MGT. The main parameter studied during the field tests was high rail curve wear. Wear measurement included gage face wear, head height and total head area loss. These measurements were taken at intervals of approximately two months using a "snap gage" of accuracy ±0.002. Profile comparisons obtained from these measurements are shown in Figure 6. From a complex analysis of this figure an average wear rate was calculated, and results are shown in Table 3.

From Table 3 and Figure 6 it could be concluded that Cr-Mo II rail performance in the dry regime was similar to most of the premium rails. However, in the lubricated regime, although its surface and gauge hardness were higher than all of the test rails with the exception of SiCr, its wear performance was virtually the same as the standard rail. Furthermore, when the wear rate was related to the gauge face hardness in both lubricated and dry conditions, the performance of Cr-Mo rail was the lowest among all premium rails.

V. Conclusions

Data presented in this paper concerning the fracture and wear characteristics of the first production of bainitic chromium-molybdenum rail steel indicates the following

i - As expected, the fracture toughness of bainitic structure is lower than the fine pearlite structure.

ii - Existence of lower bainite streaks in an upper bainite matrix does not effect the fracture toughness of the matrix.

iii - Surface wear characteristics of the bainitic steel in lubricated or dry conditions are not superior to the pearlitic steel.

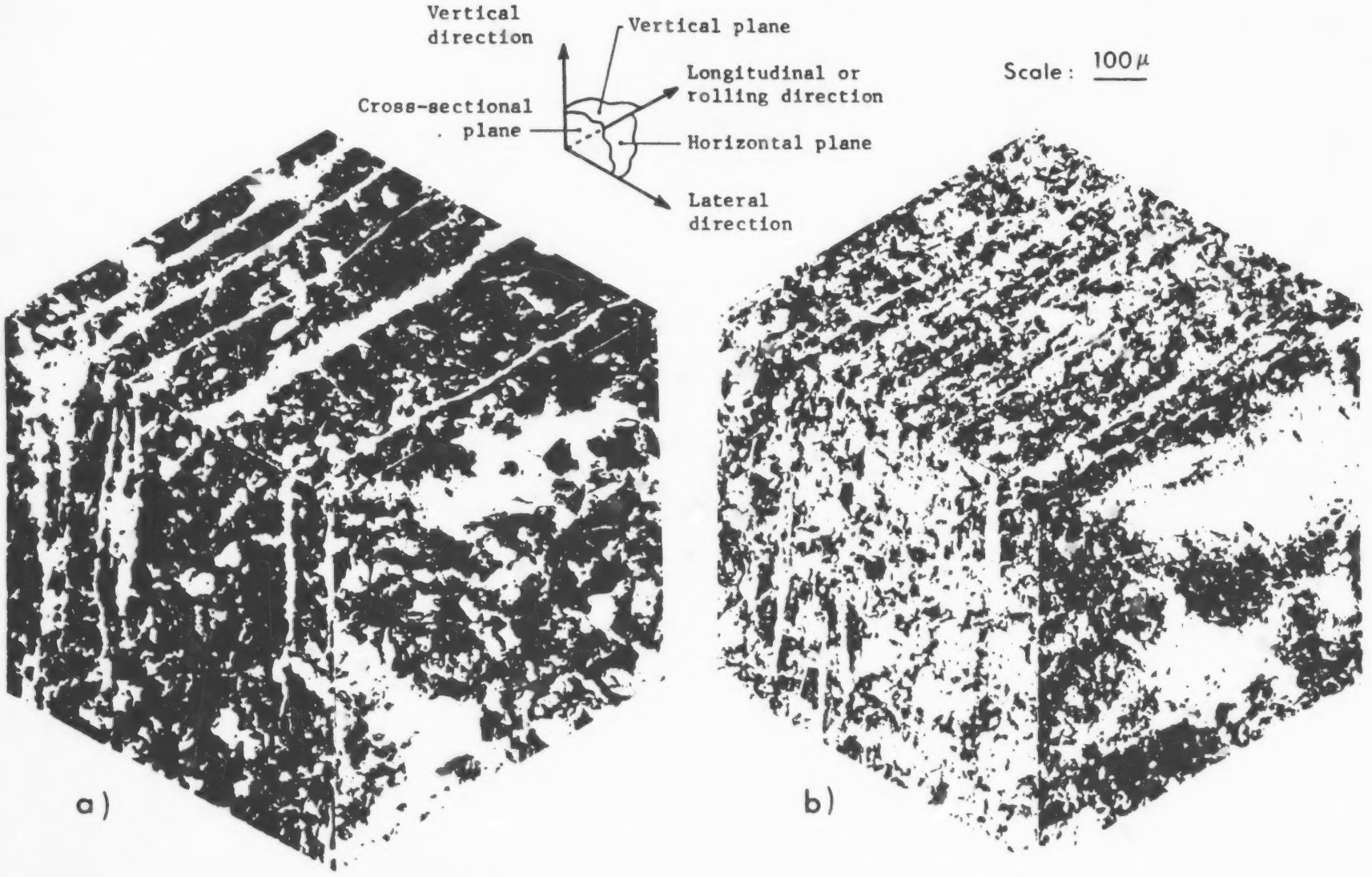

Figure 1: Microstructure of Cr-Mo Web Material, on the Three Processing Planes Depicting the Shape of 'Streaks' a) Cr-Mo I (C5599) b) Cr-Mo II (9237B)

VI. References

Kalousek, J. and Beynon, G., Canadian Pacific Tech. Rep. No. S497-75, 1975.
Parsons, D.E., Energy, Mines and Resources Canada, MRP/PMRL 76-19(R), 1976.
Kalousek, J., Parsons, D.E. and Ghonem, H., Canadian Metallurgical Quarterly, 1982.
Park, Y-J. and Bernstein, STP644, 1978.
Steele, R.K., FRA/TTC-81/07, 1981.

Steel Type	Test Temperature	Av. K_{IC} MPa $\sqrt{m}$	d_c (mm)
Cr-Mo I	Room temp.	51.3	42
	75°F	43.4	31
Cr-Mo II	Room temp.	32.0	17
	75°F	34.0	19
Fully Heat Treated	75°F	39.9	26
Plain Carbon	75°F	33.5	18

Table 1: K_{IC} and d_c Values of Bainitic and Pearlitic Cr-Mo Steels

Steel Type	Temp C°	Av. K_Q MPa $\sqrt{m}$	Av. K_{max} MPa $\sqrt{m}$
Cr-Mo I	24	45.8	45.6+
	-50	32.5	32.5
Cr-Mo II	24	38.4	37.7+
	-50	26.2	27.5
Carbon	24	40.3	40.3
	-50	23.3	
1% Cr	24	26.7	28.1
	-50	27.3	28.5

Table 2: Fracture Characteristics of Bainitic Steel Containing Streaks

Steel Type	Av. Lubricated	Av. Unlubricated
Standard	0.0010	0.0066
Heat Hardened	0.0075	0.0023
SiCr (HH)	0.00065	0.0017
1% Cr	0.00065	0.0029
Cr-Mo (CF&I)	0.00065	0.0029
Cr-Mo (II)	0.00090	0.0036
FHT	0.0007	0.0031

Table 3: Wear Rate of Cr-Mo II and Other Pearlitic Steels (In./MGT)

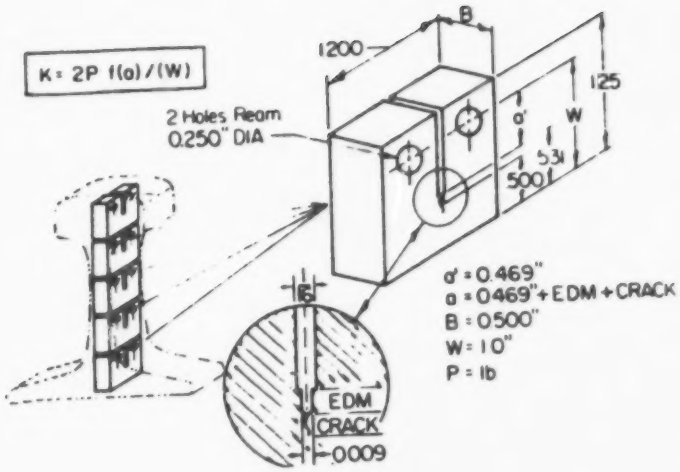

Fig. 2 Standard Compact - Tension Test Specimen

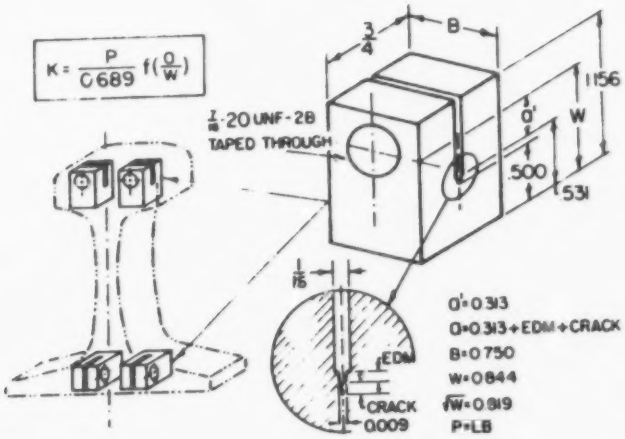

Fig. 3 WOL Test Specimen

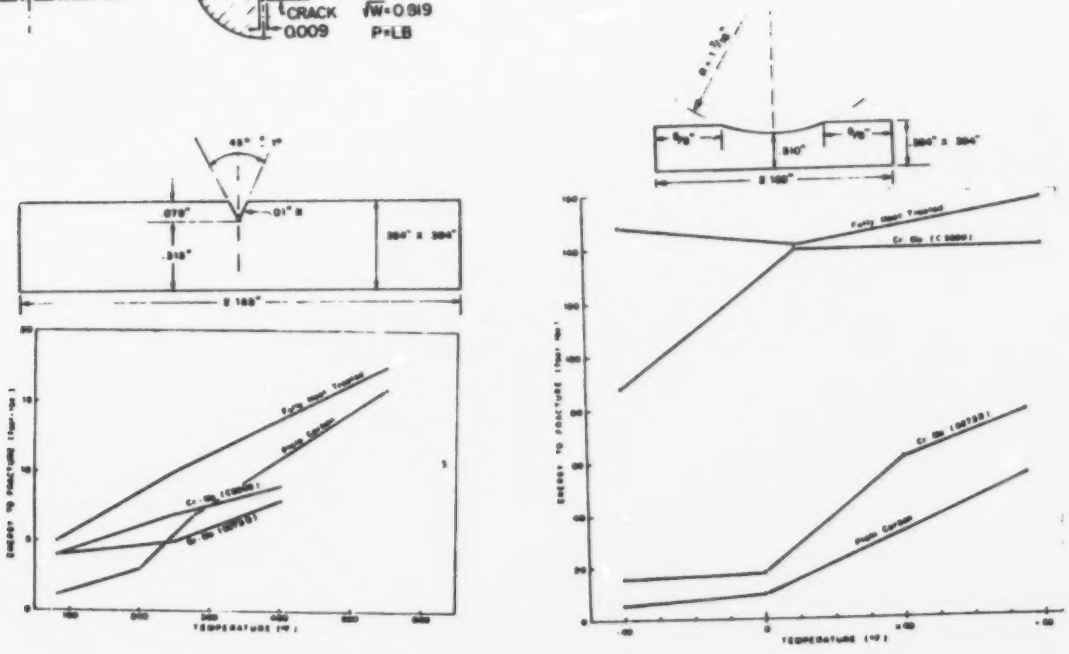

Fig. 4 Charpy Impact Energy vs Temperature

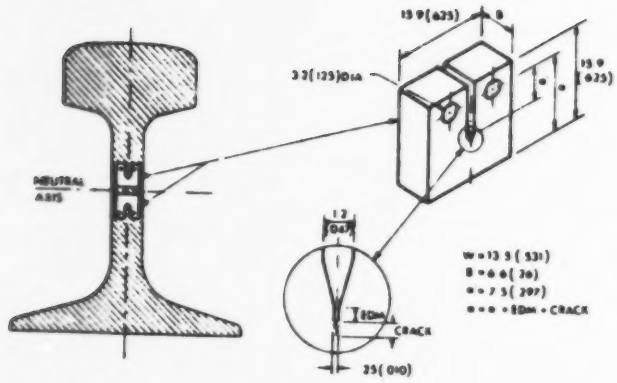

Fig. 5 Orientation and Dimension of CT Specimens Taken From the Center of the Rail Web (mm (inch)).

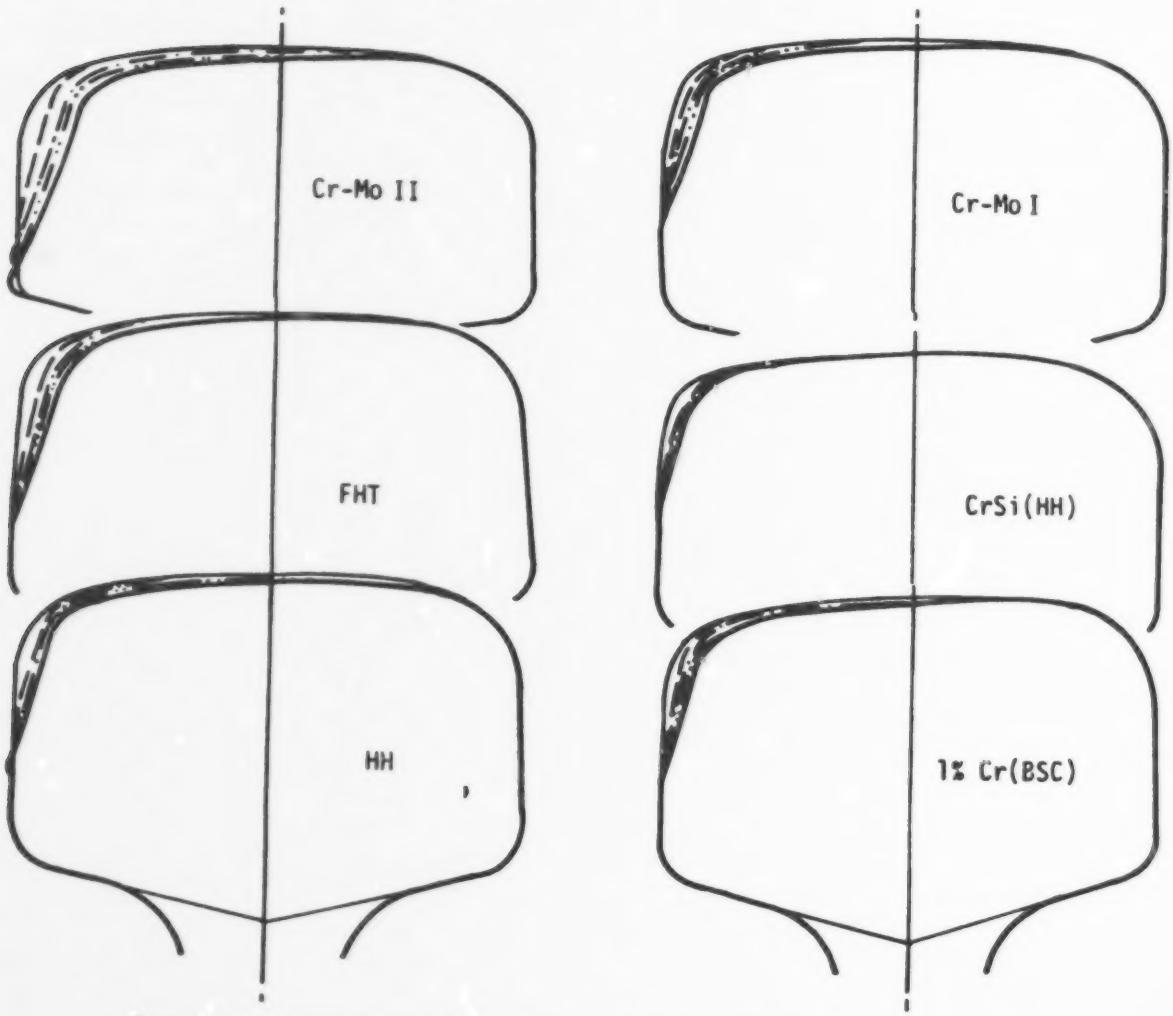

Figure 6: Comparison of Tested Rails Head Profile

POOR

QUALITY

ORIGINAL